Modeling the Transport and Inhibition Kinetics of the Human Multidrug Resistance Transporter P-Glycoprotein in MDCK-II Cells

Poulomi Acharya

B.S., Calcutta University, India, 2000

M.S., Banaras Hindu University, India, 2002

DISSERTATION

submitted by to the Faculty of The Department of Bioscience and Biotechnology

at Drexel University, Philadelphia

in partial fulfillment of the requirements

for the degree of

Doctor of Philosophy in Cellular and Molecular Biology

2007

To my Parents, Bhai

and Dia.

Acknowledgements

First and foremost I offer my sincerest gratitude to my mentor, Dr.Joe Bentz, who has been an advisor, a teacher and a friend all at the same time. He has shown patience with my ineptitude, imparted knowledge when I was ignorant, given guidance when I was lost and criticized to improve me. He showed me the right direction at each bend and also encouraged me to work in my own way, and to develop my own thought process. His eloquence in explaining complex things in a simple way amazes me and I am awed by the depth of his knowledge and the truth behind his convictions. His infallible intuition has made him as a constant oasis of novel ideas in science, which have and will exceptionally inspire and enrich my growth as a student, a researcher and a scientist I want to be. The originality of his ideas has triggered and nourished my intellectual maturity that I will benefit from, for a long time to come. I am indebted to him in more ways than he knows. Without his encouragement and effort this thesis, too, would not have been written or completed. One simply could not wish for a better or friendlier advisor to look up to.

I would like to gratefully acknowledge all the support and opportunities my co-advisor Dr. Harma Ellens, has given me. Without her efforts I would never have had the chance to work at the Drug metabolism and Pharmacokinetics research laboratories at Glaxo-SmithKline. I am thankful for her faith in me without which I would never have been able to accomplish the research that this thesis is all about. She has been a constant source of inspiration and has contributed to this work immensely with her knowledge and advice.

I thank Dr. Michael O'Connor, Dr. Aleister Saunders and Dr. Peter Lelkes for serving on my dissertation committee and guiding me with their invaluable guidance and constructive criticism. I thank Dr. Joe Polli, Dr. Andrew Ayrton at GlaxoSmithKline for helping eliminate confusions in the writing of papers. I thank Dr. Philip Handel (former Department Head) and Dr.Mary.K.Howett (Current Department Head) for their help and continual support during my stay in the Department, Dr. Laura Duwel for accommodating

my requests for teaching. I am very happy to acknowledge Dr. Jeremy Lees support and motivation during all these years.

I have been blessed to have had the opportunity to work with a handful of very helpful and intelligent group of people who have contributed in their own way to this work. Thuy Tran, a former member of Bentz lab has been instrumental in teaching me how to do the drug transport experiments and entertaining my not-so-intellectually-stimulating discussions. I thank her for her patience and time. I would also like to thank Edmund Sternberg, Jun Sun, David Robinson for their help. I also have Deep Agnani at the Bentz lab and Shilpa Jain to thank for their support and comments.

I owe special thanks to Susan Cole for her help with meeting official deadlines and friendly advice during times of confusion. I thank Brenda Jones-Bowden, Rita Berson, Blanche Haughton at the Department of Bioscience who have made my life as a graduate student simpler and Heather Morin, Margaret Schnellen at GlaxoSmithKline for making my work as a visiting student scientist enjoyable.

Finally, I offer my deepest gratitude to my parents, brother and to Vilas, for their continual love, support and inspiration.

Poulomi

Thesis Outline

This doctoral thesis includes an Introduction and the following papers:

Paper 1

P-glycoprotein expressed in a confluent monolayer of hMDR1-MDCKI cells has more than one efflux pathway with cooperative binding sites.
Poulomi Acharya, Thuy T. Tran, Joseph W. Polli, Andrew Ayrton, Harma Ellens & Joe Bentz. Published in Biochemistry; 2006; 45(51) pp 15505 - 15519.

Paper 2

Kinetic identification of membrane transporters that assist P-gp mediated drug transcytosis in a confluent monolayer of MDCKII-hMDR1 cells.
Poulomi Acharya, Joseph W. Polli, Andrew Ayrton, Harma Ellens & Joe Bentz. Manuscript to be submitted to Drug Metabolism and Disposition.

Paper 3

For P-glycoprotein-like mediated transport through a confluent cell monolayer, the IC50 of a P-gp substrate depends upon the probe substrate kinetic parameters.
Joe Bentz, Poulomi Acharya, Joseph W. Polli, Andrew Ayrton and Harma Ellens. Manuscript to be submitted to Drug Metabolism and Disposition.

Table of Contents

List of Figures viii

Abstract xi

1. Diseases and Multidrug resistance 1

1.1 Membrane transporters and the ABC family 1

1.2 ABC transporters: bacteria to humans 1

1.3 Role of ABC transporters in diseases 2

1.4 Multidrug resistance 3

1.5 P-gp and MDR 3

2. Going back in time: Literature review of work done on P-gp 4

2.1 MDR: cellular physiology and biochemistry 4

2.1.1 MDR is associated with alterations in the karyotype 4

2.1.2 Characteristic features of MDR 4

2.1.3 Finding underlying reason for MDR 5

2.2 MDR: Molecular biology and mechanism 6

2.2.1 MDR is a dominant trait 6

2.2.2 Cloning of the MDR1 gene 6

2.2.3 Characterization of function 7

2.2.4 In vivo P-gp mediated drug resistance: 8

2.3 Expression of P-gp 8

2.3.1 P-gp in normal cells 8

2.3.2 P-gp in cancer cells 9

2.3.3 P-gp in internal membranes 9

2.3.4 Regulation of P-gp expression 9

3. New directions for P-gp research 11

4. P-gp: an enigma for years 12
4.1 Structural studies 12
4.1.1 Overall structure of P-gp 12
4.1.2 P-gp structures 13
4.1.3 Crystal structures of other ABC proteins 14
4.1.4 Canonical models for drug efflux by P-gp 16
4.1.5 Recent models for drug transport 17
4.2 Drug binding site of P-gp 18
4.3 Substrates and modulators of P-gp 21
4.3.1 Substrates: their structure and binding 21
4.3.2 P-gp Pharmacophore 22
4.3.3 P-gp modulators 23
4.4 ATPase reaction and efflux of substrates 24
4.5 P-gp function and its membrane environment 26
5. Kinetic studies 28
6. My Specific aims 31
7. Summary of research papers 32
7.1 Summary of Paper 1 34
7.2 Summary of Paper 2 36
7.3 Summary of Paper 3 37
8. References 39
9. Paper 1 55
10. Paper 2 116
11. Paper 3 156

List of Figures

4.1 Figure illustrating organization of transmembrane helices involved in drug binding 20

9.1 Paper 1: Table 1 - IC50 ranges for P-gp substrates. 96

9.2 Paper 1: Table 2 - Fitted Parameter Values with Single Substrate Experiments. 97

9.3 Paper 1: Figure 1 - Model of a confluent cell monolayer 105

9.4 Paper 1: Figure 2 - Inhibition of amprenavir transport by quinidine..... 106

9.5 Paper 1: Figure 3 - Passive permeability is time-dependent. 106

9.6 Paper 1: Figure 4 - Best fit values for efflux-active P-gp density and the rate of association to it. 107

9.7 Paper 1: Figure 5a - Quinidine transport inhibited by amprenavir : Competitive inhibition at high inhibitor concentrations. 108

9.8 Paper 1: Figure 5b - No inhibitor effect provides kinetic evidence for atleast two efflux pathways through P-gp. 109

9.9 Paper 1: Figure 5c - Quinidine transport inhibited by amprenavir : competitive inhibition at high substrate concentrations. 110

9.10 Paper 1: Figure 6a - Amprenavir transport inhibited by quinidine : no inhibitor effect. 111

9.11 Paper 1: Figure 6b - Amprenavir transport inhibited by quinidine : competitive inhibition at high inhibitor concentrations. 112

9.12 Paper 1: Figure 7a - Quinidine transport inhibited by loperamide : no inhibitor effect. 113

9.13 Paper 1: Figure 7b - Quinidine transport inhibited by loperamide : competitive inhibition at high inhibitor concentrations. 114

9.14 Paper 1: Figure 8 - Microvilli morphology plays an important role in the physiological activity of P-gp. 115

10.1 Paper 2: Table 1 - Fitted Parameter Values with Single Substrate Experiments 138

10.2 Paper 2: Table 2 - List of compounds tested to identify additional transporters for loperamide and digoxin. 141

10.3 Paper 2: Figure 1 - Cartoon model of a confluent cell monolayer. 147

10.4 Paper 2: Figure 2 - 10μM Loperamide transport data can be fitted using just P-gp parameters. 148

10.5 Paper 2: Figure 3 - 1μM loperamide needs a basolateral transporter. 149

10.6 Paper 2: Figure 4 - Loperamide only needs a basolateral transporter. 150

10.7 Paper 2: Figure 5 - Digoxin transport curve generated by measuring transport over consecutive stretches of 6 hours. 151

10.8 Paper 2: Figure 6 - Digoxin transport curve upto 30 hours. 152

10.9 Paper 2: Figure 7 - Digoxin is transported by a basolateral and an apical transporter, in addition to P-gp. 153

10.10 Paper 2: Figure 8 - Digoxin cell concentration exclusion by benzbromarone. ... 154

10.11 Paper 2: Figure 9 - There is no effect of 1μM benzbromarone on the transport of 1μM digoxin. 155

11.1 Paper 3: Figure 1 - Model of a confluent cell monolayer. 178

11.2 Paper 3: Figure 2 - Simulations show IC50 for an amprenavir-like substrate transport inhibited by quinidine-like inhibitor is 1 - 2μM. 179

11.3 Paper 3: Figure 3 - The fraction of substrate bound P-gp as a function of inhibitor concentration. 180

11.4 Paper 3: Figure 4 - Overestimation of $K_{I,Aq}$ by the IC50 as a function of average passive permeability into the cytosol. 181

11.5 Paper 3: Figure 5a - The concentration of substrate-bound P-gp as a function of inhibitor concentration. 182

11.6 Paper 3: Figure 5b - Fraction of substrate-bound P-gp as a function of inhibitor concentration. 183

11.7 Paper 3: Table 1 - Fitted Parameter Values[a] 184

11.8 Paper 3: Table 2 - IC50 values and Corrections to estimate $K_{I,Aq}$ 187

Abstract

Modeling the Transport and Inhibition Kinetics of the Human Multidrug Resistance Transporter P-Glycoprotein in MDCK-II Cells

Poulomi Acharya

Advisor: Dr. Joe Bentz

The human multidrug resistance transporter P-glycoprotein (P-gp) effluxes a wide range of substrates and can be affected by a wide range of inhibitors or modulators. Many studies have presented classifications for these binding interactions, within either the context of equilibrium binding or the Michaelis-Menten enzyme analysis of the AT-Pase activity of P-gp. Our approach is to study P-gp transport and its inhibition using a physiologically relevant confluent monolayer of hMDR1-MDCKII cells. We measure the elementary rate constants for P-gp efflux of radiolabeled substrates and study inhibition using pair wise combinations with a different unlabeled substrate acting as the inhibitor. Our current kinetic model for P-gp has only a single kinetically relevant efflux-connected binding site. We conclude that there are at least two kinetically distinct efflux pathways through P-gp and the binding sites connected to these pathways may not be exclusive for any drug. Binding of these substrates must be cooperative which can be either positive or negative based on the substrate-inhibitor pair. From the transport and inhibition of digoxin and loperamide, we found that other transporters are responsible for uptake of these drugs into the cells and for recycling them into and from the apical membrane once P-gp has pumped them out. Each drug has a particular IC-50 for inhibiting transport of another. Exhaustive computer simulations of drug transport in the presence of "virtual inhibitors" showed that the fitted IC50 values overestimate the intrinsic dissociation constant, $K_{I,Aq}$ and an equation showed that this overestimate is contributed by a convolution of cell and substrate parameters. The smaller the passive permeability of the substrate,

the greater is the magnitude of the overestimate of the inhibitor's dissociation constant by its IC50. These conclusions are valid for any membrane transporter whose substrates and inhibitors must pass a permeability barrier to reach their binding site on the transporter.

Part I - Introduction

1. Diseases and Multidrug resistance

1.1 Membrane transporters and the ABC family

Various solutes, nutrients, and ions move across cell membranes with the help of transporters, which constitute 15% to 30% of membrane proteins in a cell. Transport processes consume 60% of the energy in mammalian cells (Sauna and Ambudkar, 2007). Higgins et al. (1985) defined the ATP-binding cassette (ABC) superfamily of proteins. It represents one of the largest and most diverse groups of transport proteins (Dean et al., 2001). Approximately 1,100 different transporters belonging to this family have been described in the literature (Dean and Annilo, 2005). There are 80 ABC transporters in E.coli making up 2% of its genome (Dean et al., 2001). The importance of these proteins in membrane transport is indicated by the large number of ABC genes, their ubiquitous occurrence, and primordial origin (Gottesman and Ambudkar, 2001). Luckie et al. (2003) have compiled a list of human ABC genes, their chromosomal location, and function. Dr. Michael Dean at the National Cancer Institute has an exhaustive portal for genetic information on ABC genes and the proteins encoded by them (`http://theta.ncifcrf.gov/abc_central/index.php`).

1.2 ABC transporters: bacteria to humans

Most ABC proteins are integral membrane transporters, either importing or exporting their substrates, driven by the energy of ATP hydrolysis (Dean et al., 2005; Gottesman and Ambudkar, 2001). ABC exporters extrude diverse substrates, including drugs and xenobiotics, whereas ABC importers mediate the uptake of essential nutrients. The basic ABC transporter architecture consists of two transmembrane domains (TMDs) that provide a translocation pathway through the membrane, and two cytoplasmic, water-exposed

nucleotide-binding domains (NBDs) that hydrolyse ATP.

Some of the best-studied ABC exporters are the LmrA protein from Lactococcus lactis, Pdr5 in Saccharomyces cerevisiae and P-glycoprotein (P-gp) in humans. Bacterial ABC proteins are generally expressed as 'half-transporters' (e.g. LmrA) that contain one TMD fused to an NBD, which dimerize to form the full transporter (e.g. P-gp) in higher echelons of the animal kingdom (Holland and Blight, 1999). Functionally important residues are highly conserved among the NBDs, suggesting that ABC transporters share a common mechanism of coupling ATP hydrolysis to substrate transport (Holland and Blight, 1999). It has been shown that LmrA can substitute for the human ABC transporter, P-glycoprotein, in human lung fibroblast cells, suggesting that this type of efflux pump is conserved from bacteria to man (Van Veen et al., 1998; Zgurskaya et al., 2002).

1.3 Role of ABC transporters in diseases

Out of the 50 human ABC proteins, 17 are implicated in human diseases (Gottesman and Ambudkar, 2001). In humans, mutations in ABC transporter genes cause many genetic disorders which affect various organs directly or indirectly. These include but are not limited to Tangier disease (caused by mutations in ABCA1 also called cholesterol efflux regulatory protein or CERP), Stargardt disease (affects the eye caused due to mutations in ABCA4), Wegener's granulomatosis (immune system), Dubin-Johnson syndrome (liver, ABCC2), adrenoleukodystrophy (ABCD1), Pseudoxanthoma elasticum (ABCC6). Defects in CFTR (Cystic Fibrosis Transmembrane Regulator or ABCC7) cause Cystic Fibrosis. ABC proteins are involved in conferring multidrug resistance to several cytotoxins (antibiotics, antifungals, herbicides and anti-neoplastics) in cells: starting from bacteria (Poelarends et al., 2002) to humans (Higgins and Linton, 2004). In microorganisms, they confer resistance to antibiotics and other bacteriostatic compounds via export pumps like LmrA and Pdr5 (Van Veen et al., 2001).

1.4 Multidrug resistance

Multidrug resistance (MDR) is the phenomenon by which cells develop resistance to a wide variety of structurally and functionally unrelated compounds. Multidrug resistance is an alarming and rapidly growing obstacle in the treatment of infectious diseases, cystic fibrosis, human immuno-deficiency virus (HIV), malaria, and cancer. Drug-resistant bacterial strains that cause gonorrhea, pneumonia, cholera, and tuberculosis are widespread and difficult to treat (Ouellette et al., 2001). It has been estimated that 40% of all human cancers develop multidrug resistance, making it a major obstacle to the effective treatment of cancer (Sauna and Ambudkar, 2007). In humans, ABC transporters implicated in MDR are the breast cancer resistance protein (ABCG2), P-glcoprotein (P-gp or ABCB1) and multidrug resistance protein 1 (ABCC1).

1.5 P-gp and MDR

P-gp was first recognized as a major potential hindrance to successful chemotherapy because of its over-expression in malignant cells and was later realized to function physiologically in polarized epithelia. It is involved in the absorption, distribution and elimination of diverse classes of hydrophobic xenobiotics, drug molecules, environmental and dietary toxins (Senior et al., 1995; Lown et al., 1997; Schinkel, 1998; Goh et al., 2002; Gottesman et al., 2002). P-gp can mediate clinically relevant drug-drug interactions which can even lead to fatal systemic toxicity. The mechanism in which these interactions occur is of great interest. The general potential of MDR transporters in reducing the efficacy of many hydrophobic drugs, new and old, have made P-gp a target of intense investigation. It is a challenge for researchers to get an insight into the mechanism of action of this transporter. This is central to the development of newer therapeutic approaches in the treatment of several human diseases.

2. Going back in time: Literature review of work done on P-gp

Here I will attempt to trace the sequence of milestones in P-gp related research.

2.1 MDR: cellular physiology and biochemistry

In this section I will summarize the early work done trying to understand the underlying cause for the observed genetic, physiological and biochemical changes in MDR cells. In this respect it becomes important to define the MDR phenotype. Cells selected for resistance with one drug display significant cross-resistance to other drugs. This fairly consistent pattern of cross-resistance is termed the MDR phenotype. It is a dominant trait in which cells show increased efflux and hence less accumulation of xenobiotics and MDR reversing agents can inhibit this efflux.

2.1.1 MDR is associated with alterations in the karyotype

Kessel et al. (1968) isolated multidrug resistant Chinese Hamster Ovary (CHO) cells followed by the demonstration of cytogenetic abnormalities like random chromosomal rearrangements and DNA duplication in MDR cells. These results were consistent with gene amplification (Beidler and Riehm, 1970).

2.1.2 Characteristic features of MDR

Increased drug efflux, reduced drug accumulation and cross resistance to many compounds are constitutive features of MDR. Dano (1973) showed that there is increased daunomycin efflux (resulting in decreased accumulation) in MDR cell lines (Ehrlich ascites tumor cells) in presence of ATP. MDR cells depleted of ATP resulted in less efflux and more accumulation, Daunomycin efflux was inhibited by metabolic inhibitors and

structural analogs (N-acetyl daunomycin). These observations along with the fact that the accumulated steady-state level of daunomycin increased in the presence of Vinca alkaloids, to which the tumor cells were cross-resistant, led him to conclude that an energy-dependent carrier-mediated extrusion mechanism is involved and that the Vinca alkaloids competed with daunomycin. Ling et al. (1974) showed colchicine resistance is correlated to resistance to other drugs and reduced drug uptake. In the same year, they isolated CHO cells showing reversion of MDR phenotype. Subsequently, See et al. (1974) found that colchicine accumulation in cell lines derived from colchicine resistant CHO cells denoted the CH^R was energy dependent.

2.1.3 Finding underlying reason for MDR

Ling and Thompson (1974) studied initial rates of colchicine uptake under different conditions. Ling (1975) suggested that a global effect on the cell membrane (contributed by an active permeability barrier) must be the cause for the MDR phenotype. They proposed that a "modulator" of membrane lipid fluidity could be the basis for this, perhaps involving phosphorylation /dephosphorylation of membrane proteins. In the same paper, independent revertant clones selected in a single step from the two highly resistant lines (CH^R C5 and CH^R C4) showed that the MDR and the CH^R phenotype both co-reverted. This meant that the MDR phenotype is caused by alteration in a single gene. Note that the gene encoding P-gp was isolated a few years later as described in the following section.

Juliano and Ling (1976) found that P-gp is expressed in CH^R cell lines but not in wild type cells. Riordan and Ling (1979) purified a 170000 Dalton protein as a prominent Coomassie blue stained band from CH^R cells. They named the protein in the band P-glycoprotein (P-gp) because of its association with colchicine permeability. They showed that P-gp is localized in the plasma membrane in significant amounts (estimated to be 3-4% of total plasma membrane protein) in a highly colchicine-resistant line. The results

of this study led to the possibility that isolated plasma membrane vesicles could be used for *in vitro* drug uptake studies and that P-gp could be purified (once the gene was isolated and cloned) for reconstitution studies and used to raise antisera.

These and other observations about the cellular pharmacology in MDR cells led to an acceptance of the hypothesis that P-gp, an outward transport pump of broad specificity might be responsible for increased drug efflux in MDR cells that results in altered sensitivity to multiple drugs.

2.2 MDR: Molecular biology and mechanism

In the following section I will collate the findings that attempt to show that P-gp was the protein responsible for the MDR phenotype.

2.2.1 MDR is a dominant trait

Ling and Baker (1978) showed that MDR is a dominant phenotype using hybrid CHO cells in which colchicine resistance was dominant. Debenham et al. (1982) showed that genomic DNA from CH^R cells transfected into drug-sensitive mouse cells resulted in the expression of MDR phenotype. Since such a system retains very little donor DNA in the recipient cell and non-linked genes are not normally co-transferred, they concluded that both the CH^R and MDR phenotypes are the result of a mutation in a single gene or a small number of linked genes. This confirmed that MDR is a dominant phenotype.

2.2.2 Cloning of the MDR1 gene

Roninson et al. (1984) cloned gene fragments in CH^R cell lines selected with different drugs. Kartner et al. (1985) isolated monoclonal antibodies to P-gp. Riordan et al. (1985) used these antibodies to show that P-gp is encoded by a multigene family clustered in one amplicon in MDR mammalian cell lines. Van der bliek et al. (1986) showed that there

are 5 genes clustered in this amplicon and P-gp is encoded by one of them. Gros et al. (1986a) cloned the first mdr coding sequence and demonstrated a 5 kb mdr mRNA message in multidrug-resistant hamster cell lines. In the same year, the full-length MDR1 gene was cloned and its homology to bacterial ATP-dependent transporters was demonstrated (Gros et al., 1986b). Roninson et al. (1986) found MDR1 and MDR2 genes in a human nasopharyngeal carcinoma cell line. Ueda et al. (1986) showed that the MDR1 gene encodes P-gp.

2.2.3 Characterization of function

Functional assays in-vitro:

Gerlach et al. (1986) proposed that P-gp is an export pump based on similarities between 3' half of P-gp cDNA and Hemolysin B. Ueda et al. (1987a) created a full-length clone in a retroviral expression system and showed that individual transfectant cell lines were fully multidrug-resistant. This was the first evidence that P-gp by itself can confer properties related to MDR. Cornwell et al. (1986a) showed that membranes containing P-gp bound to vinblastine and they also performed photo affinity labeling of P-gp (Cornwell et al., 1986b). Horio et al. (1988) showed that P-gp in membrane vesicles transported drugs.

It was shown that verapamil (Tsuruo et al., 1981) and quinidine (Tsuruo et al., 1984) could overcome vincristine resistance by increasing cytotoxicity of vincristine in P388 leukemia cells, a vincristine resistant P388 cell line and also in mice harboring these cells. Hamada and Tsuruo (1988) purified P-gp to homogeneity by affinity chromatography and showed that it had ATPase activity. Ambudkar et al. (1992) reconstituted purified P-gp into vesicles and showed ATPase activity stimulated by vinblastine transport. It was shown that P-gp could catalyze transepithelial transport in both transfected (Pastan et al., 1988) and naturally occurring cell lines (Horio et al., 1989). This assay, using

dog, pig, or human kidney cells, is now a standard test for transport by P-gp and other ABC transporters in polarized epithelia. This is also used to study transport in P-gp overexpressing cells like CACO cells derived from human colonic adenocarcinoma.

2.2.4 In vivo P-gp mediated drug resistance:

Galski et al. (1989) showed that mice expressing MDR1 gene in bone marrow are resistant to daunomycin. Sorrentino et al. (1992) showed retroviral transfer of MDR1 in bone marrow cells conferred *in vivo* drug resistance. Schinkel et al. (1994) showed MDR1 knock out mice have blood-brain barrier defects and exemplify altered pharmacokinetics of drugs. This shows that P-gp is responsible for defending the blood- brain barrier, controlling drug absorption and facilitating proper disposition of drugs in normal animals. These findings are important because they are based on *in vivo* studies focusing on P-gp's native function and physiologically relevant effects of MDR. Thus, research for over 30 years has advanced from one milestone to the next finally demonstrating P-gp is an efflux pump of broad specificity providing the molecular basis for MDR both *in vitro* and *in vivo*.

2.3 Expression of P-gp

2.3.1 P-gp in normal cells

Thiebaut et al. (1989) studied the expression pattern of P-gp in normal tissues by immunohistochemistry. P-gp is expressed in a large number of cells like the biliary canalicular surface of hepatocytes, apical surface of columnar epithelial cells in intestine, brush border membrane of proximal tubule in kidney, sub-apical surface of choroid plexus epithelium, endothelial cells of blood brain barrier, microvillus border of syncytiotrophoblasts of human placenta, several leukocyte lineages, endothelium of blood vessels of the heart, pan-

creatic ductules and adrenal cortex (in males only). P-gp expression shows inter-individual variations. High levels of P-gp are expressed in brain, testes, uterus, skin and eye. P-gp is localized in both the olfactory epithelium and the endothelial cells that surround the olfactory bulb. It is also present in alveolar type I epithelium within human and rat lung tissue (Srinivas et al., 2006).

2.3.2 P-gp in cancer cells

Goldstein et al. (1989) showed that MDR1 was expressed at levels thought to be sufficient to confer MDR in many epithelial cancers derived from colon, liver, and kidney, in hematopoeitic cancers (Acute myeloid leukemia or AML, Acute Lymphoblastic Leukemia, lymphoma) and solid tumors (breast, ovary) that had relapsed after chemotherapy with P-gp-affected agents, and also appeared occasionally in cancer simply as a result of the transformation process. P-gp is also over expressed in lung and bone cancers. Noonan et al. (1990) performed RT-PCR to show widespread MDR1 expression in human cancers.

2.3.3 P-gp in internal membranes

P-gp is not only expressed on cell surfaces but also in membranes of cellular organelles. P-gp is expressed and functional on the luminal side of Golgi stack membranes and in small amounts in the endoplasmic reticulum of several MDR cell lines (Molinari et al., 1994). Moreover, P-gp has also been detected by immunogold labeling along the nuclear envelope in rat microglial cells (Lee et al., 2001), and in astrocytes (Ronaldson et al., 2004).

2.3.4 Regulation of P-gp expression

Regulation of P-gp expression has been studied by several groups. Ueda et al. (1987b) identified a 1-kilobase (kb) genomic fragment containing the major transcription initiation sites for the human MDR1 gene. The 0.43-kb region upstream from the major transcrip-

tion initiation site had a consensus CAAT box and two GC box-like sequences, but no TATA sequence. Scotto (2003) has reviewed the knowledge about the transcriptional control of ABC transporter expression levels. Transcription of MDR1 is regulated by an initiator or Inr element and transcription factors like NF-Y, members of the Sp family and Kruppel family. Tumor suppressors like p53 and oncogenes (e.g. Fos and Jun families) also control its transcription. Epigenetic induction of MDR1 expression by transient exposure to different chemotherapeutic drugs was demonstrated (Chaudhary and Roninson, 1993). However, the most convincing direct evidence to date, confirming selection for MDR1 expression occurs *in vivo* in human cancers came from Mickley et al. (1997) who have shown that rearrangements involving an upstream promoter frequently occur in drug-resistant cancers.

3. New directions for P-gp research

In recent times, researchers are moving onto study drug-transporter interactions and pharmacokinetics using micro-dialysis (Bouw et al., 2001), hepatocyte cultures in collagen gel mixture or between double layers of collagen in sandwich configuration called sandwich cultures (Annaert et al., 2001) and organ perfusion systems (Booth et al., 1998; Mls et al., 2005). These systems represent the invivo milieu more realistically than confluent cell culture models. Animal models (knockouts) (Cutler et al., 2006) and whole animal imaging techniques are also emerging since the ultimate goal is to understand the biology of the MDR phenomenon and develop ways to counter it in humans. Sasongko et al. (2005) have tried to image P-gp activity using C^{11}- verapamil as the substrate at the human blood brain barrier using positron emission tomography. This is a very powerful tool that enables us to visualize *in vivo* transport and its consequences. Silicon Chips (pioneered by Dr.Linda Griffith, MIT and Dr. Sangeeta Bhatia, UCSD) designed to grow liver cells in an *in vivo* environment are being tested to study transport.

4. P-gp: an enigma for years

4.1 Structural studies

4.1.1 Overall structure of P-gp

P-gp, the product of the human MDR1 gene is a 170kDa glycosylated integral membrane protein with two identical halves. Its 1280 amino acids are organized as two homologous halves that are joined by a linker region. Each half consists of a transmembrane domain (TMD) comprising of 6 transmembrane helices which together form the drug-binding site(s) and one nucleotide (ATP in this case) binding domain (NBD) which projects into the cytosol. Thus, P-gp has discrete NBDs and drug-binding sites and the protein is believed to perform two separate, yet coupled, functions: ATP hydrolysis and substrate transport. The nature of interaction between the transporter and its substrates still remains largely unknown.

TMD structure:

Each of the 12 membrane-spanning segments consist of 21 amino acids in length predicted to exist as an α-helix and are separated by six extra cellular hydrophilic loops, one of which is glycosylated. Among the transmembrane domains, Loo and Clarke (1999) demonstrated that TM6 and TM12 might be particularly important for drug transport because they directly connect the two transmembrane domains to their respective ATP-binding domains. Both transmembrane segments may interact and undergo essential conformational changes during drug binding or during ATP hydrolysis. There are intra-cytoplasmic domains or ICDs which are believed to relay events at the NBDs to the TMDs (Loo and Clarke, 2005b).

NBD structure:

Although the TMDs show little sequence homology, the NBDs of all ABC proteins show extensive amino acid sequence identity and conserved motifs. These include the Walker A and Walker B, common to most proteins that bind nucleotide, and the signature motif (LSGGQ motif, linker peptide, or C motif), which is diagnostic of ABC proteins (Loo et al., 2003). The Walker A motif (Gly-X-X-Gly-X-Gly-Lys-Ser/Thr-Ser/Thr) is a glycine-rich loop. Residues within this motif interact with the phosphate groups of the bound nucleotide complex. The Walker B motif is (H-H-H-H-Asp), where H is a hydrophobic residue. This sequence constitutes a buried β-strand within the core of the NBD (Smith and Rayment, 1996). The C motif (Leu-Ser-Gly-Gly-Gln-Gln/Arg/Lys-Gln-Arg) exists within each NBD of all the ABC proteins. This motif is located immediately next to the N-terminal of Walker B motif and is believed to be involved in interactions with the TMDs. The Walker A and Walker B motifs hydrogen bond extensively to the bound ATP. Walker B also contributes the catalytic base. In addition, they contain the D-loop, H-loop, and Q-loop and it has recently been proposed that a highly conserved A-loop (an aromatic residue 25 amino acids upstream of the Walker A) is also an integral part of the ABC core structure (Ambudkar et al., 2006a; Kim et al., 2006). These domains from each NBD interact to form dimers and the characteristic ABC structural motifs are critical in ATP binding and hydrolysis.

4.1.2 P-gp structures

Low-resolution structures of P-gp have been reported in Rosenberg et al. (1997) and Lee et al. (2002) by electron microscopy and more recently, in Lugo and Sharom, (2005b) based on FRET (Fluorescence Resonance Energy Transfer) studies. Rosenberg et al. (2003, 2005) have presented a three-dimensional structure for P-gp at $8\mathring{A}$ resolution obtained by cryo-electron crystallography of two-dimensional crystals. These structures have

the highest resolution for any eukaryotic ABC transporter and the first to show the organization of the transmembrane helices. Comparing nucleotide-analog-bound-P-gp with free P-gp it was seen that upon binding of nucleotide, the transmembrane domains reorganize into three compact structures that are each 2-3 nm in diameter and 5-6 nm in depth. This opens a central pore along its length, potentially facilitating movement of hydrophobic compounds from the lipid bilayer to the aqueous pore of the transporter. Fluorescence studies (Lugo and Sharom, 2005b) have led to the belief that the drug binding site is at the base of the central pore within the inner monolayer of the cell membrane. Since ATP-analog binding led to significant changes in the packing of TMDs within the membrane, it was proposed that ATP binding, rather than hydrolysis, drives the conformational changes associated with transport.

The vanadate trapped complex of P-gp displayed a different conformation, suggesting that rotation of TM helices takes place during the catalytic cycle. TM 4, 5, 6 in the N-terminal half, and TM 9, 10, 11, and 12 in the C-terminal half of P-gp line the drug binding pocket and rotation of helices 2/11 and 5/8 open and close as gates during drug binding according to Loo and Clarke (2005a). It has been shown that TM6 and TM12 can also undergo rotation or tilting during ATP hydrolysis (Loo and Clarke, 1997; 2001a). Moreover rearrangement of TM11 may contribute to the release of drug substrate during ATP hydrolysis (Loo and Clarke, 2005b; Loo et al., 2005)

4.1.3 Crystal structures of other ABC proteins

Recently, two multidrug resistance proteins, AcrB (2.8$\AA$ resolution), a principal multidrug efflux transporter in Escherichia coli (Murakami et al., 2006) and sav1866 (3.0$\AA$ resolution) from Staphylococcus aureus were crystallized. Both of these proteins export a wide variety of substrates.

AcrB structure:

The cystal structures of AcrB-drug complex consists of three forms, each of which has a different conformation corresponding to one of the three functional states of the proposed transport cycle. Bound substrates (minocycline and doxorubicin) were in the periplasmic domain of one of the three protomers indicated that the there is provision for multi-site binding. They found that the binding pocket is voluminous and lined by aromatic residues. Based on the structures it has been proposed that drugs are exported by a three-step helix rotating mechanism in which substrates gain access to the binding site, bind and are extruded. The shrunken drug binding pocket in the extrusion protomer led to the suggestion that the substrates are squeezed out through a channel in the membrane. The central α-helices seem to have an important role as a valve to open and shut the exit from the binding pocket. Opening and closing of gates to access the drug binding site/s by movement of transmembrane helices have been proposed for P-gp by Loo and Clarke (2005a). Since AcrB cooperates with an outer-membrane channel, TolC, and a membrane-fusion protein, AcrA, it is difficult to draw structural and functional homology to P-gp. No test of functionality was performed to ensure the structure could indeed export drugs.

sav1866 structure:

Sav1866 shows significant sequence similarity to human ABC transporters of the sub-family B that includes MDR1 (Dawson and Locher, 2006). From the sav1866 structure a scheme for transport of substrates has been proposed. An inward-facing conformation coincides with the substrate binding site being accessible from the cell interior, and an outward-facing conformation with an extrusion pocket exposed to the external medium. The structure reveals that tight interaction of the NBDs in the ATP-bound state is coupled to the outward-facing conformation of the TMDs. In this conformation, bound substrates may escape into the outer leaflet of the lipid bilayer or into the aqueous medium surround-

ing the cell, depending on their hydrophobicity. Hydrolysis of ATP is expected to return the transporter to an inward-facing conformation, again granting access to the binding site from the cell interior. It was proposed that ABC transporters may thus use an "alternating access and release" mechanism. The crystal structure is V shaped, the open face towards the extracellular side. The *in vitro* ATPase activity of the protein was found similar to that *in vivo*.

It should be noted that ADP, rather than ATP, was bound to the sav1866 crystal structure although the authors claimed that the NBDs in sav1866 exhibit the conformation of the ATP-bound state since the TMDs face outwards.

4.1.4 Canonical models for drug efflux by P-gp

The following models resulted from some of the early work done on P-gp and had formed the basis for understanding the mechanistic details of P-gp mediated drug efflux.

Hydrophobic vacuum cleaner model:

Raviv et al. (1990) showed that daunorubicin, when photoactivated, transferred energy to INA (iodonaphthalene azide, a non-specific, hydrophobic affinity probe) which specifically labels P-gp. Since INA is only present in hydrophobic regions of membranes, the interaction of daunorubicin with P-gp must have been within the plasma membrane. This resulted in the "hydrophobic vacuum cleaner" model of P-gp. In this model, drugs are detected and extruded from the lipid bilayer into an aqueous environment; thus, P-gp works like a phase separator that takes drugs from a hydrophobic environment and places them in an aqueous environment. This model was supported by transport experiments with fluorescent drugs (Bolhuis et al., 1996; Shapiro and Ling, 1997a, b, 1998; Shapiro et al., 1997) and more recently by EPR studies employing spin-labeled verapamil (Omote and Al-Shawi, 2002) in which ATPase activity and the movement of drugs from a hydrophobic

to a hydrophilic environment is monitored.

Lipid flippase model:

Higgins and Gottesman (1992) proposed the flippase model which is based on the resemblance of the drug transport process to lipid flipping. It proposes that drugs from the inner leaflet are flipped to the outer leaflet by P-gp, where they can diffuse into the aqueous environment around the cell, or bind to proteins such as albumin, present in medium. This idea is supported by substantial experimental evidence with fluorescent substrates (Sharom, 1997). The MDR3 protein, the product of the human ABCB4 gene is primarily expressed in the bile canalicular membrane of hepatocytes and acts as a phosphatidyl choline (PC) flippase translocating PC to the outer plasma membrane (Van Helvoort et al., 1996). It was shown that P-gp transported several short chain analogs of membrane lipids in transfected LLC-PK cells (Van Helvoort et al., 1996). The MDR3 protein displays 80% homology with P-gp and therefore it is possible that P-gp acts as a broad specificity flippase.

4.1.5 Recent models for drug transport

Omote and Al-shawi (2002) have conducted kinetic experiments using spin-labeled verapamil and purified P-gp in proteoliposomes. They measure the K_M, K_I for the drug and also measure activation of ATPase activity. Using EPR (Electron paramagnetic resonance) spectroscopy they tried to locate the movement of SL-verapamil in the membrane and also determined the concentration of SL-verapamil in the lipid and aqueous phases. They found that on addition of ATP, the external aqueous concentration of SL-verapamil was reduced and the lipid-bound component increased until steady state was achieved. In these studies, there is no direct evidence of P-gp mediated transport but by indirectly linking ATPase activity and movement of drug, they have tried to describe the transport

process. Al-shawi and Omote (2005) proposed a new drug transport model of P-gp from the results of mutagenic, quantitative thermodynamic and kinetic studies. The model advocated that drug binds first to a high-affinity loading site followed by ATP binding to the NBD. After passing through the high-energy transition state, drug is released to the other side of the membrane (successful transport). Different transport drugs lead to different energy levels of the rate-limiting coupling transition state (Al-Shawi et al., 2003; Omote et al., 2004). Omote and Al-Shawi (2006) suggest that most transported drugs can diffuse from the surface zone of the inner leaflet of the apical plasma membrane into the initial high affinity drug-binding site of P-gp through an open cleft. This is similar to but not identical to the drug entry "gates" proposed by Loo and Clarke (2005a) and observed in the two dimensional crystal of P-glycoprotein (Rosenberg et al., 2003). The mechanisms for binding of a broad range of substrates agree with Loo and Clarke's reported rotation of helices 6 and 12 by ATP hydrolysis based on the cross-linking experiments (Loo and Clarke, 2001a). Omote and Al-Shawi (2006) proposed that a "solvation" exchange mechanism involving dehydration and rehydration of substrates is responsible for P-gp mediated drug transport.

4.2 Drug binding site of P-gp

P-glycoprotein substrates generally partition into the lipid bilayer due to their hydrophobicity. Partitioning of drugs into the lipid bilayer is a requirement for transport and is a major determinant of the apparent K_M of the drug molecule and activation of transport by P-gp. This was the outcome of work by various groups (Shapiro and Ling, 1995; Romsicki and Sharom, 1999; Seelig and Landwojtowicz, 2000). Several groups have localized the drug-binding sites of P-gp to the cytoplasmic membrane leaflet (Shapiro and Ling, 1997a, 1998; Ferry et al., 2000; Qu and Sharom, 2002; Lugo and Sharom, 2005a).

Photo-reactive drugs label the transmembrane domains 3, 4, 5, 6, 7, 8, 11 and 12 of

P-glycoprotein (Greenberger et al., 1991; Pleban et al., 2005). In addition, mutations in one face of TM 5, 6, 11 and 12 change substrate specificity (Loo and Clarke, 1993; Ambudkar et al., 1999). Choi et al. (1988) also showed that point mutations change the substrate specificity of P-gp which means individual residues are crucial for recognition and binding. Loo and Clarke (1997, 1999, 2000, 2001a, 2003, 2005a; Loo et al., 2005) have used Cysteine scanning mutagenesis and cross-linking agents to map the drug binding sites of P-gp. Their studies revealed that the drug-binding site is formed by the TM regions of both halves of P-gp, especially TM4, TM5, and TM6 in the N-terminal half, and TM9, TM10, TM11, and TM12 in the C-terminal half (Loo and Clarke, 2005b). These studies reveal the important amino acids involved in substrate binding since binding is altered when these crucial residues are mutated.

Recent work suggests that the drug-binding sites of P-gp lie in a large funnel-shaped "binding pocket" with overlapping sites formed by multiple helices from both TMDs (Loo and Clarke, 2001b, 2005a; Loo et al., 2004; Sauna et al., 2004; Ambudkar et al., 2006b). It is narrower at the cytoplasmic side, where TM2-TM11 and TM5-TM8 come together (Loo and Clarke, 2005a). It may lie at the interface between the N- and C-terminal halves of the protein (Pleban et al., 2005). In the sav1866 crystal structure described above, the open end of the "V" faces the extra cellular side in absence of substrate or ATP. P-gp on the other hand has the structure of an inverted "V" the open end facing the cytosol. The nucleotide analog bound-P-gp, has a large central water filled pore through the protein which can be compared to the "V" of the sav1866 structure. Several fluorescence based methods have been used to measure drug binding affinity and stoichiometry. These include covalently attached fluorophores, intrinsic Trp fluorescence, fluorescent nucleotides and drugs. Binding affinity for several drugs have been estimated based on MIANS (2-(4'-maleimidoanilino)-naphthalene-6-sulfonic acid) fluorescence quenching by drugs and/or ATP (Sharom, 1997). Shapiro, Ling, and Sharom have been proponents of two functionally

distinct drug binding sites which interact allosterically in complex ways (Shapiro et al., 1997; Shapiro and Ling, 1997b, 1998; Lugo and Sharom 2005a, b). They are named as the R-site, which interacts preferentially with rhodamine 123, and the H-site, which interacts preferentially with Hoechst 33342. These sites were reported to be in the hydrophobic membrane environment (Qu and Sharom, 2002; Lugo and Sharom, 2005a). In Lugo and Sharom (2005a) it was reported that LDS-751 and R123 bind to different overlapping regions, or minipockets, within the large flexible R site. It is not clear whether the putative drug binding sites, H and R, are distinct from one another because they both have been localized within a few angstroms of the membrane-cytosol interface.

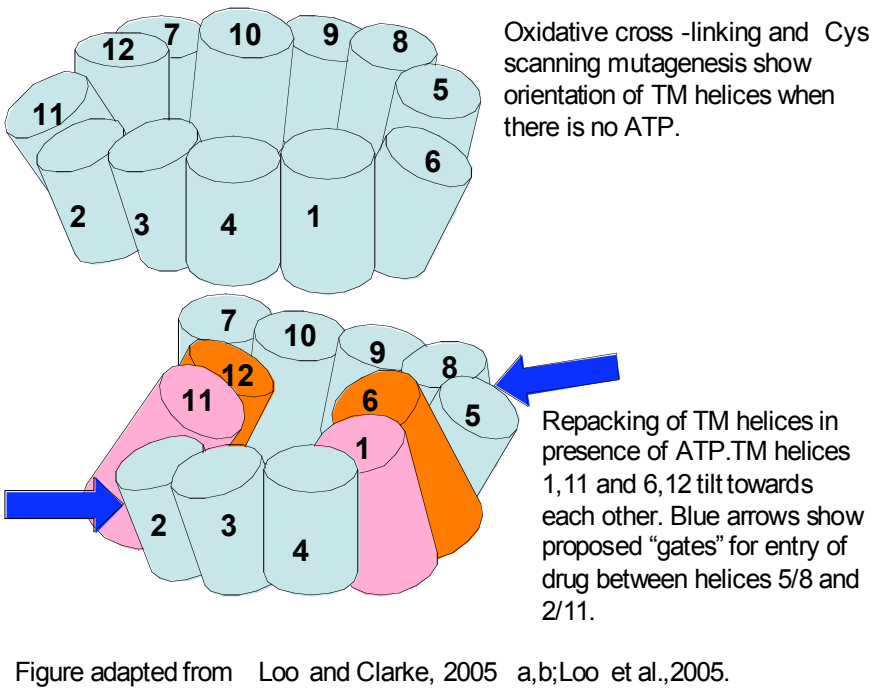

Figure 4.1: Figure illustrating organization of transmembrane helices involved in drug binding

As mentioned above, suggestions about many separate drug-binding sites with overlapping specificities exist but the current consensus is that there is a single, large, flexible drug-binding pocket. Drugs are believed to interact with the amino acid residues that line this pocket by an "induced-fit" type of mechanism, involving multiple Van der Waals and hydrophobic interactions which can be different for each compound (Loo et al., 2003).

The transport pathway of P-gp is initiated by the binding of drug and/or ATP. It is largely believed that the drug binds to the protein at an inward (cytoplasmic) facing high-affinity site and is expelled via a conformational change that transforms it to a low-affinity outward (extra cellular) facing site (Loo and Clarke, 2005b). Homology modeling, molecular dynamics simulations and, quantitative structure activity relationship (QSAR) studies are evolving into useful ways of understanding structure activity relationships of P-gp (Srinivas et al., 2006).

4.3 Substrates and modulators of P-gp

4.3.1 Substrates: their structure and binding

P-gp seems to have an exceptionally broad specificity for structurally dissimilar compounds (Borst & Elferink, 2002; Gottesman, 2002; Ambudkar et al., 2003). P-gp substrates include but are not limited to neutral or cationic cytotoxic drugs and metabolites. Examples of P-gp substrates are anthracyclines, vinca-alkaloids, epipodophyllotoxins, taxol, colchicine and actinomycin D, steroid hormones, cyclic and linear peptides, fluorescent dyes, lipids, immunosuppressive agents, and calcium channel blockers (Holland and Blight, 1999). A comprehensive list of P-gp substrates, inhibitors/modulators/inducers are available at the transporters database (source: `http://www.tp-search.jp/`). A majority of these compounds were identified indirectly by resistance to cytotoxicity in cells that over express P-gp. Sparreboom et al. (1997) have shown that P-gp reduces the

oral availability of amphipathic drugs, e.g., Taxol. Likewise, most substrates are weakly amphipathic and relatively hydrophobic; many (but not all) contain aromatic rings and a positively charged tertiary N atom. The positive charge is often associated with 2 to 3 characteristic hydrogen bond acceptors arranged in a fixed spatial separation (Seelig, 1998; Ecker et al., 1999; Cianchetta et al. 2005).

4.3.2 P-gp Pharmacophore

A pharmacophore is the ensemble of steric and electronic features which define the molecular framework within the active site of P-gp in 3D space based on its ability to interact with substrates of known structures. A pharmacophore does not represent a real molecule or a real association of functional groups, but a purely abstract concept that accounts for the common molecular interaction capacities of a group of compounds (substrates, modulators, inducers etc) with the active site. Typical pharmacophore features are based on where a molecule is hydrophobic, aromatic, a hydrogen bond acceptor, a hydrogen bond donor, a cation, or an anion. Pharmacophores provide conceptual templates for designing new drugs and probing the active site of a protein where these drugs interact.

Seelig (1998) presented a basic pharmacophore model for P-gp substrates, inducers and inhibitors using 100 compounds from literature. According to this study there are two pharmacophore models. Type I is two electron donor groups separated by 2.5±0.3 $\mathring{A}$. Type II contains two electron donors separated by 4.6±0.6 $\mathring{A}$, possibly with a third electron donating group between the other two. All the compounds with at least one of these features were found to be substrates. Most of them contain at least two of these pharmacophores, some contain as many as eight. Inducers were found to contain at least one Type II pharmacophore but some also contain multiple Type I pharmacophores.

Wiese et al. (2001) proposed an alternate pharmacophore model for a variety of P-

gp substrates. This study was based on a highly diverse data set and relates to the verapamil-binding site of the protein. This model consists of two hydrophobic points, three hydrogen bond (HB) acceptor points and one HB donor point. In a P-gp substrate recognition study of 129 diverse compounds by 3D-QSAR, a new pharmacophoric feature emerged. The recognition elements were two hydrophobic groups 16.5 $\AA$ apart and two hydrogen bond acceptor groups 11.5 $\AA$ apart and the dimensions of the molecule also played a role in substrate recognition (Cianchetta et al., 2005).

4.3.3 P-gp modulators

It has been shown that certain compounds, known as modulators (also called chemosensitizers, reversers, or inhibitors), are able to reverse MDR in intact cells by blocking the drug efflux activity of P-gp (Tan et al., 2000). Most modulators which are structurally similar to transport substrates appear to bind to P-gp at the substrate-binding pocket, and compete with them in a complex fashion. Indeed, many modulators, including verapamil and cyclosporine A, are known to be transported by P-gp. P-gp modulators also belong to many different structural classes, and have molecular features similar to transport substrates (Wiese and Pajeva, 2001). Drugs and modulators have been shown to affect P-gp ATPase activity (Borgnia et al., 1996). Pascaud et al. (1998) worked on ATPase activities of membrane vesicle suspensions and have shown that P-glycoprotein has distinct but interacting binding sites for various modulators of its ATPase function. Clinically, co-administration of modulators with drugs has the potential to improve uptake in the gut and delivery to the brain as well as to increase the cytotoxicity of anticancer drugs to tumor cells. Clinical trials showed survival advantage for patients with Acute Myeloid Leukemia or AML treated with MDR inhibition plus chemotherapy (List et al., 2001). This might help in overcoming the challenge of selectively targeting malignant cells without toxic repercussions on the surrounding normal cells. Several promising

third-generation modulators are already being used in clinical trials (Modok et al., 2006).

4.4 ATPase reaction and efflux of substrates

The biochemistry of the ATPase reaction of human, mouse, and hamster P-gp have been studied since the early 1990s, and these studies have been extensively reviewed (Al-Shawi and Senior, 1993; Borgnia et al., 1996; Senior et al., 1998; Omote and Al-Shawi, 2002).

It has been a long drawn challenge to understand the events at the NBDs leading to substrate efflux. It was shown that there is a very high basal (in the absence of any added transport substrates) ATPase level (3-5 mmol/min/mg of protein) in purified P-gp (Al-Shawi and Senior, 1993; Urbatsch et al., 1994). This has usually been ascribed to the presence of an unidentified endogenous transport substrate or to lipids being flipped in purified preparations (Borgnia et al., 1996; Romsicki and Sharom, 2001; Druley et al., 2001). In their quest to understand the mechanism of coupling of ATP hydrolysis to transport, Urbatsch et al. (1995) used orthovanadate to trap P-gp in the post-ATP-hydrolysis transition state.

Following this, many groups have focused their research on the ATPase activity of P-gp particularly trying to find out which step in the ATP binding and hydrolysis cycle provides the "power stroke" for transport and several theories have been proposed. Ramachandra et al. (1998) found that P-gp shows reduced affinity for photo affinity analog of drug-substrate in the Vi trapped transition state and proposed its use to monitor conversion of high affinity "ON" site to a low affinity "OFF" site. They proposed that ATP hydrolysis was needed to power transport and restore ability of P-gp molecule to bind substrate. Hrycyna et al. (1999) proposed that P-gp mediated ATP hydrolysis could be used both for transport and to 'reset' P-gp conformation. Rosenberg et al. (2001) supported the latter. It has been suggested that ATP binding rather than ATP hydrolysis provides

the power stroke (Higgins and Linton, 2004; Al-shawi and Omote, 2005; Loo and Clarke, 2005a, b). The stoichiometry of ATP binding (and/or hydrolysis) during one catalytic cycle has been under investigation for a long time. Senior et al. (1995), suggested that P-gp operates by alternating-sites mechanism, in which only 1 catalytic site can be in the transition state at any instant in time and the 2 sites alternate in catalysis. The energy from ATP hydrolysis has been proposed to drive drug transport via relaxation of a high-energy intermediate, with 1 ATP hydrolyzed for each drug molecule translocated (Senior et al, 1995). Senior et al. (1998) proposed that there is cooperativity between the ATP binding sites. It is known that P-gp binds and hydrolyses ATP molecules at two steps during each transport cycle (Sauna and Ambudkar, 2000). Ambudkar et al. (2006b) support that 2 molecules of ATP are hydrolyzed per cycle, the first to transport the substrate molecule, the second to "re-set" the protein for another round of transport. Thus the estimate ranges from 1-2 and still remains the centre of ongoing research and intense debate.

Crystal structures of isolated NBD subunits or domains from diverse transporters have been visualized as symmetric dimers with two molecules of ATP bound at the NBD dimer interface (Chen et al., 2003; Hopfner et al., 2000; Smith et al., 2002; Zaitseva et al., 2005a). FRET studies using fluorescent probes attached to the Walker A Cys residues, are compatible with the sandwich dimer model (Qu and Sharom, 2001). Biochemical studies of isolated NBDs have identified dimer species with 2 mol of nucleotide bound per dimer for P-gp (Horn et al., 2003; Janas et al., 2003; Moody et al., 2002; Verdon et al., 2003; Zaitseva et al., 2005b). However the "occluded" state contains only 1 mol ATP/mol P-gp (Tombline et al., 2005). Sauna and Ambudkar (2007) have proposed after loose binding of 2 ATP molecules, the sandwich dimer forms, and the tightly bound nucleotide is then committed to hydrolysis and rapidly enters the transition state.

Ambudkar et al. (2006b) proposed a general sequence of events: ATP binding at 2

NBDs causes the formation of NBD sandwich dimer followed by asymmetrical occlusion of ATP from one NBD which causes conformational changes in TMDs which in turn results in a switch from high affinity to low affinity for the substrate. Finally, the occluded ATP is hydrolyzed and the transporter is reset to its original conformation. Higgins and Linton (2004) have drawn analogy to several other ABC transporters and have suggested that cooperative ATP binding and hydrolysis can enhance the kinetics for closed dimer formation and its subsequent dissociation to the open conformation. This means that ATP hydrolysis per se drives the thermodynamic destabilization of the nucleotide sandwich dimer and enables the pump to "reset". Experimental evidence is yet to be obtained to support any one of these hypotheses.

Understanding the coupling between ATP hydrolysis and drug transport would require high resolution structures of intact P-gp including both the NBDs and the TMDs captured in the ground state and various intermediate steps during the catalytic cycle.

4.5 P-gp function and its membrane environment

The membrane lipid phase provides the hydrophobic environment to integral membrane proteins like P-gp, and has a profound impact on their functional activity. Among the membrane enzymes and transporters, P-gp is highly sensitive to its lipid environment (Sharom, 1997) because of the fact that P-gp recognizes its transport substrates within the bilayer. Romsciki and Sharom, (1998) have shown that when P-gp is reconstituted in gel phase lipid, the Michaelis constant for ATP is lower than in liquid-crystalline lipid. Romsciki and Sharom, (1999) found that binding of vinblastine, daunorubicin and verapamil presents a 2- to 4- fold higher affinity in gel phase lipid than in liquid-crystalline lipid. There is more transport of tetramethylrosamine, a P-gp fluorescent substrate, in the rigid gel phase possibly due to better binding of drugs to the gel-phase, not because of changes in P-gp function per se. In cells, lipid heterogeneity can complicate the relationship between

P-gp function and the membrane environment (Orlowski et al., 2006).

5. Kinetic studies

More often than not, several groups have studied the kinetics of the ATPase activity of P-gp in presence and absence of substrates and the results of these studies have been used to conclude about transport. Binding of drugs to P-gp and their transport have been studied using purified and reconstituted P-gp in inside-out plasma membrane vesicles or proteoliposomes (Shapiro and Ling, 1997a, b; Shapiro et al., 1997; Sharom and Eckford, 2003; Lugo and Sharom, 2005a, b; Loo and Clarke, 2005b). Some groups have used cells in suspension (Ayesh et al., 1996) or unpolarized adherent cells over-expressing P-gp (Spoelstra et al., 1994; Seelig and Gatlik-Landwojtowicz, 2005). Commonly fluorescent (Shapiro and Ling,1997a, b, 1998; Shapiro et al., 1997; Lugo and Sharom, 2005a, b) or radiolabelled substrates (Ayesh et al., 1996) are used to quantify binding or transport. I will summarize the salient findings derived from studies on some of these systems.

Wang et al. (2000) measured the rate of phosphate release for ATP hydrolysis during Hoechst transport in presence of different concentrations of other substrates in membrane microsome preparations (derived from a drug resistant cell line) containing P-gp. Change in fluorescence of substrates was monitored and this was correlated to their movement between aqueous and lipid phase but this was a separate experiment and there was no way to correlate transport to ATPase activity. They performed graphical kinetic analysis (Lineweaver Burk, Dixon, Cornish Bowden plots) to determine K_M, Vmax, K_I for the substrates tested. The aim was to determine the inhibition type and hence characterize the modes of interaction of substrate pairs at the transport site(s). They reported that P-gp has two unequal sites and drug binding at one site precludes, or lowers the affinity for binding at the other site. There was no definite proof of binding to P-gp or transport by P-gp per se. There was no way to distinguish ATPase activity due to transport of

Hoechst from that due to transport of other substrates.

Omote and Al-shawi's kinetic experiments using spin-labeled verapamil are explained earlier. For many years, Sharom and associates have used purified P-gp reconstituted in proteoliposomes and employed biochemical and fluorescent spectroscopic techniques to measure transport into the proteoliposomes. They showed that P-gp mediated transport is a saturable process, generating 6 to 8 fold substrate concentration gradient and is inhibited by other drugs and modulators. This was quite remarkable. However, there are are a few caveats of using this system. It is difficult to generate and measure transmembrane drug gradients with proteoliposomes in solution. Furthermore, the hydrophobicity of the drugs could lead to nonspecific binding with lipids within the encapsulated volume of the proteoliposomes causing low signal to noise ratios. In Lu et al. (2001) a high affinity fluorescent substrate tetramethylrosamine (TMR) was used to monitor real time transport in proteoliposomes containing reconstituted P-gp. TMR accumulates in the aqueous phase within the lumen of the proteoliposomes. This means that the nonspecific binding to the lipids within the encapsulated volume, as explained before, was not an issue. The TMR concentration gradient generated by P-gp was collapsed by the addition of the ATPase inhibitor, vanadate, or P-gp modulators. Michaelis Menten constants for ATP binding and hydrolysis during TMR transport were compared to those in presence and absence of ATPase inhibitor or P-gp modulators. TMR transport was inhibited in a concentration-dependent fashion by verapamil and cyclosporin A, and activated (probably by a positive allosteric effect) by the transport substrate colchicine. For membrane transporters like P-gp whose substrates reside in the inner monolayer of the apical membrane, the Michaelis Menten analysis cannot yield the correct K_M because of convolution of substrate passive permeability parameters into the calculated K_M (Bentz et al., 2005). Therefore the Michaelis Menten analysis peformed in these studies is not an accurate way to explain the mechanism of efflux.

Transport of drugs are studied in confluent cell monolayers but only single time point measurements are taken and efflux ratios are calculated in either direction (Rautio et al., 2006). Single time point data cannot be used to find best-fit values for kinetic parameters. Continous time course measurements for transport are needed to quantitate the best fit estimates for the elementary kinetic parameters that govern the mechanism of efflux.

6. My Specific aims

The experimental aims of this thesis were designed to gain better insight into the molecular mechanism of drug efflux by the human multidrug resistance transporter P-gp. The kinetics of drug efflux and inhibition were studied using a robust kinetic model for transport in a physiologically relevant cell culture system. This has led to a better understanding of the structure-function relationship underlying the extrusion of a wide variety of xenobiotics by this much-studied and clinically relevant membrane-associated transporter protein. The specific aims are:

1. Generate consensus fits for elementary rate constants for association to, dissociation from and efflux by P-gp in addition to its functionally-relevant density on the membrane. This will help us explain the fundamental rules of operation for this transporter.

2. Determine the number of independent efflux-connected drug binding sites/pathways in P-gp by studying the kinetics of inhibition using two P-gp substrates.

3. Understand the nature of cross talk between the drug binding sites/efflux pathways. This will enable us to predict functionally relevant interactions within in the protein.

4. To find out if and how the presence of putative basolateral and apical transporters in addition to P-gp, contribute to uptake and recycling of substrates in the cells.

5. Deconvolve the contribution of substrate and cell-related parameters in understanding the relation between the IC50 values generated from the inhibition studies and the aqueous dissociation constant of the inhibitor.

Once we can accomplish these, we would be one step ahead in unraveling the physiological basis of the multidrug resistance phenomenon.

7. Summary of research papers

Having presented the context and goals for our research, I embark on the journey of telling a story about the structure and function of this intriguing protein that I have been trying to put together for the past few years. A consensus understanding of P-gp is that there are multiple substrate/inhibitor/modulator binding sites within the large binding pocket in the inner apical monolayer (Lugo and Sharom, 2005a; Loo and Clarke, 2005b).

The main theme of the work presented here is to understand the salient features of the P-gp mediated transport process. We apply the most rigorous kinetic analysis to the transport and inhibition kinetics data obtained from the most physiologically relevant P-gp expression system with the hope that the basic operating mechanism of this transporter *in vivo* can be explained.

A confluent monolayer of **M**adine **D**arby **C**anine **K**idney (MDCK)-II cells constitutively over-expressing the human MDR1 gene that encodes P-gp in the apical plasma membrane is used to measure transport of substrates radiolabeled with tritium or C^{14} over a period of 6 hours. The cells are grown in Transwell plates with a polycarbonate membrane insert which serves as basement membrane for the cells to attach and grow. It is a more complex expression system to analyze than conventional studies on re-constituted systems like proteoliposomes, membrane vesicles, suspension cells or unpolarized adherent cells. It has the advantage of studying P-gp in a tissue-like bed of cells which mimic the *in vivo* environment, without the uncertainties of how purification and reconstitution affect function.

To start with, transport experiments were done using amprenavir (HIV protease inhibitor which doesn't show saturation during P-gp mediated transport), quinidine (Na+ channel blocker and prototype drug which has clinical relevance) and loperamide (an-

tidiarrheal agent which showed 50% loss during transport).

Inhibition of P-gp mediated drug transport was studied using pair-wise combinations of two substrates which had simultaneous access to P-gp. One of them is radiolabelled and therefore acts as the substrate and the other one is unlabelled and thus acts as the inhibitor-substrate. The radiolabelled drug can be added to either the basolateral or the apical chamber and active transport is measured in both directions. To measure passive permeation, P-gp is inhibited by a potent inhibitor GF120918 and trans/paracellular movement of substrates is measured in either direction. The difference helps us quantify the amount of P-gp mediated efflux and inhibition.

The data for the transport and inhibition experiments are subjected to a hierarchical fitting algorithm which generates best fit values for each elementary rate constant for association to, dissociation from and efflux by P-gp for all concentrations of a particular drug along with the efflux-active P-gp density. The details of the kinetic model are published in Tran et al. (2004, 2005).

At this point I would like to briefly discuss a hurdle we faced while trying to identify additional transporters contributing to flux of Loperamide and digoxin. It is generally believed that membrane transporters mediate the transcytosis (efflux and uptake) of compounds across the epithelial cells of the colon, kidney and liver, and across the endothelial cells of the blood brain barrier, it has proven very difficult to identify which transporters are involved *in vivo* (Lau et al., 2006). Over expression (based on increased mRNA) of a particular transporter in a model cell line can identify its substrates and inhibitors (Dresser et al., 2001; Shitara et al., 2006), but the extension of this knowledge to a physiological model system which shows how the transporters function together has been lacking. This issue serves as a backdrop for the third chapter. Kathleen Giacomini and her group had worked extensively on the pharmacogenomics of organic anion and organic cation transporters/transporting peptides and hence we chose the compounds primarily based on her

research, (Dresser et al., 2001). There is not much information available on dog kidney transporters and therefore we based our search on known transporters in mammalian (rat, mice and human) cells.

Now that the basic premise and experimental set up for the experiments and analysis is explained, I will summarize the highlights of each chapter in this thesis which has been (or will be) submitted as an original research paper.

7.1 Summary of Paper 1

The first chapter attempts to evaluate the number of functional binding sites and efflux pathways in a complex protein like P-gp and to explore the nature of the communication between them. The fits from transport of amprenavir, quinidine and loperamide could explain some of the key characteristics of P-gp function.

The same fitted value for the surface density of efflux active P-gp for all three drugs, validated the fitting algorithm. The association rate constant of drug into the P-gp binding site, is lipid lateral diffusion controlled, which agrees with the drug binding site being a large open vestibule in the inner apical membrane monolayer as suggested by structural studies. A large association rate constant requires rapid dissociation back into the membrane, for P-gp to maintain relatively weak binding for a very broad class of substrates. In other words, for every substrate molecule pumped out, several thousands of them return to the monolayer.

P-gp protects the cell against the cytosolic build-up of harmful compounds by maintaining an efflux rate much faster than the rate of dissociation of the substrate from the inner apical monolayer back into the cytosol. Substrates must be amphipathic and therefore have large membrane/water partition coefficients to bind to P-gp within the membrane in the first place. Amongst all the substrates binding to P-gp, only the one bound at the moment when the ATP binding step is accomplished (Al-shawi and Omote,

2005; Loo and Clarke, 2005), is the one which gets effluxed.

To probe the number of kinetically functional efflux pathways we conducted inhibition studies using pairwise combinations of substrates. These have shown that there is competitive inhibition with high concentrations of either a substrate or an inhibitor. The elementary rate constants fitted independently for each of the substrates alone quantitatively predicted the efflux curves assuming that binding at the "one site" was competitive. This is a strong validation of our kinetic model and fitting algorithm. Remarkably, at low concentrations of either the substrate and/or the inhibitor, we found no inhibition of the substrate efflux, despite the fact that there was substantial efflux of the inhibitor. This provides the first quantitative proof that the substrate and the inhibitor are being extruded by multiple pathways through P-gp. Increasing the substrate concentration above the "low" concentration caused the inhibition to become competitive, i.e. the inhibitor became more effective. These results indicate that there are atleast 2 efflux pathways through P-gp. There was no reason to believe that the efflux-connected binding sites and pathways through P-gp are exclusive for any substrate. A rigorous analysis of a two site binding model shows that binding of these substrates must be cooperative, either positive or negative, based on the substrate-inhibitor pair.

We found that the density of efflux active P-gp, and the steady state passive permeability coefficient for all three substrates is about 2-3 times larger than those reported in Tran et al. (2004). Preliminary simulations testing the probability of escape of a substrate after efflux predicted that only substrates released at the tip of the microvilli on the apical membrane will have a reasonable chance of diffusing directly into the apical chamber. In our assay only those molecules which appear directly in the apical chamber are counted and this count is attributed to transport mediated by efflux-active P-gp or passive permeability. Since the changes we see occur within the time scale of membrane recycling, we hypothesized that change in microvilli dimension/morphology would affect the probability

of direct escape and, hence, the number of efflux active P-gp and the membrane area for passive permeability. This implies that cells in culture do change and the result we observe is really an example of the analytical power of our kinetic analysis to detect them.

7.2 Summary of Paper 2

For all concentrations of loperamide transport, we did not get consensus fits for the elementary rate constants (Tran et al., 2005; Acharya et al. 2006). The low concentrations showed there was more transport than could be justified by setting efflux rates for P-gp to infinity. This led us to believe that transporters other than P-gp contribute to loperamide transport in the MDCK-hMDR1 cells. As the first step to evaluate this possibility, additional transporters were modeled to compensate for the difference in the nmoles transported by P-gp alone and the data. Based on this approach, we found kinetic evidence that there is a basolateral transporter that helps loperamide get into cells much faster than possible by its passive permeability.

We moved onto studying transport and inhibition of a clinically relevant P-gp substrate digoxin (treats cardiac arrhythmias) which did not yield any fits at all. Digoxin has a very slow passive permeability compared to quinidine, yet is a good inhibitor of quinidine transport. This suggests that additional transporters help digoxin enter cells so that it can compete with quinidine during transport. Using the same approach as before, we found that a basolateral transporter causes digoxin uptake into cells and an apical transporter helps it re-enter cells from the receiver side. Each of these transporters is fully inhibited by GF120918 which necessitates using specific inhibitors to identify them.

In order to experimentally prove the presence and identity of these additional transporters, we have attempted to screen members of the Organic anion/cation family of transporters (Shitara et al., 2006) using more than 10 different compounds (good substrates/inhibitors) for digoxin and loperamide inhibition experiments. This has resulted

in no direct hits for OCT, OAT, OATP, URAT or MRP families of membrane transporters. However this enables us to narrow down the list of possibilities. A future direction is to find out whether loperamide and digoxin use the same or different basolateral transporter. We also tried the typical cell concentration exclusion assay which shows benzbromarone selectively inhibits digoxin accumulation but has no effect on the transport of digoxin. The simplest hypothesis for explaining this is that benzbromarone reduces the cell's cytosolic volume, so less digoxin can accumulate, which would have no necessary change in transport of digoxin, since it passes through the inner monolayer of the plasma membrane. This suggests that cell concentration exclusion assays must be carefully controlled when used with amphiphilic compounds effluxed from a transporter whose binding sites are within the plasma membrane, like P-gp.

7.3 Summary of Paper 3

The inhibition experiments showed that all combinations of substrate-inhibitor pairs showed substantial inhibition of substrate transport and at concentrations near the IC50 (concentration of inhibitor that reduces drug transport by 50%) the inhibition between substrates was simply competitive. For membrane transporters like P-gp, whose drug binding site resides in the lipid bilayer, we suspected that the membrane may act as a permeability barrier for the binding of drug since the drug is initially added in the extra cellular space. Therefore passive permeability through the plasma membrane may affect the correlation between the inhibitor's dissociation constant with respect to water ($K_{D,Aq}$) and its IC50.

Our objective was to delineate the contribution of the substrate parameters that could be convolved with the IC50, as was shown to be the case for the K_M when the Michaelis-Menten equations are used to analyze P-gp transport (Bentz et al., 2005). To address this issue, simulations of substrate transport in the presence of "virtual inhibitors" based on

the elementary kinetic parameters fitted in chapter 1 were used.

The simulations show that the IC50 over-estimates the dissociation constant of the inhibitor to P-gp relative to the cytosol, $K_{I,Aq}$, by a factor which depends upon probe substrate kinetic parameters (partition coefficient into the membrane from cytosol, binding constant to P-gp, passive permeability from both apical and basolateral sides into the cell) and cell parameters (volume of apical membrane, P-gp efflux active density, area of the transwell insert on which the cells grow). The smaller the passive permeability of the substrate, the greater the overestimate of the inhibitor's dissociation constant by its IC50 will be.

8. References

Acharya, P., Tran, T.T, Polli, J.W., Ayrton, A., Ellens, H. and Bentz, J. (2006) P-glycoprotein (P-gp) Expressed in a Confluent Monolayer of hMDR1-MDCKII Cells Has More Than One Efflux Pathway with Cooperative Binding Sites. Biochemistry; 45(51):15505-19.

Al-Shawi, M. K., and Senior, A. E. (1993) Characterization of the Adenosine Triphosphatase Activity of Chinese Hamster P-glycoprotein. J. Biol. Chem. 268: 4197-4206.

Al-Shawi, M. K., Omote, H. (2005) The remarkable transport mechanism of P-glycoprotein: A multidrug transporter. J.Bioenergetics and Biomembr., 37(6):489-96.

Al-Shawi, M.K., Polar, M. K., Omote, H., and Figler, R. A. (2003) Transition State Analysis of the Coupling of Drug Transport to ATP Hydrolysis by P-glycoprotein. J. Biol. Chem. 278:52629-40.

Ambudkar, S.V., Lelong, I.H., Zhang, J., Cardarelli, C.O., Gottesman, M.M. and Pastan, I. (1992) Partial Purification and Reconstitution of the Human Multidrug-Resistance Pump: Characterization of the Drug-Stimulatable ATP Hydrolysis. Proc. Natl. Acad. Sci. USA 89; 8472-76.

Ambudkar, S. V., Dey, S., Hrycyna, C. A., Ramachandra, M., Pastan, I. and Gottesman, M. M. (1999) Biochemical, cellular, and pharmacological aspects of the multidrug transporter. Annu. Rev. Pharmacol. Toxicol. 39:361-98.

Ambudkar, S.V., Kimchi-Sarfaty, C., Sauna, Z.E. & Gottesman, M. M. (2003) P-glycoprotein: from genomics to mechanism, Oncogene. 22:7468-85.

Ambudkar, S.V., Kim, I.W., Xia, D., Sauna, Z.E.(2006a) The A-loop, a novel conserved aromatic acid subdomain upstream of the Walker A motif in ABC transporters, is critical for ATP binding. FEBS Lett. 580:1049-55.

Ambudkar,S.V., Kim, I.W., Sauna, Z.E. (2006b) The power of the pump: mechanisms of action of P-glycoprotein (ABCB1) Eur. J. Pharm. Sci. 27:392-400.

Annaert,P.P., Turncliff,R.Z., Booth,C.L., Thakker,D.R. and Brouwer,K.L.R. (2001) P-Glycoprotein-mediated In Vitro biliary excretion in sandwich-cultured rat hepatocytes. Drug Metab. Disp. 29(10);1277-83.

Ayesh,S., Shao,Y.M., Stein,W.D. (1996) Co-operative, competitive and non-competitive interactions between modulators of P-glycoprotein. Biochim. Biophys. Acta 1316:8-18.

Bentz, J., Tran, T. T., Polli, J. W. , Ayrton, A. and Ellens, H. (2005) The steady-state Michaelis-Menten analysis of P-glycoprotein mediated transport through a confluent cell monolayer cannot predict the correct Michaelis constant K_M. Pharm. Res. 22:1667-77.

Bolhuis, H., van Veen, H. W., Molenaar, D., Poolman, B., Driessen, A. J. and Konings, W. N.(1996) Multidrug resistance in Lactococcus lactis: evidence for ATP-dependent drug extrusionfrom the inner leaflet of the cytoplasmic membrane. EMBO J. 15:4239-45.

Booth, C.L., Brouwer, K.R. and Brouwer, K.L.R. (1998) Effect of multidrug resistance modulators on the hepatobiliary disposition of doxorubicin in the isolated perfused rat liver. Cancer Res. 58:3641-48.

Borgnia, M. J., Eytan, G. D., and Assaraf, Y. G. (1996) Competition of hydrophobic peptides, cytotoxic drugs, and chemosensitizers on a common P-glycoprotein Pharmacophore as revealed by its ATPase activity. J. Biol. Chem. 271:3163-71.

Borst, P. & R. O. Elferink. (2002) Mammalian ABC transporters in health and disease, Ann. Rev.Biochem. 71:537-92.

Bouw, R., Ederoth, P., Lundberg, J., Ungerstedt, U., Nordstrm, C.-H., Hammarlund-Udenaes, M.(2001) Increased blood-brain barrier permeability of morphine in a patient with severe brain lesions as determined by microdialysis. Acta Anaesthesiologica Scandinavica 45(3):390-92.

Chaudhary, P.M. and Roninson, I.B. (1993) Induction of Multidrug Resistance in Human Cells by Transient Exposure to Different Chemotherapeutic Drugs. J. Natl. Cancer Inst. 85:632-39.

Chen, J., Lu, G., Lin, J., Davidson, A. L., and Quiocho, F. A. (2003) A Tweezers-like Motion of the ATP-Binding Cassette Dimer in an ABC Transport Cycle.Mol. Cell.12:651-61.

Choi, K.H., Chen, C.J., Kriegler, M. and Roninson, I.B. (1988) An altered pattern of cross-resistance in multidrug-resistant human cells results from spontaneous mutations in the mdr1 (Pglycoprotein) gene. Cell. 53:519-29.

Cianchetta, G., Singleton, R.W., Zhang, M., Wildgoose, M., Giesing, D., Fravolini, A., Cruciani, G., and Vaz, R.J. (2005) A pharmacophore hypothesis for P-glycoprotein substrate recognition using GRIND-based 3D-QSAR. J. Med. Chem. 48: 2927-35.

Cornwell, M.M., Gottesman, M.M. and Pastan, I. (1986a) Increased vinblastine binding to membrane vesicles from multidrug-resistant KB cells. J. Biol.Chem. 261, 7921-28.

Cornwell, M.M., Safa, A.R., Felsted, R.L., Gottesman, M.M. and Pastan, I. (1986b) Membrane Vesicles from Multidrug-Resistant Human Cancer Cells Contain a Specific 150- to 170-kDa Protein Detected by Photoaffinity Labeling. Proc. Natl. Acad. Sci. USA 83, 3847-51.

Cutler, L., Howes, C., Deeks, N.J., Buck,T.L., Jeffrey, P.(2006) Development of a P-glycoprotein knockout model in rodents to define species differences in its functional effect at the blood-brain barrier. J. Pharm Sci. 95(9);1944-53.

Dano, K. (1973) Active outward transport of daunomycin in resistant Ehrlich ascites tumor cells. Biochim. Biophys. Acta 323, 466-83.

Dawson, J.P.R.& Locher, K.P.(2006) Structure of a bacterial multidrug ABC transporter Nature: 443;180-85.

Dean M, Annilo T. (2005) Evolution of the ATP-binding cassette (ABC) transporter superfamily in vertebrates. Annu. Rev. Genomics Hum. Genet.; 6:123-42.

Dean M, Hamon Y, Chimini G. (2001)The human ATP-binding cassette (ABC) transporter superfamily. J. Lipid Res.; 42:1007-17.

Debenham, P.G., Kartner, N., Siminovitch, L., Riordan, J.R. and Ling, V. (1982) DNA-mediated transfer of multiple drug resistance and plasma membrane glycoprotein expression. Mol. Cell. Biol. 2: 881-889.

Dresser, M.J., Leabman, M.K. and Giacomini, K.M. (2001) Transporters involved in the elimination of drugs in the kidney: Organic Anion Transporters and Organic Cation Transporters. J. Pharm. Sci. 90(4):397-421.

Druley, T. E., Stein, W. D., and Roninson, I. B. (2001) Analysis of MDR1 P-Glycoprotein conformational changes in permeabilized cells using differential immunoreactivity. Biochemistry. 40:4312-22.

Ecker, G., Huber, M., Schmid, D., and Chiba, P. (1999) The Importance of a Nitrogen Atom in Modulators of Multidrug Resistance. Mol. Pharmacol.56:791-796.

Ferry, D., Boer, R., Callaghan, R., and Ulrich, W.R. (2000) Localization of the 1,4-dihydropyridine drug acceptor of P-glycoprotein to a cytoplasmic domain using a per-

manently charged derivative N-methyl dexniguldipine. Int. J. Clin. Pharmacol. Ther. 38:130-140.

Galski, H., Sullivan, M., Willingham, M.C., Chin, K.V., Gottesman, M.M., Pastan, I. and Merlino, G.T. (1989) Expression of a human multidrug-resistance cDNA (MDR1) in the bone marrow of transgenic mice: resistance to daunomycin-induced leukopenia. Mol. Cell. Biol. 9, 4357-63.

Gerlach, J.H., Endicott, J.A., Juranka, P.F., Henderson, G., Sarangi, F., Deuchars K.L. and Ling, V. (1986) Homology between P-glycoprotein and a bacterial haemolysin transport protein suggests a model for multidrug resistance. Nature, 324, 485-89.

Goh, L. B., Spears, K. J., Yao, D., Ayrton, A., Morgan, P., Roland, W. C. and Friedberg, T. (2002) Endogenous drug transporters in *in vitro* and *in vivo* models for the prediction of drug disposition in man. Biochem. Pharmacol. 64:1569-78.

Goldstein, L.J., Galski, H., Fojo, A., Willingham, M., Lai, S.-L., Gazdar, A., Pirker, R., Green, A., Crist, W., Brodeur, G., Grant, C., Lieber, M., Cossman, J., Gottesman, M.M. and Pastan, I. (1989) Expression of a multidrug resistance gene in human cancers. J. Natl. Cancer Inst. 81:116-24.

Gottesman, M.M., Ambudkar, S.V. (2001) Overview: ABC transporters and human disease. J. Bioenerg. Biomembr.; 33:453-8.

Gottesman, M.M., Fojo, T., Bates, S.E. (2002) Multidrug resistance in cancer: role of ATP-dependent transporters. Nat. Rev. Cancer; 2:48-58.

Gottesman, M. M. (2002) Mechanisms of cancer drug resistance. Annu. Rev. Med. 53:615-27.

Greenberger, L. M., Lisanti, C. J., Silva, J. T. and Horwitz, S. B.(1991) Domain mapping of the photoaffinity drug-binding sites in P-glycoprotein encoded by mouse mdr1b. J. Biol. Chem. 266:20744-51.

Gros, P., Croop, J., Roninson, I., Varshavsky, A. and Housman, D.E. (1986a) Isolation and Characterization of DNA Sequences Amplified in Multidrug-Resistant Hamster Cells. Proc. Natl. Acad. Sci. USA 83, 337-341.

Gros, P., Croop, J. and Housman, D.E.(1986b) Mammalian multidrug resistance gene: Complete cDNA sequence indicates strong homology to bacterial transport proteins Cell. 47:371-390.

Hamada, H. and Tsuruo, T. J. (1988) Purification of the 170- to 180-KDa membrane glycoprotein associated with multidrug resistance. Biol. Chem.263: 1454-58.

Higgins, C.F. and Gottesman, M.M. (1992) Is the multidrug transporter a flippase? Trends Biochem. Sci. 17, 18-21.

Higgins, C.F. and Linton, K. (2004) The ATP switch model for ATP transporters. Nature Struct. & Mol. Biol. 11(10):918-26.

Higgins, C.F., Hiles, I.D., Whalley, K. and Jamieson, D.J. (1985) Nucleotide binding by membrane components of bacterial periplasmic binding protein-dependent transport systems. EMBO J. 4:1033-39.

Holland, I. B., and Blight, M. A. (1999) ABC-ATPases, adaptable energy generators fuelling transmembrane movement of a variety of molecules in organisms from bacteria to humans. J. Mol. Biol. 293, 381-99.

Hopfner, K. P., Karcher, A., Shin, D. S., Craig, L., Arthur, L.M., Carney, J. P., and Tainer, J. A. (2000) Structural biology of Rad50 ATPase: ATP-driven conformational control in DNA double-strand break repair and the ABC-ATPase superfamily. Cell. 101:789-800.

Horio, M., Chin, K.-V., Currier, S.J., Goldenberg, S., Williams, C., Pastan, I., Gottesman, M.M. and Handler, J. (1989) Transepithelial transport of drugs by the multidrug transporter in cultured Madin-Darby canine kidney cell epithelia. J. Biol. Chem. 264: 14880-84.

Horio, M., Gottesman, M.M. and Pastan, I. (1988) ATP-Dependent Transport of Vinblastine in vesicles from human multidrug-resistant cells. Proc. Natl. Acad. Sci. USA 85:3580-84.

Horn, C., Bremer, E., and Schmitt, L.(2003) Nucleotide Dependent Monomer/Dimer Equilibrium of OpuAA, the Nucleotide-binding protein of the osmotically regulated ABC transporter OpuA from Bacillus subtilis. J.Mol. Biol. 334, 403-19.

Hrycyna, C.A., Ramachandra, M., Germann, U.A., Cheng, P.W., Pastan, I. and Gottesman, M.M. (1999) Both ATP Sites of human P-Glycoprotein are essential but not symmetric. Biochemistry 38:13887-99.

Janas, E., Hofacker, M., Chen, M., Gompf, S., van der Does, C., and Tampe, R. The ATP hydrolysis cycle of the nucleotide-binding domain of the mitochondrial ATP-binding Cassette transporter Mdl1p.(2003) J. Biol. Chem. 278:26862-69.

Juliano, R.L. and Ling, V.(1976) A surface glycoprotein modulating drug permeability in Chinese hamster ovary cell mutants. Biochim. Biophys.Acta 455:152-162.

Kartner, N., Evernden-Porelle, D., Bradley, G. and Ling, V. (1985) Detection of P-glycoprotein in multidrug-resistant cell lines by monoclonal antibodies. Nature 316: 820-823.

Kessel, D., Botterill, V. and Woodinsky, I. (1968) Uptake and retention of daunomycin by mouse leukemic cells as a factor in drug response. Cancer Res. 28:938-941.

Kim, I.W., Peng, X.H., Sauna, Z.E.(2006) The conserved tyrosine residues401 and 1044 in ATP sites of human P-glycoprotein are critical for ATP binding and hydrolysis: evidence for a conserved subdomain, the A-loop in the ATP-binding cassette. Biochemistry:45: 7605-16.

Lau, Y.Y., Okochi, H., Huang, Y., Benet, L.Z. (2006) Multiple transporters affect the disposition of atorvastatin and its two active hydroxy metabolites: application of *in vitro* and ex situ systems. J. Pharmacol. Exp. Ther. 316:762-71.

Lee, G., Schlichter, L., Bendayan, M. and Bendayan, R. (2001) Functional expression of P-glycoprotein in rat brain microglia. J. Pharmacol. Exp. Ther. 299: 204-12.

Lee, J.Y., Urbatsch, I.L., Senior, A.E., and Wilkens, S.(2002) Projection structure of P-glycoprotein by electron microscopy-evidence for a closed conformation of the nucleotide binding domains.J. Biol. Chem. 277: 40125-31.

Ling, V. (1975) Drug resistance and membrane alteration in mutants of mammalian cells. Can. J. Genet. Cytol. 17:503-515.

Ling, V. and Baker, R.M. (1978) Dominance of colchicines resistance in hybrid CHO cells. Somatic Cell Genet. 4:193-200.

Ling, V. and Thompson, L.H. (1974) Reduced permeability in CHO cells as a mechanism of resistance to colchicine. J. Cell. Physiol. 83:103-116.

List, A.F., Kopecky, K.J., Willman, C.L., Head, D.R., Persons, D.L., Slovak, M.L., Dorr, R., Karanes, C., Hynes, H.E., Doroshow, J.H., Shurafa, M. and Appelbaum, F.R.(2001) .Benefit of cyclosporine modulation of drug resistance in patients with poor-risk acute myeloid leukemia: a Southwest Oncology Group study. Blood: 98: 3212-20.

Loo, T. W. & D. M. Clarke.(1993) Functional consequences of phenylalanine mutations in the predicted transmembrane domain of P-glycoprotein. J. Biol.Chem. 268:19965-72.

Loo, T. W. & Clarke, D.M. (1997) Correction of defective protein kinesis of human p-glycoprotein mutants by substrates and modulators. J. Biol. Chem. 272:709-12.

Loo, T. W. & Clarke, D. M. (1999) Determining the structure and mechanism of the human multidrug resistance P-glycoprotein using cysteine-scanning mutagenesis and thiol-modification techniques. Biochem. Biophys. Acta. 1461(2): 315-25.

Loo, T. W. & Clarke, D. M. (2000) Drug-stimulated ATPase activity of human P-glycoprotein is blocked by disulfide cross-linking between the nucleotide-binding sites. J. Biol. Chem 275:19435-19438.

Loo, T. W. & Clarke, D. M.(2001a) Cross-linking of human multidrug resistance P-glycoprotein by the sSubstrate, Tris-(2-maleimidoethyl)amine, is altered by ATP hydrolysis. J. Biol. Chem. 276(34):31800-5.

Loo, T.W., Clarke, D.M. (2001b) Determining the dimensions of the drug-binding domain of human P-glycoprotein using thiol cross-linking compounds as molecular rulers. J Biol Chem. 276:36877-80.

Loo, T. W., Bartlett, M. C. & Clarke, D. M.(2003) Substrate-induced conformational changes in the transmembrane segments of human P-glycoprotein. J. Biol. Chem. 278 (16):13603-6.

Loo, T.W., Bartlett, M.C., Clarke, D.M. (2004) The drug-binding pocket of the human multidrug resistance P-glycoprotein is accessible to the aqueous medium. Biochemistry. 43:12081-9.

Loo, T.W., Clarke,D.M. (2005a) Do drug substrates enter the common drug-binding pocket of P-glycoprotein through "gates"? Biochem.Biophys.Res.Comm. 329:419-22.

Loo, T.W. and Clarke, D.M. (2005b) Recent progress in understanding the mechanism of P-glycoprotein-mediated drug efflux. J. Membr. Biol. 206:173-185.

Loo, T.W., Bartlett, M.C, and Clarke,D.M. (2005) ATP hydrolysis promotes interactions between the extracellular ends of transmembrane segments 1 and 11 of human multidrug resistance P-Glycoprotein. Biochemistry, 44, 10250-10258.

Lown, K. S., Mayo, R. R., Leichtman, A. B., Hsiao, H. L., Turgeon, D. K., Schmiedlin-Ren, P., Brown, M. B., Guo, W., Rossi, S. J., Benet, L. Z. and Watkins, P. B.(1997) Role of intestinal P-glycoprotein (mdr1) in interpatient variation in the oral bioavailability of cyclosporine. Clin. Pharmacol. & Therap. 62 (3):248-60.

Luckie,D.B., Wilterding,J.H., Krha,M. and. Krouse,M.E.(2003) CFTR and MDR: ABC transporters with homologous structure but divergent function.Curr.Genomics. 4:109-21.

Lu, P., Liu,R. and Sharom, F. J. (2001) Drug transport by reconstituted P-glycoprotein in proteoliposomes:Effect of substrates and modulators, and dependence on bilayer phase state. Eur. J. Biochem. 268: 1687-97.

Lugo, M.R., and Sharom, F.J. (2005a) Interaction of LDS-751 with P-glycoprotein and mapping of the location of the R drug binding site. Biochemistry, 44: 643-655.

Lugo, M. R. and Sharom, F.J. (2005b) Interaction of LDS-751 and Rhodamine 123 with P-Glycoprotein: evidence for simultaneous binding of both drugs. Biochemistry. 44:14020-29.

Mickley, L.A., Spengler, B.A., Knutsen, T.A., Biedler, J.L. and Fojo, T. (1997) Gene rearrangement: a novel mechanism for MDR-1 gene activation. J. Clin. Invest. 99, 1947-57.

Modok, S., Mellor, H.R., and Callaghan, R. (2006) Modulation of multidrug resistance efflux pump activity to overcome chemoresistance in cancer. Curr. Opin. Pharmacol. 6: 350-54.

Molinari, A., Cianfriglia, M., Meschini, S., Calcabrini, A. and Arancia, G. (1994) P-glycoprotein expression in the golgi apparatus of multidrug-resistant cells. Int. J. Cancer. 59: 789-95.

Mls, M., Heikkinen, T., Hakkola, J., Hakala, K., Wallerman, O., Wadelius, M., Wadelius, C., Laine, K.(2005) Functional role of P-glycoprotein in the human blood-placental barrier. Clin. Pharm.Therap., 78(2):123-31.

Moody, J. E., Millen, L., Binns, D., Hunt, J. F., and Thomas, P. J. (2002) Cooperative, ATP-dependent association of the nucleotide binding cassettes during the catalytic cycle of ATP-binding Cassette Transporters. J. Biol. Chem. 277:21111-14.

Murakami,S., Nakashima1,R.,Yamashita, E., Matsumoto,T., Yamaguchi,A.(2006) Crystal structures of a multidrug transporter reveal a functionally rotating mechanism. Nature, 443:173-9.

Noonan, K.E., Beck, C., Holzmayer, T.A., Chin, J.E., Wunder, J.S., Andrulis, I.L., Gazdar, A.F., Willman, C.L., Griffith, B., Von Hoff, D.D. and Roninson, I.B.(1990) Quantitative analysis of MDR1 (Multidrug Resistance) gene expression in human tumors by

polymerase chain reaction. Proc. Natl. Acad. Sci. USA 87:7160-4.

Omote, H., and Al-Shawi, M. K.(2002) A novel electron paramagnetic resonance approach to determine the mechanism of drug transport by P-glycoprotein. J. Biol. Chem. 277:45688-94.

Omote, H. and Al-Shawi, M. K.(2006) Interaction of transported drugs with the lipid bylayer and P-glycoprotein through a solvation exchange mechanism. Biophys.J, doi:10.1529/biophysj.105.077743.

Omote, H., Figler, R. A., Polar, M. K., and Al-Shawi, M. K. (2004) Improved energy coupling of human P-glycoprotein by the Glycine 185 to Valine mutation. Biochemistry 43:3917-28.

Orlowski,S., Martin,S.and Escargueil,A.(2006) P-glycoprotein and 'lipid rafts': some ambiguous mutual relationships (floating on them, building them or meeting them by chance?) Cell. Mol. Life Sci. 63:1038-59.

Ouellette, M., Legare, D., Papadopoulou, B. (2001) Multidrug resistance and ABC transporters in parasitic protozoa. J. Mol. Microbiol. Biotechnol. 3(2):201-6.

Pascaud,C., Garrigos,M., Orlowski,A. (1998) Multidrug resistance transporter P-glycoprotein has distinct but interacting binding sites for cytotoxic drugs and reversing agents. Biochem. J. 333:351-8.

Pastan, I., Gottesman, M.M., Ueda, K., Lovelace, E., Rutherford, A.V. and Willingham, M.C. (1988) A retrovirus carrying an MDR1 cDNA confers multidrug resistance and polarized expression of P-glycoprotein in MDCK cells. Proc. Natl. Acad. Sci. USA 85:4486-90.

Pleban, K., Kopp, S., Csaszar, E., Peer, M., Hrebicek, T., Rizzi, A., Ecker, G. F.and Chiba, P. (2005) P-glycoprotein substrate binding domains are located at the transmembrane domain/transmembrane domain interfaces: a combined photoaffinity labeling-protein homology modeling approach. Mol. Pharmacol. 67:365-74.

Poelarends,G.J., Mazurkiewicz, P.& Konings, W. N.(2002) Multidrug transporters and antibiotic resistance in Lactococcus lactis. Biochim Biophys Acta. 1555:1-7.

Qu, Q., and Sharom, F.J.(2001) FRET analysis indicates that the two ATPase active sites of the P-glycoprotein multidrug transporter are closely associated. Biochemistry, 40:413-22.

Qu, Q., and Sharom, F.J. (2002) Proximity of bound Hoechst 33342 to the ATPase cat-

alytic sites places the drug binding site of Pglycoprotein within the cytoplasmic membrane leaflet. Biochemistry, 41: 4744-52.

Ramachandra, M., Ambudkar, S.V., Chen, D., Hrycyna, C.A., Dey, S., Gottesman, M.M. and Pastan, I. (1998) Human P-Glycoprotein exhibits reduced affinity for substrates during a catalytic transition state.Biochemistry 37:5010-19.

Rautio, J., Humphreys, J. E., Webster, L. O., Balakrishnan, A., Keogh, J. P., Kunta, J. R., Serabjit-Singh, C.J. and Polli, J. W.(2006) In Vitro P-glycoprotein Inhibition Assays for Assessment of Clinical Drug Interaction Potential of New Drug Candidates: A Recommendation for Probe Substrates. Drug. Metab. Dispos. 34: 786-92.

Raviv, Y., Pollard, H.B., Bruggemann, E.P., Pastan, I. and Gottesman, M.M. (1990) Photosensitized labeling of a functional multidrug transporter in living drug-resistant tumor cells. J. Biol. Chem. 265:3975-80.

Riordan, J.R. and Ling, V. (1979) Purification of P-glycoprotein from plasma membrane vesicles of Chinese hamster ovary cell mutants with reduced colchicine permeability. J. Biol. Chem. 254, 12701-5.

Riordan, J.R., Deuchars, K., Kartner, N., Alon, N., Trent, J. and Ling, V. (1985) Amplification of P-glycoprotein genes in multidrug-resistant mammalian cell lines. Nature 316:817-19.

Romsicki, Y. and Sharom, F.J. (1999) The membrane lipid environment modulates drug interactions with the P-glycoprotein multidrug transporter. Biochemistry, 38:6887-96.

Romsicki, Y. and Sharom, F. J. (2001) Phospholipid flippase activity of the reconstituted P-Glycoprotein multidrug transporter. Biochem., 40:6937-47.

Ronaldson, P. T., Bendayan, M., Gingras, D., Piquette-Miller, M. and Bendayan, R. (2004) Cellular localization and functional expression of P-glycoprotein in rat astrocyte cultures. J. Neurochem.89: 788-800.

Roninson, I.B., Abelson, H.T., Housman, D.E., Howell, N. and Varshavsky, A. (1984) Amplification of specific DNA sequences correlates with multidrug resistance in Chinese hamster cells. Nature, 309:626-28.

Roninson, I.B., Chin, J.E., Choi, K.G., Gros, P., Housman, D.E., Fojo, A., Shen, D.W., Gottesman, M.M. and Pastan, I. (1986) Isolation of human mdr DNA sequences amplified in multidrug resistant KB carcinoma cells. Proc. Natl. Acad. Sci. USA 83,4538-42.

Rosenberg, M.F., Callaghan, R., Ford, R.C., and Higgins, C.F.(1997) Structure of the multidrug resistance P-glycoprotein to 2.5 nm resolution determined by electron microscopy and image analysis. J. Biol. Chem. 272: 10685-94.

Rosenberg, M.F., Velarde, G., Ford, R.C., Martin, C., Berridge, G., Kerr, I.D., Callaghan, R., Schmidlin, A., Wooding, C., Linton, K.J. and Higgins, C.F. (2001) Repacking of the transmembrane domains of P-glycoprotein during the transport ATPase cycle EMBO J. 20:5615-25.

Rosenberg, M. F., Kamis, A. B., Callaghan, R., Higgins, C. F. & Ford, R.C.(2003) Three-dimensional structures of the mammalian multidrug resistance P-glycoprotein demonstrate major conformational changes in the transmembrane domains upon nucleotide binding. J. Biol. Chem. 278(10):8294-9.

Rosenberg,M.F., Callaghan,R., Modok, S., Higgins,C.F.and Ford,R.C. (2005) Three-dimensional structure of P-glycoprotein the transmembrane regions adopt an asymmetric configuration in the nucleotide-bound state. J. Biol. Chem. 280(4):2857-62.

Sasongko, L., Link, J., Muzi, M., Mankoff, D., Yang, X., Collier, A., Shoner, S., Unadkat, J. (2005) Imaging P-glycoprotein transport activity at the human blood-brain barrier with positron emission tomography. Clin.Pharm.Therap.77(6); 503-14.

Sauna,Z.E., Andrus, M.B., Turner, T.M., Ambudkar, S.V.(2004) Biochemical basis of polyvalency as a strategy for enhancing the efficacy of P-glycoprotein (ABCB1) modulators: stipiamide homodimers separated with defined length spacers reverse drug efflux with greater efficacy. Biochemistry;43:2262-71.

Sauna, Z. E. & Ambudkar, S. V. (2000) Evidence for a requirement for ATP hydrolysis at two distinct steps during a single turnover of the catalytic cycle of human P-glycoprotein. Proc. Natl Acad. Sci. USA 97, 2515-20.

Sauna,Z.E. and Ambudkar,S.V. (2007) About a switch: How P-glycoprotein (ABCB1) harnesses the energy of ATP binding and hydrolysis to do mechanical work. Mol. Cancer Ther.; 6(1):13-23.

Schinkel, A. H. (1998) Pharmacological insights from P-glycoprotein knockout mice. Intl. J. Clin. Pharmacol. & Therap. 36(1):9-13.

Schinkel, A.H., Smit, J.J., van Tellingen, O., Beijnen, J.H., Wagenaar, E., van Deemter, L., Mol, C.A., van der Valk, M.A., Robanus-Maandag, E.C. and te Riele, H.P. (1994) Cell Disruption of the mouse mdr1a P-glycoprotein gene leads to a deficiency in the blood-brain barrier and to increased sensitivity to drugs. Cell,77:491-502.

Scotto, K.W. (2003) Transcriptional regulation of ABC drug transporters. Oncogene 22: 7496-7511.

See, Y.P., Carlsen, S.A., Till, J.E. and Ling, V. (1974) Increased drug permeability in Chinese hamster ovary cells in the presence of cyanide. Biochem. Biophys. Acta 373, 242-52.

Seelig, A. (1998) A general pattern for substrate recognition by P-glycoprotein Eur. J. Biochem. 251:252-61.

Seelig, A., and Gatlik-Landwojtowicz, E. (2000) Structure-activity relationship of P-glycoprotein substrates and modifiers. Eur. J. Pharm. Sci. 12: 31-40.

Seelig, A. and Gatlik-Landwojtowicz, E. (2005) Biophysical characterization of inhibitors of multidrug efflux transporters: their membrane and protein interactions. Med. Chem., 5(2):135-151.

Senior, A. E., Al-Shawi, M. K., and Urbatsch, I. L. (1995) The catalytic cycle of P-glycoprotein FEBS Lett. 377:285-89.

Senior, A. E., Al-Shawi, M. K., and Urbatsch, I. L. (1998) ATPase activity of Chinese hamster P-glycoprotein. Methods Enzymol. 292:514-23.

Shapiro, A. and Ling, V. (1995) Using purified P-glycoprotein to understand multidrug resistance. J. Bioenerg. Biomembr. 27:7-13.

Shapiro, A.B. and Ling, V. (1997a) Extraction of Hoechst 33342 from the cytoplasmic leaflet of the plasma membrane by P-glycoprotein Eur. J. Biochem. 250, 122-9.

Shapiro, A. B., Corder, A. B. and Ling, V. (1997) P-glycoprotein-mediated Hoechst 33342 transport out of the lipid bilayer. Eur. J. Biochem. 250:115-21.

Shapiro, A. B., and Ling, V. (1997b) Positively cooperative sites for drug transport by P-glycoprotein with distinct drug specificities. Eur. J. Biochem. 250:130-37.

Shapiro, A. B., and V. Ling. (1998) Transport of LDS-751 from the cytoplasmic leaflet of the plasma membrane by the rhodamine-123-selective site of P-glycoprotein. Eur. J. Biochem. 254:181- 8.

Sharom, F.J. (1997) The P-glycoprotein efflux pump: how does it transport drugs? J. Membr. Biol. 160: 161-75.

Sharom, F.J. and Eckford, P.D. (2003) Reconstitution of membrane transporters. Meth. Mol Biol. 227:129-54.

Shitara,Y., Horiea,T., Sugiyama,Y. (2006) Transporters as a determinant of drug clearance and tissue distribution. Eur. J. Pharm. Sci. 27:425-46.

Smith, C.A. and Rayment, I. (1996) Active site comparisons highlight structural similarities between myosin and other P-loop proteins. Biophys. J., 70(4):1590-1602.

Smith, P. C., Karpowich, N., Millen, L., Moody, J. E., Rosen, J., Thomas, P. J., and Hunt, J. F. (2002) ATP binding to the motor domain from an ABC transporter drives formation of a nucleotide sandwich dimer. Mol. Cell.10:139-49.

Sorrentino, B.P., Brandt, S.J., Bodine, D., Gottesman, M., Pastan, I., Cline, A. and Nienhuis, A.W. (1992) Retroviral transfer of the human MDR1 gene permits selection of drug resistant bone marrow cells *in vivo*. Science 257:99-103.

Sparreboom, A., van Asperen, J., Mayer, U., Schinkel, A.H., Smit, J.W., Meijer, D.K., Borst, P., Nooijen, W.J., Beijnen, J.H. and van Tellingen, O. (1997) Limited oral bioavailability and active epithelial excretion of paclitaxel (Taxol) caused by P-glycoprotein in the intestine. Proc. Natl. Acad. Sci. USA 94:2031-2035.

Spoelstra, E. C., Westerhoff, H. V., Pinedo, H. M., Dekker, H., & Lankelma, J. (1994) The multidrug-resistance-reverser verapamil interferes with cellular P-glycoprotein-mediated pumping of daunorubicin as a non-competing substrate, Eur. J. Biochem.221:363-73.

Tan, B., Piwnica-Worms, D., and Ratner, L. (2000) Multidrug resistance transporters and modulation. Curr. Opin. Oncol. 12: 450-58.

Thiebaut, F., Tsuruo, T., Hamada, H., Gottesman, M.M., Pastan, I. and Willingham, M.C. (1989) Immunohistochemical localization in normal tissues of different epitopes in the multidrug transport protein, P170: evidence for localization in brain capillaries and cross-reactivity of one antibody with a muscle protein. J. Histochem. Cytochem. 37,159-64.

Tombline, G., Muharemagic, A., White, L. B., and Senior, A. E. (2005) Involvement of the "Occluded Nucleotide Conformation" of P-Glycoprotein in the catalytic pathway. Biochemistry. 44,12879-86.

Tran, T. T. , Mittal, A., Gales, T., Maleeff, B., Aldinger, T., Polli, J.W., Ayrton, A., Ellens, H. and Bentz, J. (2004) An exact kinetic analysis of passive transport across a

polarized confluent MDCK cell monolayer modeled as a single barrier. J. Pharm. Sci. 93:2108-23.

Tran, T. T., Mittal, A., Aldinger, T., Polli, J.W. , Ayrton, A., Ellens, H. and Bentz, J. (2005) The elementary mass action rate constants of P-gp transport for a confluent monolayer of MDCKII-hMDR1 cells. Biophys. J., 88:715-38.

Tsuruo, T., Iida, H., Tsukagoshi, S. and Sakurai, Y. (1981) Overcoming of vincristine resistance in P388 leukemia *in vivo* and *in vitro* through enhanced cytotoxicity of vincristine and vinblastine by verapamil. Cancer Res. 41, 1967-1972.

Tsuruo, T., Iida, H., Kitatani, Y., Yokota, K., Tsukagoshi, S. and Sakurai,Y.(1984) Effects of quinidine and related compounds on cytotoxicity and cellular accumulation of vincristine and adriamycin in drug-resistant tumor cells. Cancer.Res. 44:4303-7.

Ueda, K., Cornwell, M.M., Gottesman, M.M., Pastan, I., Roninson, I.B., Ling, V. and Riordan, J.R. (1986) The mdr1 gene responsible for multidrug-resistance codes for P-glycoprotein. Biochem. Biophys. Res. Commun. 141, 956-62.

Ueda, K., Cardarelli, C., Gottesman, M.M. and Pastan, I. (1987a) Expression of a full-length cDNA for the human "MDR1" (Pglycoprotein) gene confers multidrug resistance to colchicine, doxorubicin, and vinblastine. Proc. Natl. Acad. Sci. USA 84, 3004-8.

Ueda, K., Pastan, I. and Gottesman, M.M. (1987b) Isolation and sequence of the promoter region of the human multidrugresistance (P-glycoprotein) gene. J. Biol. Chem. 262:17432-6.

Urbatsch, I. L., Al-Shawi, M. K., and Senior, A. E. (1994) Characterization of the ATPase activity of purified chinese hamster P -glycoprotein. Biochem.33:7069-76.

Urbatsch, I.L., Sankaran, B., Weber, J. and Senior, A.E. (1995) P-glycoprotein is stably inhibited by vanadate-induced trapping of nucleotide at a single catalytic site. J. Biol. Chem. 270:19383-90.

Van der Bliek, A.M., Van der Velde-Koerts, T., Ling, V. And Borst, P. (1986) The overexpression and amplification of five genes in a multidrug-resistant Chinese hamster ovary cell line. Mol. Cell. Biol. 6:1671-78.

Van Helvoort, A., Smith, A.J., Sprong, H., Fritzsche, I., Schinkel, A.H., Borst, P., van Meer, G.(1996) MDR1 P-glycoprotein is a lipid translocase of broad specificity, while MDR3 P-glycoprotein specifically translocates phosphatidylcholine. Cell ;87: 507-17.

Van Veen, H.W., Callaghan,R., Soceneantu,L., Sardini,A., Konings,.W.N & C.F. Higgins.(1998) Abacterial antibioticresistance gene that complements the human multidrug-resistance P-glycoprotein gene. Nature,391:291-5.

Van Veen,H.W, Higgins,C.F, Konings, W. N.(2001) Multidrug transport by ATP binding cassette transporters: a proposed two-cylinder engine mechanism.Res. Microbiol. 152:365-74.

Verdon, G., Albers, S. V., van Oosterwijk, N., Dijkstra, B.W., Driessen,A. J. M., and Thunnisen, A. M.(2003) Formation of the Productive ATP-Mg2+-bound Dimer of GlcV, an ABC-ATPase from Sulfolobus solfataricus J. Mol. Biol. 334:255-67.

Wang,E., Casciano,C.N., Clement,R.P., Johnson,W.W. (2000) Two transport binding sites of P-glycoprotein are unequal yet contingent: initial rate kinetic analysis by ATP hydrolysis demonstrates intersite dependence.Biochim. Biophys. Acta.1481:63-74.

Wiese, M., and Pajeva, I.K. (2001) Structure-activity relationships of multidrug resistance reversers. Curr. Med. Chem. 8: 685-713.

Zaitseva, J., Jenewein, S., Jumpertz, T., Holland, I. B., and Schmitt, L.(2005a) H662 is the linchpin of ATP hydrolysis in the nucleotide-binding domain of the ABC transporter HlyB EMBO J. 24, 1901-10.

Zaitseva, J., Jenewein, S., Wiedenmann, A., Benabdelhak, H.,Holland, I. B., and Schmitt, L. (2005b) Functional characterization and ATP-induced dimerization of the isolated ABC-domain of the Haemolysin B transporter. Biochem.44:9680-90.

Zgurskaya, H. I.and Nikaido H. (2002) Mechanistic Parallels in Bacterial and Human Multidrug Efflux Transporters. Curr. Prot. and Peptide Sci. 3:531-40.

Part II - Papers

9. Paper 1

P-gp expressed in a confluent monolayer of hMDR1-MDCKII cells has more than one efflux pathway with cooperative binding sites.

Poulomi Acharya[1,2], Thuy T. Tran[1,2], Joseph W. Polli[3], Andrew Ayrton[4], Harma Ellens[2] & Joe Bentz[1*]

[1] Department of Bioscience & Biotechnology, Drexel University, Philadelphia, PA19104, USA

[2] Preclinical Drug Metabolism and Pharmacokinetics, GlaxoSmithKline, King of Prussia, PA, 19406.

[3] Preclinical Drug Metabolism and Pharmacokinetics, GlaxoSmithKline, Research Triangle Park, NC 27709

[4] Preclinical Drug Metabolism and Pharmacokinetics, GlaxoSmithKline, Welwyn, England

[*] Address correspondence to Dr. Joe Bentz, email: bentzj@drexel.edu, FAX: 215-895-1273.

Running Title: P-gp cooperative binding and multiple efflux pathways.

Keywords: Transcellular Efflux; Elementary Rate Constants; amprenavir; quinidine; loperamide; Hoechst 33342; rhodamine 123

Abbreviations: P-gp, the P-glycoprotein product of the hMDR1 gene; A:B>A or A:A>B, concentration in the apical chamber when the basolateral or apical chamber is the donor; B:B>A or B:A>B, concentration in the basolateral chamber when the basolateral or apical chamber is the donor.

Abstract

The multidrug resistance transporter P-gp effluxes a wide range of substrates and can be affected by a wide range of inhibitors or modulators. Many studies have presented classifications for these binding interactions, either within the context of equilibrium binding or the Michaelis-Menten enzyme analysis of P-gp's ATPase activity. Our approach is to study P-gp transport and its inhibition using a physiologically relevant confluent monolayer of hMDR1-MDCKII cells. We measure the elementary rate constants for P-gp efflux of substrates and study inhibition using pairwise combinations with a different unlabelled substrate acting as the inhibitor. Our current kinetic model for P-gp has only a single binding site, because a previous study proved that the mass action kinetics of efflux of a single substrate were not sensitive to whether there are one or more substrate binding and efflux sites. In this study, using this 1-site model, we found that with "high" concentrations of either a substrate or an inhibitor, the elementary rate constants fitted independently for each of the substrates alone quantitatively predicted the efflux curves, simply applying the assumption that binding at the "one site" was competitive. On the other hand, at "low" concentrations of both the substrate and the inhibitor, we found no inhibition of the substrate efflux, despite the fact that both substrate and inhibitor were being well effluxed. This was not an effect of excess "empty" P-gp molecules, since the competitive efflux model takes site occupancy into account. Rather, it is quantitative evidence that the substrate and the inhibitor are being effluxed by multiple pathways within P-gp. Remarkably, increasing the substrate concentration above the "low" concentration, caused the inhibition to become competitive, i.e. the inhibitor became effective. These data and their analysis show that binding of these substrates must be cooperative, either positive or negative.

Introduction

The human multidrug resistance transporter P-glycoprotein, P-gp (1), is the product of the hMDR1 gene, ABCB1, and is widely expressed in human epithelial tissue as a protection against xenobiotics. It is one of the 48 members of the ABC family of membrane transporters within the human genome (2). The biological and clinical significance of P-gp has been demonstrated through a large number of *in vitro*, preclinical and clinical studies (3-10). A wide variety of *in vitro* expression systems have been used to study P-gp structure and function: purified protein (11), lipid reconstitutions of purified P-gp (12-14), plasma membrane vesicles (15), suspension or unpolarized adherent cells over-expressing P-gp (16-18), and more recently polarized confluent cell monolayers (19-25).

A key question about P-gp, and any similar transporter, is how many functional binding sites and efflux pathways it contains, as well as the nature of the communication between these sites. It is generally believed that the two transmembrane domains, TMD, of P-gp form a large binding pocket (11, 14, 26, 27). Each TMD is composed of 6 transmembrane α-helices and the binding pocket appears to be within the interface between α-helices 4, 5 and 6 of TMD 1 and α-helices 9, 10, 11 and 12 in TMD 2 (14). If P-gp has more than one substrate binding site and each can lead to efflux, whether through a common or a different route within P-gp, it will need to be analyzed by a multi-pathway kinetic model. In this case, the next question is whether the pathways are independent or cooperative.

The binding of substrates to P-gp has been assayed in many different ways, each of which is consistent, at least in some studies, with multiple substrate/inhibitor/modulator binding sites within the P-gp binding pocket. Lugo & Sharom (13) and Loo & Clarke (14) have recently reviewed the current hypotheses about the number of binding sites on P-gp and their possible interrelationships. There are many different proposals on both topics.

To address these questions, we use a polarized MDCKII-hMDR1 confluent cell monolayer, which constitutively overexpresses P-gp in the apical plasma membrane. It has the advantage of studying P-gp in a physiologically relevant expression system, without the uncertainties of how purification and reconstitution affect function. It has the disadvantage of being a more complex expression system to analyze. We believe that all expression systems will be needed to elucidate the structure-function relationship of P-gp, however the molecular parameters derived from P-gp transport from the confluent cell monolayer system will be essential to understand the extent to which the purified systems or other reconstituted expression systems predict the "native" function of P-gp. In particular, the sensitivity which P-gp activity appears to be showing to lipid composition (28, 29) makes the confluent cell monolayer, with an asymmetric lipid composition across the apical plasma membrane, more likely to mimic the *in vivo* environment than proteoliposomes, membrane vesicles, suspension cells or unpolarized adherent cells.

Materials and Methods

Materials. Amprenavir and GF120918 were from GlaxoSmithKline (USA), loperamide was from Sigma and quinidine was from Fisher Scientific. ^{3}H-loperamide (10 Ci/mmole) and ^{3}H-amprenavir (21 Ci/mmole) were custom synthesized by Amersham Pharmacia Biotech, England. ^{3}H-quinidine (20 Ci/mmole) was from ICN Biomedical, Inc. USA. Hoechst 33342 and rhodamine 123 was purchased from Invitrogen (Eugene, OR). DMSO was from Sigma-Aldrich. Dulbecco's Modified Eagle Medium (DMEM) was from MediaTech, VWR. DMEM with 25 mM HEPES buffer, high glucose (4.5 g/L), L-Glutamine, pyridoxine hydrochloride, w/o sodium pyruvate, and with phenol red was from Gibco. The same medium without phenol red was used for transport experiments. Transwell 12-well plates with polycarbonate inserts (0.4μm pore size and 12 mm diameter) were obtained from Costar (Acton, MA).

Substrate Selection. Amprenavir, quinidine, and loperamide use were chosen because they are good P-gp substrates, they are chemically unrelated and show different transport and mass balance problems (23, 24). Hoechst 33342 and rhodamine 123 are commonly used fluorescent substrates of P-gp (27).

Cell line and culture conditions. The Madin-Darby Canine Kidney II cell line overexpressing human MDR1 (MDCKII-hMDR1) was purchased from the Netherlands Cancer Institute (Amsterdam, Netherlands) (30). MDCK II cells were grown in 175 cm^2 culture flasks using DMEM with 10% fetal bovine serum, 1% L-glutamine and 50 U/mL penicillin, 50 mg/mL streptomycin at 37°C in 5% CO_2 atmosphere. Cells were split twice a week at 70-80% confluence in a ratio of 1:40, after at least 2 washes in PBS, and trypsinized with 0.25% trypsin/EDTA. All transport assays were done with cells from passages 30 to 55. Cells were kept at 37°C in 5% CO_2.

Single substrate efflux assay. Cells were seeded in 12 well Costar-Transwell plates

with polycarbonate membrane inserts at a density of 175,000 cells per insert and grown for four days in culture medium. Cells were given fresh media 1 day after seeding. On the day of the experiment, culture medium was removed and cells were pre-incubated for 30 minutes with either transport medium alone or transport medium with 2μM GF120918, a potent inhibitor of P-gp. Efflux of a range of substrates across the confluent monolayer of cells was measured in both directions, that is, apical to basolateral (A>B) and basolateral to apical (B>A) in the presence and absence of GF120918. 0.5 mCi/mL ^{3}H-amprenavir, ^{3}H-quinidine, or ^{3}H-loperamide was added to each respective substrate concentration to allow quantitation of efflux from donor to receiver chambers. Lucifer yellow (100μM) was added to the donor chamber to monitor integrity of confluent cell monolayer. 25 μL samples were taken over a period of 6 hours, from both donor and receiver chambers into 96-well Lumaplates, dried overnight and the radioactivity counted by TopCount Model 9912 (Perkin Elmer, USA). The initial concentration measurement was taken at 6 min after the addition of substrate in the first well (23, 24) and subsequent measurements taken at multiple time points up to 6 hours for all experiments (24). After taking a 25 μL aliquot, the plates were replaced in a shaker at a speed of 30 rpm, at 37°C in 5% CO_2. Fluorescence of lucifer yellow (Ex max = 438nm, Em max = 530nm) was measured at time zero from aliquots taken directly from the vials and compared to samples taken after 6 hours from both the basolateral and apical chambers into transparent bottom 96- well plates. The fluorescence was analyzed using a SpectraMax microplate reader. Passive permeability of lucifer yellow was always <20 nm/s over the 4 hr experiment.

Inhibition studies with two substrates. Cells were seeded and fed as described above and on the day of the experiment culture medium was removed by aspiration. The cells were then preincubated with the inhibitor/substrate in both chambers for 30 min. Note that all inhibitors used here are also P-gp substrates. During the preincubation, half the wells receive inhibitor solution without GF120918 (to study active transport) and the

other half receives inhibitor solution with GF120918 (to study passive transport). After 30 minutes, the preincubation solutions were removed by aspiration and the labeled substrate was added to the donor chamber, while refilling fresh inhibitor solution in both chambers, again one half without GF120918 and the other half with it.

For quinidine efflux experiments using the fluorescent compounds Hoechst 33342 or rhodamine 123 as the inhibitor, the same protocol was followed. Initially, Hoechst 33342 was dissolved in distilled water and rhodamine 123 was dissolved in absolute ethanol. Cells were pre-incubated for 30 minutes with a solution of the fluorophor in transport medium with and without GF120918 to study passive and active transport respectively. The maximum ethanol concentration in the rhodamine transport media was $<0.1\%$. Both basolateral and apical chambers received the same pre-incubation solution. After 30 minutes, the preincubation solution was aspirated. Donor solutions contain appropriate concentrations of quinidine and both chambers received a fresh refill of the fluorophor, with and without GF120918. Inhibition of quinidine efflux by either of these fluorophores was studied over a period of 6 hours. The radioactivity from the aliquoted samples was read using a TopCount Model 9912. Lucifer yellow was present in the donor solutions in all cases. For the rhodamine 123 inhibition of quinidine efflux, lucifer yellow was used since fluorescence from rhodamine 123 has a significant fluorescence spectra overlap. However, the continuity of the kinetic trace of quinidine transport over 6 hours showed that the monolayer remained intact.

Transport studies were done with rhodamine 123 following the same protocol as all single substrate transport assays. The 25μL aliquots at specific time points were collected in transparent bottom black-sided 96-well Costar plates and fluorescence from the aliquots was read in a Cytofluor fluorescence plate reader at Excitation wavelength of 485nm and Emission wavelength of 530nm with a bandwidth of 20nm.

Cell stability and substrate metabolism. We showed that the stability of the cell

monolayer and plasma membrane with respect to passive and active transport was not affected by the prolonged exposure times to amprenavir for at least 6 hr (data not shown; 24). It was also shown that metabolism or decomposition was insignificant for amprenavir, quinidine and loperamide on this time scale using radio-HPLC (data not shown).

Numerical integrations. We used the stiffest integrator in MATLAB, ode23s, with absolute and relative tolerances set between 10^{-8} and 10^{-10}, depending upon the data being analyzed (24). Other MATLAB integrators, while faster, were not accurate enough at the later times of simulations. In data fitting, all concentration curves are simultaneously fitted, so that despite the fact that the A:B>A curve, i.e. substrate concentration in the apical chamber when the basolateral chamber is the donor, is the most visually striking, all curves contribute to minimizing the difference between data and simulated curve. MATLAB fminsearch minimizes the coefficient of variation between the data and the simulated curves. Further details can be found in (24) and (31).

Mass Action Kinetic Model

Figure 1 is a cartoon of a confluent cell monolayer, showing the polarized MDCKII-hMDR1 cells, where the basolateral membrane is attached to the polycarbonate filters and P-gp (upward arrows) expressed on the apical surface (32). The apical and basolateral chambers are kept separate by the tight junctions. Active transport by P-gp occurs vectorally, with substrate binding to a site on P-gp within the apical membrane inner monolayer and with efflux into the apical chamber (6, 24, 27, 33). For many substrates, including those we use, passive permeability is a significant fraction of total transport and is quantitatively analyzed separately using a potent P-gp inhibitor, GF120918 (23, 24).

With the confluent cell monolayer system, we measure the concentration of substrate in the apical chamber, denoted C_A, and the basolateral chamber, denoted C_B. However, the concentration of substrate in the cytosol, denoted C_C, and in the inner plasma membrane in contact with the P-gp binding site, denoted C_{PC}, cannot (yet) be measured rigorously in real time. These internal concentrations are variables of a mass action model and fitted by elementary rate constants for well-defined kinetic barriers, according to the measured values of C_B and C_A over time (24).

Previously, we have fitted the P-gp elementary rate constants, the passive permeability coefficients across the cell monolayer and estimates for partition coefficients for three P-gp substrates: amprenavir (an HIV protease inhibitor), quinidine (a Na+ channel blocker), and loperamide (an antidiarheal drug), chosen because of their very distinct behaviors as P-gp substrates (24). P-gp was modeled by the simplest mass action reaction (8, 17, 24, 34), where the binding reaction takes place within the apical membrane inner monolayer (27, 35):

$$T_0 + C_{pc} \underset{k_r}{\overset{k_1}{\rightleftarrows}} T_1 \xrightarrow{k_2} T_0 + C_A \tag{9.1}$$

where T_0 is the empty transporter, C_{PC} the substrate in the apical membrane inner monolayer, T_1 is the transporter bound by substrate and C_A the substrate after efflux into the apical chamber. The elementary rate constants which we seek to fit are: k_1, the association rate of the substrate to P-gp from the inner apical monolayer; k_r, the dissociation rate constant of substrate from P-gp back into the inner apical membrane; and k_2, the efflux rate constant of the substrate from P-gp into the apical chamber. We calculated the binding constant of a substrate to P-gp, relative to being in the inner apical monolayer, by the ratio of the fitted association rate constant, k_1, and the fitted dissociation rat constant, k_r, i.e. $K_C = k_1/k_r$, which is shown in Table 2 below. This means that our binding constants are for the binding sites connected to the efflux pathway. Since these binding constants are relative to the bilayer of the apical plasma membrane, they must be multiplied by the appropriate partition coefficient to get the value relative to the aqueous phase.

This reaction model has a single efflux pathway per P-gp. While it is known that P-gp can bind more than one substrate molecule, Tran et al. (24) showed that with a single substrate, since the rate constant of association, k_1, was so large, the predicted efflux curves were the same whether there was one or two or, presumably, more efflux pathways in P-gp. Basically, if the binding site for one efflux pathway were filled by the substrate, then "all" sites would be filled. Thus, the number of kinetically functional efflux pathways can be probed only with the simultaneous usage of two, or more, different substrates.

The confluent cell monolayer is a challenging system to use when the aim is to obtain the elementary rate constants for P-gp activity. However, we found for this system that the standard steady-state Michaelis-Menten analysis for P-gp efflux, while commonly used and typically yielding "good fits" to data, does not provide anywhere close to accurate estimates for the Michaelis constant K_M (31). This was because the passive permeability across the cell membranes becomes convolved in the fitting of the K_M value, with no ob-

vious means to de-convolve the two parameters. This suggests that classifications of P-gp transport inhibition based upon the classical Michaelis-Menten steady-state kinetic formalism in other expression systems, reviewed in (13,14), should be reevaluated to confirm that the analysis is valid in the expression system used.

Results

Amprenavir transport inhibited by quinidine. Figure 2 shows the passive and total transport, which equals passive+active, of 100 μM amprenavir, initially in the donor chamber across the MDCKII-MDR1 cell monolayers, inhibited by increasing concentrations of the P-gp substrate quinidine. The passive permeability was determined in the presence of 2 μM GF120918, a potent inhibitor of P-gp (23, 24, 36, 37). As expected for a static passive barrier (23), when active efflux is inhibited with GF120918, the nmol of quinidine transported is symmetric (i.e. the same for B>A and A>B) over time, as shown by the closed symbols.

Without GF120918, P-gp increases total amprenavir transport in the B>A direction and decreases of total transport in the A>B direction. Quinidine, a P-gp substrate, was used as the inhibitor over the concentration range of 1-10 μM. Quinidine is pre-incubated with the cells, in both chambers, for 30 min before the chambers are emptied by aspiration and fresh quinidine is added to both chambers, along with radiolabelled amprenavir added to the donor chamber. Thus, during the amprenavir transport, the quinidine concentration is maintained close to the concentration initially added, despite its own transport by P-gp. Clearly, the active transport of amprenavir is inhibited by increasing quinidine concentrations.

Passive permeability is time dependent and is not affected by inhibitors. Tran et al. (23) derived an exact equation for calculating the passive permeability coefficient at multiple time points, even when there is loss of substrate into the cells, e.g. due to binding to intracellular components. Figure 3 shows the passive permeability coefficient for quinidine over time in the presence of many amprenavir or loperamide concentrations, as well as with GF120918. We have aggregated all passive permeability coefficients for the for 0.1-5μM quinidine data in both directions, B>A and A>B, either alone or with

inhibitors: amprenavir (50 and 100μM) or loperamide (0-10 μM). There are 34 different data sets represented in this figure.

Clearly the passive permeability coefficient of quinidine increases for the first hour of transport and is basically constant thereafter, where the arrow shows the steady-state passive permeability coefficient across the confluent cell monolayer to be about 500 nm/s in both transport directions. There is no significant dependence on inhibitor concentration or the direction of transport. The same basic results were found for amprenavir passive permeability coefficient in the presence of quinidine, which increased for the first 0.5 hr before reaching the steady state (data not shown; 24).

For amprenavir and quinidine, this early time dependent increase in the passive permeability coefficient is not due to substrate "loading" into the cells, since there is no significant loss of these substrates into the cells (data not shown; 23, 24). The change occurs on the time scale of plasma membrane recycling and may be due to changes in cell membrane area or cell microvilli morphology, as discussed below and in Tran et al. (23). This is true because the passive permeability coefficient we calculate is per unit area of insert of the Transwell apparatus, i.e. 1.13 cm^2. For the fitting of P-gp transport, this is not a problem, since the passive permeability is fitted independently, in order to accurately calculate the active transport due to P-gp.

Loperamide's passive permeability coefficient shows an asymmetric time dependent change, with a greater increase for A>B than B>A, which appears to be coupled with its absorption within the cells (data not shown; 23). However, the presence of quinidine did not affect the time dependence of the change of loperamide's passive permeability coefficient. We conclude that the presence of these inhibitors, at the concentrations used, do not significantly affect the (time-dependent) passive permeability coefficients of substrates through the confluent cell monolayer, which certainly implies that they do not affect the bilayer structure significantly.

Inhibition as measured by IC50. We began the analysis of substrate inhibition of P-gp in a semi-quantitative way. Inhibition is typically represented by a curve showing the reduction of P-gp specific transport at a particular time versus the inhibitor concentration. In the B>A direction, P-gp transport is defined as the total nmol transported, solid lines in Figure 2, minus the passive transport (+GF120918), dotted lines in Figure 2. This P-gp specific transport is normalized by dividing each value by the value in the absence of inhibitor, yielding the fraction of P-gp transport. Thus, in the B>A direction, the fraction of P-gp transport is 1 without inhibitor and decreases as the inhibitor concentration increases. The inhibitor concentration at which the fraction of P-gp transport is 0.5 is defined as the IC50. In the A>B direction, this calculation would give negative numbers, since P-gp inhibits total transport, so we used the absolute value to show the fraction of P-gp transport.

We have collected our measured IC50 values in Table 1, measured after 2 hours of transport, which looks basically the same as the curves calculated at 4 hours of transport. It is important to note here that these times are chosen to focus on steady state P-gp transport. For the substrates we use with the confluent cell monolayer, it requires 1 to 3 hours for binding to P-gp to reach steady state (24, 31). Using shorter times for "initial rates", predominantly measures just the passive permeability coefficients. This semi-quantitative analysis has been done for each of the P-gp substrates we use and they all can inhibit each other. For the transport of loperamide, inhibition by quinidine in the B>A direction has an IC50 in the range of 5-8μM quinidine, but in the A>B direction, inhibition seems to stall around a fraction of 0.5 for 10-30 μM quinidine, suggesting a more complex interaction for loperamide with P-gp and the cells. Our IC50 values agree with those published in Rautio et al. (25).

Ling and co-workers have made the case that Hoechst 33342 and rhodamine 123 bind to different sites in P-gp and that rhodamine 123 binding can enhance the efflux of Hoechst

33342 (15, 35, 38). Their studies used plasma membrane vesicles purified from P-gp expressing CH*B30 cells. The membrane vesicles were assayed to be about 50% inside out, so the fluorophores would not have to pass through a bilayer to reach the P-gp binding site of these vesicles, i.e. within the cell's inner monolayer of its plasma membrane. We found that Hoechst 33342 inhibited quinidine with an IC50 which was about the same as quinidine's own IC50 for amprenavir and loperamide.

On the other hand, we found no inhibition of quinidine transport with up to 100μM rhodamine 123. Tang et al. (39) claimed that there were fluorescence quenching artifacts between Hoechst 33342 and rhodamine 123, which obscured the interpretations of the studies by Ling and co-workers. We measured the transport of rhodamine 123 across the confluent cell monolayer and found that its passive permeability coefficient is about 20 nm/s B>A and 10 nm/s A>B, i.e. more than an order of magnitude smaller than quinidine, Fig. 2, and close to values reported by Tang et al. (39). This implies that it would take over 24 hours for 50% transport to occur (23). This is not a reliable experiment to follow with this cell line, since is it enough time for these cells to start overgrowing themselves and obscuring the analysis. Interestingly, because the intracellular volume of the entire confluent cell monolayer is so small, crudely estimated at 1μL (24), the intracellular concentration would be predicted to be essentially the same as the donor side concentration after 2 hrs, using the equations in Tran et al. (23), although this would be difficult to prove.

We also found that the transport of rhodamine 123 was enhanced over passive permeability in the B>A direction, which would be expected if it were a P-gp substrate. However, there was no inhibition of transport in the A>B direction, as would be expected if it were not a P-gp substrate. The ambiguity of these findings will require additional work, beyond the scope of this study.

These IC50 analyses show that each of the P-gp substrates we use can inhibit the other,

but that proves nothing about the inhibition mechanism. Since we have shown for the confluent monolayer system that the classical Michaelis-Menten analysis cannot predict K_M values to better than 1-3 orders of magnitude (31), there is no reason to assume that the canonical textbook Lineweaver-Burke or Eadie-Hofstee curves for competitive, uncompetitive and/or mixed competition are applicable to the confluent cell monolayer system. Instead, we will pursue the question of mechanism with a rigorous analysis of the mass action transport by P-gp.

Inhibition as measured by mass action kinetic analysis of a 1-site model for P-gp. Our current P-gp transport model only has a single binding site for P-gp (24, 31). However, writing a two-binding site model and fitting the data does not prove that the model is correct, since more parameters will be available to fit the data. More importantly, writing such a model and implementing it requires a clear idea of the most important molecular parameters. With this in mind, here we are asking the simpler, but essential, question of what kind of mechanisms can be tested by a one-site model. This is a prerequisite to writing a minimal 2-site model, i.e. the one that captures the important mechanisms with the fewest number of parameters. Since we use only P-gp substrates, neither uncompetitive nor mixed-type competition are relevant, as defined by the classical Michaelis-Menten analysis. Basically, there are two classical Michaelis-Menten mechanisms and one other mechanism that can be tested against the data:

1. Competitive inhibition: Inhibitor replaces the substrate in "the single" P-gp binding site. This is the simplest case expected for combinations of substrates. When transport data fits this model it does not prove that P-gp has only one binding site.

2. Noncompetitive inhibition: All P-gp bound initially to inhibitor is thereafter "inactivated", since inhibitor concentration is constant throughout our experiments. This classical mechanism is simple to test, but it is rare with soluble enzymes. The

transport data present here is nowhere near the predictions from this mechanism and we will not consider it further.

3. No Inhibitor Effect: Despite substantial transport of the inhibitor, there is no effect on substrate transport. Setting the inhibitor concentration to zero in the simulation of substrate transport tests this mechanism, i.e. ignoring its presence and its known P-gp mediated efflux. This is direct kinetic evidence of substrate and inhibitor being effluxed by independent pathways within P-gp, under the specific conditions used. This caveat is very important, because it foreshadows our finding that the "mechanism" will shift according to pathway occupancy. This mechanism has also been called noncompetitive in the transport literature. We believe the nomenclature used here is less likely to be confused with mechanism 2, above.

For this study, we have refitted all of the elementary kinetic parameters for single substrate studies of amprenavir (AMP), quinidine (QND) and loperamide (LPM) using new data. Since Tran et al. (24) described the kinetic analysis in detail, we will only discuss the outcomes. The fitting algorithm developed in Tran et al. (24) finds all of the possible values of the parameters {T(0), k_1, k_r, k_2} which can best fit the data for each of the substrate concentrations used. T(0) denotes the initial density of efflux active P-gp, Not surprisingly, there are many different combinations which give essentially the same best fits to the data, but they are clustered into a compact set, i.e. a seemingly random collection of equally good fitting parameters within a closed area, which is a benchmark for the validity of this kinetic analysis, as shown in Figure 4.

Figure 4 shows the final fitting for the best fit {T(0), k_1 } pairs found in this study for amprenavir transport, without any inhibitor. This different colored symbols denote different amprenavir concentrations, from many separate experiments. The subset of {T(0), k_1} pairs within the blue box, which looks like a tilted trapezoid, fit all of the

substrate data equally well and are called the consensus fits (24). The pairs outside of the box only fit the data for some substrate concentrations. Values of the association rate constant $k_1 > 1\text{x}10^{10} M^{-1}s^{-1}$ are excluded because that is at or near an upper bound for substrate lateral diffusion through the bilayer (24). P-gp densities above 8000 P-gp/μm^2, or 0.01 M in the apical membrane (see footnote b in Table 2), are excluded because that would require the plasma membrane be entirely covered by close packed P-gp (24). P-gp densities below 1 P-gp/μm^2, i.e. 4 orders of magnitude lower than the maximum, are excluded as being too small. Otherwise, the fitting algorithm has no constraints.

The blue arrows in the "center of the box" show the values for each parameter which are the values shown in Table 2, only to 1 significant digit. All of the fitted parameters come from the "center of the box" of parameter values for the substrates tested, with a range of about a factor of three for T(0) and the rate constants (see below). More precise estimates are limited by experimental error and computational expense. These values are quite adequate for our purposes here and are best fits for the data.

From Table 2, we see that the efflux active density of P-gp, T(0), is independent of the substrate, which was a crucial test of the model and the fitting algorithm, since it should not depend on the identity of the substrate (24). The association rate constant, k_1, is also independent of the substrate, which agrees with the open structure of P-gp for substrates with similar molecular weights (24, 40).

On the other hand, the efflux rate constants, k_2, the passive permeability coefficients in both directions across the confluent cell monolayer, P_{BA} and P_{AB}, the binding constants to P-gp from the inner apical monolayer, K_C, and the partition coefficients, K_{PC}, are all substrate specific, as expected.

In the column showing the binding constants of the substrates to P-gp, there is also shown an effective aqueous dissociation constant for each substrate, $K_{D,Aq}$, which is calculated as the inverse of the product of the binding constant times the partition coefficient

to the liposomes, composed of 1/1/1::PE/PS/chol as the mimic of the inner apical monolayer. It estimates the aqueous concentration expected to give 50% binding to P-gp, in the absence of inhibitor. This number is not near the steady state K_M that would be fitted using a standard Michaelis-Menten steady state analysis (31), because that analysis doesn't work for the confluent cell monolayer. These effective dissociation constants are 20-100 times smaller than the IC50 values shown in Table 1, showing that the IC50 cannot predict the dissociation constant of the substrate when it is used as an inhibitor. For the confluent cell monolayer, an IC50 is purely phenomenological and dependent upon many factors besides the substrate binding constant, e.g. the substrate passive permeability. This result will be elucidated in a separate study.

There are two significant differences between some of these values and those published in Tran et al. (24). The first difference is minor, in that the binding constants for loperamide and quinidine to P-gp found here are just above the upper bounds found in Tran et al. (24). The values quoted here fit all of the data better.

The other difference is physiologically quite interesting. In Figure 4, the shape of the consensus box for the $\{T(0),k_1\}$ pairs is somewhat different than that found in Tran et al. (24), which yields roughly a 2-3 fold larger estimate for the center of the box value for the density of efflux active P-gp, T(0), while the estimate for k_1 is essentially the same. In addition, the passive permeability coefficients for all three substrates are roughly 2-3 fold larger than reported in Tran et al. (24). The similar increase in two biophysically "unrelated" parameters suggests a common mechanism. These differences do not affect our analysis of the inhibition mechanism, but they are very important for the *in vivo* activity of P-gp, which will be discussed below. This kinetic modeling is providing a high resolution view of the transport data and can uncover differences which would be very difficult to notice or prove otherwise.

For the inhibition experiments, the inhibitor is preincubated with the cells in both

chambers for 30 min before the substrate is added to the donor chamber, with a refreshment of the inhibitor concentration in both chambers at that time to ensure that transport of the inhibitor does not change its concentration dramatically during the transport experiment. A crucial part of the fitting process is using the passive permeability coefficients at all time points to correct the total transport for the contribution of passive permeability. As explained in Tran et al. (24), this correction must be done within the mass action equations for transport, rather than simply subtracting the nmol transported passively from the total nmol transported, which neglects transport reversibility. All these passive permeability coefficients increase in time until a steady state is reached, as shown in Figure 3 for quinidine. For fitting active transport, we use the individual values for each time point, e.g. up to 1 hour for quinidine, until the steady state is reached. Thereafter, the average value within the steady state period is used, as shown in Figure 3 for quinidine by the arrow at about 500nm/s. This approach avoids fitting the noise of the passive permeability coefficient (24).

Competitive Inhibition versus No Inhibitor Effect. We can now move to the mechanism of inhibition of P-gp efflux by P-gp substrates. These data will be shown as the substrate concentration over time in both chambers, since this is the form of the data actually being fitted. The different concentrations are labeled in the figures by a short notation. For example, A:B>A is read as the concentration of substrate in the Apical chamber when the Basolateral chamber is the donor and the Apical chamber is the receiver.

Figure 5 shows a sample of the data and fits for the P-gp mediated transport of quinidine when amprenavir is the inhibitor. Figure 5A shows 0.3μM quinidine transport in the presence of 100μM of the inhibitor amprenavir. Data are shown by the symbols with error bars defined by the standard deviation of triplicate measurements. All simulations used the single substrate parameters shown in Table 2, i.e. there is no fitting of these data

with inhibitor. The solid lines show the case where binding to the "single P-gp site" is competitive, using the binding constants shown in Table 2. The dashed lines show the case where there is no inhibitor effect, i.e. the concentration of amprenavir is set to zero in the simulation of the dashed line in the figure. This is equivalent to amprenavir following a different efflux pathway within P-gp than the one used by quinidine. Clearly, competitive inhibition fits the data much better than the no inhibitor effect curve. Note that the color of the data, blue for basolateral and red for apical, must match the color of the simulation curves for the data to fit. Likewise the data symbols must match, with squares for B>A flux, where the basolateral chamber is the donor, and triangles for A>B flux, where the apical chamber is the donor.

Competitive inhibition is the simplest expectation for two substrates. This does not prove that P-gp has only one efflux pathway. Doubling the number of "competitive" pathways in P-gp would have little effect on the total transport because one of the most important fitted parameters is the product of the efflux rate constant and the density of efflux active P-gp, k_2T(0), which is the equivalent of Vmax in the language of the Michaelis-Menten analysis (24). This parameter is very tightly fixed (24), so that if we simply proposed that P-gp had twice the number of pathways, the efflux rate constant k_2 would become half as large as that shown in Table 2. This makes sense, since the overall substrate efflux would be the same in both cases and that is what is being fitted.

Figure 5B shows the data and fits for the P-gp mediated transport of 0.3μM quinidine, now in the presence of only 50μM of the inhibitor amprenavir, i.e. half the concentration as in Figure 5A. If quinidine and amprenavir still competitively bind to the "single P-gp site", then the solid curves should fit the data just as well as the case above. The fact that less amprenavir and more quinidine would be bound is taken into account by the equations for competitive inhibition. Remarkably, the data is fitted better by the case of no inhibitor effect. It is important to pay attention here to the donor side curves, B:B>A

and A:A>B, where the no inhibitor effect simulations predict a slower loss of quinidine from the apical donor side than for the basolateral donor side, which is what the data shows. The competitive inhibition simulations predict the same rate of quinidine loss from both donors, which was what was observed in Figure 5A with the larger amprenavir concentration, but not with 50μM amprenavir.

Before continuing, it is important to explain that we decided to use this plot format because it can prove mechanism most compactly. The conventional plot of nmol transported per μM of inhibitor will show inhibition only at adequately high concentrations, regardless of whether inhibition is always competitive or there is no inhibitor effect at the low concentrations. If binding is competitive, then inhibition will only occur when enough inhibitor had bound to replace some bound substrate. However, if the mechanism transitions from no inhibitor effect to competitive once the "amounts bound" exceed some limits, which is the case here, then the conventional curve will show no inhibitor effect until the mechanism shifts over to competitive inhibition. The qualitative inhibition curve will look the same, except that the "binding constant" of the inhibitor will appear weaker than it actually is. In order to prove that no inhibitor effect occurs, it must be shown that the amount of inhibitor needed to cause competitive inhibition is greater than that predicted by the independent binding constants. The plot format we use shows this comparison simply and directly.

We will see below that there is substantial amprenavir transport by P-gp under similar conditions, thus this P-gp mediated transport of amprenavir must be through a different pathway than that used by quinidine here. All of the combinations of concentrations shown in Table 1 have been analyzed. The data presented in the figures were picked to show roughly the minimal concentrations needed to provide competitive inhibition and the maximal concentrations allowed to show no inhibitor effect. The message is simple. When the substrate and inhibitor concentrations are both small enough, there is no inhibitor

effect, despite the fact that there is P-gp mediated transport of the inhibitor transport. For example, Fig. 6A below, 50μM amprenavir shows substantial transport in the presence of 2μM quinidine, i.e. 7 times more quinidine than in Fig. 5B.

The next result is even more interesting. Figure 5C shows the data and fits for the P-gp mediated transport of 3μM quinidine, i.e. a 10-fold increase of the substrate concentration with the same 50μM of amprenavir as the inhibitor. Here the best fit is back to competitive inhibition. So when amprenavir is relatively saturating of P-gp, 100μM versus 50 μM, or quinidine is relatively saturating of P-gp, 3μM versus 0.3μM, then the inhibition is competitive. An increase in substrate concentration, 0.3 to 3 μM quinidine, causes the inhibitor, 50 μM amprenavir, to transition from no inhibitor effect to competitive inhibition. This novel result proves that the binding sites for efflux pathways are cooperative, as shown in the Appendix-Supplementary Material (`http://pubs.acs.org/subscribe/journals/bichaw/suppinfo/bi060593b/bi060593bsi20060919_032146.pdf`). So we are seeing a mixing of mechanisms driven by binding site occupancy.

Here we want to show other substrate combinations to determine the generality of this observation. Figure 6 shows the data and fits for the P-gp mediated transport of amprenavir when quinidine is the inhibitor. Figure 6A shows the data and fits for the P-gp mediated transport of 50μM amprenavir in the presence of 2μM of quinidine. The best fit is for no inhibitor effect. So even 2 μM quinidine is not enough to yield competitive inhibition. However, as shown in Figure 6B, the P-gp mediated transport of 50μM amprenavir in the presence of 5μM of the inhibitor quinidine is mostly competitive. So the transition from no inhibitor effect to competitive inhibition is gradual rather than abrupt, at least on a population average.

We now turn to loperamide, which appears to have a more complex interaction with these cells than quinidine and amprenavir (23, 24). Figure 7 shows the data and fits for the P-gp mediated transport of quinidine when loperamide is the inhibitor. Figure 7A shows

the data and fits for the P-gp mediated transport of 1μM quinidine in the presence of 2μM loperamide. The best fit is for no inhibitor effect. Figure 7B shows the data and fits for the P-gp mediated transport of 3μM quinidine in the presence of 10μM of the inhibitor loperamide. The best fit is competitive. We also studied the P-gp mediated transport of 50 and 100μM amprenavir when loperamide is the inhibitor. There was no inhibitor effect with 50μM amprenavir inhibited by 1 μM loperamide and competitive inhibition with 2-10 μM loperamide. The transport of 100 μM amprenavir was competitively inhibited by 1-10 μM loperamide (data not shown).

Loperamide is inhibited by quinidine, however the inhibition was incomplete in the A>B direction, Table 1. Complete inhibition of P-gp mediated transport of loperamide can only be achieved with very high quinidine concentrations, >20μM, where there is little P-gp mediated transport (data not shown). This suggests that loperamide has an additional interaction with these cells and/or P-gp beyond those that are well modeled for amprenavir and quinidine, as noted previously in Tran et al. (24). Our current hypothesis is that there is another transporter in the basolateral membrane, which admits loperamide and which is completely inhibited by GF120918. Since the cell line used is canine kidney epithelial, there are many candidates (41). We can say that quinidine and amprenavir have no significant interaction with this putative transporter, at any concentration used (data not shown). When loperamide is an inhibitor, the putative transporter only makes more certain that the preincubation achieves steady state in loperamide. We will present the inhibition of loperamide transport by these other P-gp substrate in a separate paper, since this is outside the scope of this work. The bottom line is that the existence of this putative loperamide transporter does not affect our conclusion that P-gp has multiple pathways, at least for amprenavir and quinidine.

Discussion

It is known that P-gp can bind more than one substrate at a time (13, 14). However, Tran et al. (24) showed that the efflux kinetics of a substrate, without any inhibitor, was predicted to be the same whether each P-gp had one or two efflux binding sites. Because the association rate constant to P-gp was so large, effectively lipid lateral diffusion controlled, if one site was occupied, then all sites were occupied. Equilibrium binding and/or ATPase activity could not have predicted this. To understand the activity of P-gp efflux with the confluent cell monolayer, the mass action kinetics of efflux must be studied directly and rigorously, i.e. not with the steady-state Michaelis-Menten equations (31). In order to determine the number of efflux pathways of P-gp, it is necessary to use more than one substrate at a time.

Inhibition of P-gp by its substrates and modulators has been intensely studied, as reviewed by Lugo & Sharom (13) and Loo & Clarke (14). From many assays, including transport, it has been found that some pairs of substrates do not compete with one another, at the particular concentrations studied, which has been called a noncompetitive interaction. We define this mechanism as no inhibitor effect, so as not to confuse it with the classical noncompetitive inhibition mechanism for enzymes. This observation lent support to the work of Ling and co-workers, who have made the case that Hoechst 33342 and rhodamine 123 are P-gp substrates which bind to different sites in P-gp and that rhodamine 123 binding can enhance the efflux of Hoechst 33342, suggesting distinct pathways through P-gp (15, 35, 38; see also 27 and 39). Additional quasi-independent pathways have been proposed (42). Of course, there may be other binding sites for modulators of P-gp activity that do not lead to efflux of that modulator.

For single substrates, we show binding constants to P-gp from the inner apical monolayer in Table 2. In fact, these binding constants were calculated from ratio of the fitted

values of the association rate constant k_1 and the dissociation rate constant k_r, from P-gp back into the inner apical monolayer, i.e. $K_C = k_1/k_r(M^{-1})$. This means that the binding constants we measured are for the binding sites of the efflux pathways.

Our analysis yields a fairly simple picture of substrate binding and efflux for P-gp, at least for quinidine and amprenavir, as well as inhibition by loperamide, a trio of drugs chosen solely because of their different behaviors as P-gp substrates (23, 24). Using the elementary rate constants fitted for these substrates alone, we found that at "high" concentrations of substrate and/or inhibitor, the substrate efflux curve was fitted very well with the sole assumption that substrate and inhibitor competed for the "single" P-gp binding site. The fit does not imply that each P-gp has only one binding site, but only that all sites behave as though they are independent at the substrate and inhibitor concentrations used.

At low concentrations of substrate and inhibitor, the efflux of the substrate was unaffected by the presence (and efflux) of the inhibitor. Under these conditions, we found that the efflux of the substrate was still quantitatively predicted using the elementary rate constants fitted for each of the substrates alone, with the sole assumption that inhibitor did not bind to the substrate's "single site", i.e. it must use another site and efflux pathway. This proves that P-gp has two or more efflux pathways. The gradual transition from no inhibitor effect to competitive inhibition as the concentration of either substrate or inhibitor increases suggests that both substrate and inhibitor can bind to all the efflux connected binding sites, as their individual binding constants prescribe. It has been proposed that these binding sites are flexible or to some extent inducible (43). We will need to build the 2-site efflux model to fit and simulate the gradual transition from no inhibitor effect to competitive inhibition to better understand the mechanistic implications of this finding.

It is very important to mention that the ability of the one site model to fit the compet-

itive inhibition data is a strong validation of our kinetic model and fitting algorithm. The analysis presented in Tran et al. (24) is rather complex within the field of P-gp transport kinetics. That was a consequence of our belief that a clear understanding of P-gp efflux activity *in vivo* could only come from applying the most rigorous kinetic analysis to the most physiologically relevant expression system. The fact that the density of efflux active P-gp in the cell membrane was found to be independent of substrate type was required if the model and the fitting algorithm were valid. The lipid lateral diffusion controlled value of the association rate constant, k_1, was also independent of substrate type, which agrees with the predicted openness of the structure of P-gp within the plasma membrane (24, 40).

However, since the fitted value of k_2 is different for each substrate, it could be argued that the parameter we fit is not really the efflux rate constant from P-gp, but rather represents a distinct and unknown barrier for each substrate. We just fit a parameter in an equation, which does not prove the parameter is the claimed rate constant for P-gp efflux. There are good reasons why our assignment of k_2 to the efflux rate constant of P-gp is reasonable (24), but that does not eliminate the question. Since we are fitting 3 rate constants and a P-gp membrane density simultaneously, such an argument must be constantly checked against the data.

The fact that the single substrate parameters for amprenavir and for quinidine can quantitatively fit the competitive inhibition data would be hard to explain if the fitted k_2 were not the P-gp efflux rate constant for each substrate. It is nearly certain now that the fitted k_2 must come from the same barrier for all three substrates. The fitting process is so blind and so exhaustive, leaving no potential fit undiscovered, that we are now far more confident that the k_2 we fit is the efflux rate constant for P-gp.

Spoelstra et al. (16) found evidence of inhibitor concentration affecting the "mechanism" of P-gp efflux. They studied the interaction of daunorubicin with verapamil, both

P-gp substrates, in multidrug resistant cell lines grown as a monolayer on plates and fitted their data with a Michaelis-Menten steady-state model for no inhibitor effect, using our terminology. However, at a higher daunorubicin concentration there was a shift away from this model. They proposed two daunorubicin binding sites in P-gp, with verapamil binding to the weaker site, so that high concentration of daunorubicin would be required to competitively inhibit verapamil transport.

What do our kinetic findings about transport tell us about the interaction between the efflux binding sites, i.e. cooperativity? The key observation was that increased substrate concentration causes the inhibitor to increase its competitive inhibition of substrate transport. Without inhibitor, increased substrate concentrations do not "inhibit" transport in any way, as shown here and in Tran et al. (24). A single binding constant and a single efflux rate constant fits all the substrate concentration curves. Of course, this must not be confused with the fact that P-gp mediated transport does become saturated with increased substrate concentration, thus making the fraction of total transport due to P-gp smaller relative to passive permeation. The transition from no inhibitor effect to competitive inhibition means that the efflux of substrate is less than it would have been without inhibitor.

Basically, the increased substrate concentration must increase the efficacy of the inhibitor either through the binding constants, $K_C = k_1/k_r$, or the efflux rate constants, k_2. Obviously, an increase in substrate concentration must cause an increase in the amount of substrate bound. If the efflux rate constants, k_2, are responsible for the transition to competitive inhibition, then bound substrate must inhibit the flow of other substrate molecules or enhance the flow of inhibitor molecules through the other efflux pathways, relative to having inhibitor bound to those other efflux binding sites. How this could happen, when substrate alone does not show the same effect, is very unclear. Any proposed mechanism along these lines will require a complex feedback loop and there is no data, or

theory, supporting such a concept at this time.

It is easy to believe that cooperative binding between the two, or more, efflux binding sites could cause the transition from no inhibitor effect to competitive inhibition with increased substrate concentration. To prove this, we have carried out a rigorous and general analysis of the 2-site binding model in the Appendix (which is posted in Supplementary Material).

Interestingly, many different combinations of positive and/or negative cooperativity can predict the increased inhibitory effect with an increased substrate concentration. This is an important finding in order for the binding model to be robust, since all the different pairs of P-gp substrates may have very different interactions within the binding pocket, see also (14).

While there has been much speculation about P-gp efflux cooperativity based upon equilibrium binding and/or ATPase activity, this is the first prediction about binding based upon efflux kinetics alone, insofar as we are aware. In fact, since our binding constants are obtained from efflux kinetics, they are for the efflux binding sites of the active P-gp in the plasma membrane. While the binding model analyzed here is "only" 2-site, which entails a fair amount of complexity, the rigorous analysis of a 3 or 4 site binding model would likely reach the same conclusion. It is interesting that recently published theoretical structures for P-gp only proposed two or three binding sites, while the binding pocket appeared to be fairly "crowded" with transmembrane helices (44, 45), providing ample possibilities for cooperativity.

This study provides important guidance for our construction of the 2-site transport model for P-gp, since we now know that cooperativity must be part of that model. The cooperativity terms in the model will not just be extra parameters for fitting the data, but rather will be required to fit the transition between no inhibitor effect and competitive inhibition observed for the substrates used here.

Now we can discuss our finding that two of the fitted parameters changed from values published in (24). We now find that the density of efflux active P-gp, T(0), is about 2-3 times larger and that the steady state passive permeability coefficient for all three substrates is about 2-3 times larger than the respective values reported in Tran et al. (24), as shown in Table 2. We note that k_1 and k_2 did not change significantly, strongly suggesting that the change is not in P-gp, per se. Cells in culture do change or respond to subtle changes in support composition (32) and the result we observe is really an example of the analytical power of our kinetic analysis. We know which parameters changed and by how much, which would not be possible using, for example, the Michaelis-Menten steady state equations (31).

Although the confluent cell monolayers were cultured the same way in all studies, to the extent possible, there was a hiatus of about a year between the end of data acquisition for Tran et al. (24) and the beginning of the studies reported here. The parameter values in Table 2 have been found consistently, e.g. Figure 3 incorporates 17 separate experiments completed over the course of more than a year. The fact that the P-gp efflux active density changed and that the passive permeability coefficients changed, and both changes are about the same magnitude, suggests that the simplest explanation will be one which affects both "equally". An increase in the expression level of P-gp is unlikely to change passive permeability coefficients, and vice versa.

The simplest explanation which ties the density of efflux active P-gp with the passive permeability coefficient is the random walk the substrate must make between the microvilli subsequent to leaving the outer apical monolayer, either by efflux by P-gp or by permeation through the bilayer or tight junction. Figure 8 shows a roughly scale model cartoon of a pair of microvilli, which are about 10 μm high, 1 μm in diameter and separated by 1μm.

By definition in the kinetic model, the P-gp which are efflux active are those which send their substrate directly into the apical chamber, where it equilibrates "instantly" between

the sampling volume of the apical chamber and the outer apical monolayer, according to the partition coefficients. Tran et al. (24) found that the surface density of efflux active P-gp was probably 10-20 times smaller than the total P-gp estimated in Ambudkar et al. (47) for a related cell line. While the cell lines were not identical and expression levels for our line have not been quantitiated, we felt the difference was significant and we hypothesized that only those P-gp at the tips of the microvilli will be efflux active for our fitting. This does not mean that the rest of the P-gp do not efflux, but rather the random walk of substrate released from P-gp into the aqueous space at the base of a microvillus will almost certainly encounter the same or a neighboring microvillus rather than escaping non-stop into the apical chamber. Absorption back into the outer apical monolayer and flip-flop into the inner apical monolayer would put the substrate back to where it started and the cycle would have to be restarted. Only those substrate molecules that are released from P-gp at or near the tips of the microvilli would have a reasonable probability of escaping directly into the apical chamber. Our current data increases the efflux active P-gp to about 3-10 times smaller than that estimated in (47) for the related cell line.

The 2-3 times larger steady state passive permeability coefficient for all three substrates reported here, relative to values reported in (24), can be explained by the same hypothesis. Recall that the passive permeability coefficients are calculated relative to the surface area of the plastic inserts the cells are grown on, i.e. 1.13 cm^2, since we cannot know the true membrane surface area (23, 24). A change in the cell monolayer surface area that can directly release substrate into the apical chamber will change the passive permeability coefficient we report. Obviously, microvilli morphology can change this true membrane surface area and the changes we see occur on the time scale of membrane recycling, e.g. Fig. 3 (48). Thus, in Figure 8, the diffusion pathway shown will also apply to a substrate released at the base of the microvilli by passive diffusion through the bilayer or

tight junction. Changes in the morphology of the microvilli would have to change both the number of efflux active P-gp and the passive permeability. It is difficult to conjure another mechanism that explains both changes so parsimoniously. If this hypothesis is correct, then the morphology of the microvilli is an important component of P-gp's *in vivo* activity, as well as for this cell line.

We have performed a simple test calculation for this hypothesis using a very simple model for the aqueous space between adjacent microvilli. We have simulated a random walk away from a square well sunk into an infinite plane, 1μm on all 4 sides and 10μm deep. The question is whether a particle released from the side of the well, like the side of the microvilli, will escape to the apical chamber or be reabsorbed into the wall or the plane. The test particle was released 1nm from the wall, or the plane, and its 3D random walk was followed until it hit another wall of the square well, the infinite plane or escaped into the apical chamber by reaching 10μm from the top of the plane. To get reliable statistics, we examined 108 test particle releases. Relative to the escape frequency from the plane 1um away from the edge of the well, like the tip of the microvillus, the probability of escape starting from the top edge of the well, midway between the corners of the well, was just 0.38. Particles which had entered into the well had a much smaller chance of eventually escaping than particles that never entered the well. This probability of escape was reduced nearly exponentially as the test particle was released further down the side of the well, mimicking being released from the sides of the microvilli, to 0.013 when release was 1μm into the well and to 0.00083 when release was 2μm into the well. Escape from the bottom of the well, like the release point shown in Figure 8, was at least 8 orders of magnitude less probable, i.e. not one out of 108 released particles escaped. It is a highly simplified model of escaping from the microvilli without being reabsorbed, but it shows that the basic hypothesis is physically sound.

Conclusions: We have three general conclusions about P-gp efflux kinetics. The

first is that the specific mechanism of binding and inhibition does not change the efflux kinetics of P-gp by a large amount, about 2-fold at most, as shown in Figures 5-7. The no inhibitor mechanism predicts greater efflux by P-gp than does the competitive inhibition mechanism, as it must. Based upon our findings and the literature, it seems that the general model for P-gp substrates moves from no inhibitor effect to competitive inhibition as P-gp becomes saturated with either substrate or the inhibitor. However, this difference appears not produce much selective pressure on P-gp to extend the concentration range wherein the no inhibitor effect operated and, thus, where the kinetics of substrate efflux would be somewhat larger.

The second general observation concerns the long-standing speculation about whether P-gp effluxes the substrate into the apical aqueous space or delivers the substrate in the outer apical monolayer as a flippase, followed by passive diffusion into the aqueous space, (14, 49). Our kinetic model for P-gp has efflux into the apical aqueous space with an instantaneous equilibration between the apical chamber and the outer apical monolayer, based upon the estimated partition coefficients, Eq. (1) and (24). If we had chosen to follow the flippase model, then what was delivered to the outer apical membrane would be instantaneously equilibrated with the apical aqueous chamber. The assumption of instant equilibration was based upon data showing that similar types of molecules bind to liposomes very rapidly, within seconds, compared with the kinetics of efflux over hours from the confluent cell monolayer (24). Explicitly including the kinetics of substrate permeation from the outer apical monolayer to the aqueous space of the apical chamber, or vice versa, would have doubled the number of mass action differential equations needed to fit the data, in order to fit these on and off rate constants to the bilayer. That would have been computationally too expensive.

Loo & Clarke (14) are quite right that determining which of these two mechanisms P-gp follows will require very rapid stopped-flow kinetic techniques. However, if P-gp

efflux is into the aqueous space, due to the initial ATP binding or its hydrolysis, then the mechanism of release is likely passive diffusion of the substrate out of the binding pocket subsequent to a decrease in its binding constant to P-gp. That means that after leaving the extracellular domain of P-gp, the "effluxed" substrate will be within a nanometer, or so, of the bilayer. The random walk back to the bilayer would be common, and not take long, according our simple random walk simulation described just above. Seen from the perspective of kinetics, there is very little difference between the two mechanisms. Our kinetic model fits the efflux data assuming a maximal recycling of substrate, where it is free to rebind to the outer apical monolayer as soon as it leaves P-gp. This shows, regardless of whether it is a flippase or a transporter, that P-gp protects the cell in part by keeping the xenobiotics occupied at the plasma membrane, as well as by facilitating their diffusion away from the apical bilayer of the cell.

Our fitted rate constants support this view of how P-gp does its job. Comparing the efflux rate constant, k_2, with the dissociation rate constant, k_r, shows that bound substrate is 10^4 - 10^5 times more likely to be released back into the inner apical membrane than being effluxed into the apical aqueous compartment. Since the association rate constant, k_1, is so large, rapid dissociation back into the membrane is required for P-gp to maintain relatively weak binding for a very broad class of substrates. This means that the selective pressure on P-gp, with respect to keeping xenobiotics out of the cytosol, is to keep k_2 larger than the passive permeation rate of the substrate through the inner apical monolayer into the cytosol. We do not know this permeability coefficient, but using the overall permeability coefficients shown in Table 2, we estimate the rate constant for release into the cytosol is at least an order of magnitude smaller than the efflux rate constants, k_2, shown in that Table.

The third general observation concerns the similarity of efflux mechanism between P-gp and the related multidrug resistance-related transporters, MRPs. Borst et al. (50)

review the current transport data of MRPs and favor a model in which the binding pocket can bind more than one ligand, allowing cooperative interactions between ligands, rather than the alternative model of requisite co-transport of two different ligands. The similarity with P-gp mechanism is clear.

References

1. Juliano, R.L. and Ling, V.(1976) A surface glycoprotein modulating drug permeability in Chinese hamster ovary cell mutants. Biochim. Biophys.Acta 455:152-162.

2. Dean, M., Rzhetsky, A. and Allikmets, R.(2001) The human ATP-binding cassette (ABC) transporter superfamily. Genome Res. 11:1156-1166.

3. Lown, K. S., Mayo, R. R., Leichtman, A. B.,Hsiao, H. L., Turgeon, D. K., Schmiedlin-Ren, P., Brown, M. B., Guo, W., Rossi, S. J., Benet, L. Z. and Watkins, P. B.(1997) Role of intestinal P-glycoprotein (mdr1) in interpatient variation in the oral bioavailability of cyclosporine. Clin. Pharmacol. & Therap. 62 (3):248-260.

4. Schinkel, A. H. (1998) Pharmacological insights from P-glycoprotein knockout mice. Intl J. Clin. Pharmacol. & Therap. 36(1):9-13.

5. Goh, L. B., Spears, K. J., Yao, D., Ayrton, A., Morgan, P., Roland, W. C. and Friedberg, T. (2002) Endogenous drug transporters in *in vitro* and *in vivo* models for the prediction of drug disposition in man. Biochem. Pharmacol. 64:1569-1578.

6. Borst, P. and Elferink, R. O. (2002) Mammalian ABC transporters in health and disease. Ann. Rev. Biochem. 71:537-592.

7. Gottesman, M. M. (2002) Mechanisms of cancer drug resistance. Annu Rev Med. 53:615-27.

8. Ambudkar S.V., Kimchi-Sarfaty, C., Sauna, Z.E. and Gottesman., M. M. (2003) P-glycoprotein: from genomics to mechanism. Oncogene. 22:7468-7485.

9. Englund G, Hallberg, P., Artursson, P., Michaelsson, K. and Melhus, H.(2004) Association between the number of coadministered P-glycoprotein inhibitors and serum digoxin levels in patients on therapeutic drug monitoring. BMC Med. 2:1-8.

10. Balayssac, D., Authier, N., Cayre, A., and Coudore, F. (2005) Does inhibition of P-glycoprotein lead to drug-drug interactions? Toxicol Lett 156: 319-329.

11. Higgins, C.F. and Linton, K. (2004). The ATP switch model for ATP transporters. Nature Struct. & Mol. Biol.11:918-926.

12. Sharom, F.J. and Eckford, P.D. (2003) Reconstitution of membrane transporters. Methods Mol Biol. 227:129-154.

13. Lugo, M. R. and Sharom, F.J.(2005b) Interaction of LDS-751 and Rhodamine 123 with P-Glycoprotein: Evidence for Simultaneous Binding of Both Drugs. Biochemistry. 44:14020-14029.

14. Loo, T.W. and Clarke, D.M. (2005) Recent Progress in Understanding the Mechanism of P-Glycoprotein-mediated Drug Efflux. J. Membr. Biol. 206:173-185.

15. Shapiro, A. B., and Ling, V. (1997) Positively cooperative sites for drug transport by P-glycoprotein with distinct drug specificities, Eur. J. Biochem. 250, 130-137.

16. Spoelstra, E. C., Westerhoff, H. V., Pinedo, H. M., Dekker, H., & Lankelma, J. (1994) The multidrug-resistance-reverser verapamil interferes with cellular P-glycoprotein-mediated pumping of daunorubicin as a non-competing substrate, Eur. J. Biochem.221, 363-373.

17. Stein, W. D. (1997) Kinetics of the multidrug transporter (P-glycoprotein) and its reversal. Physiolog. Rev. 77(2):545-590.

18. Seelig, A. and Gatlik-Landwojtowicz, E. (2005) Biophysical characterization of inhibitors of multidrug efflux transporters: Their membrane and protein interactions. Med. Chem., 5(2):135-151.

19. Tang, F., Horie, K. and Borchardt, R.T. (2002a) Are MDCK cells transfected with the human MRP2 gene a good model of the human intestinal mucosa? Pharm Res.;19:765-772.

20. Tang, F., Horie, K. and Borchardt, R.T. (2002b) Are MDCK cells transfected with the human MDR1 gene a good model of the human intestinal mucosa? Pharm Res. 19: 773-779.

21. Troutman, M.D., and Thakker, D.R. (2003a) Novel Experimental Parameters to Quantify the Modulation of Absorptive and Secretory Transport of Substrates by P-Glycoprotein in Cell Culture Models of Intestinal Epithelium. Pharm. Res. 220:1210-1224.

22. Troutman, M.D., and Thakker, D.R. (2003b) Efflux Ratio Cannot Assess P-Glycoprotein-Mediated Attenuation of Absorptive Transport: Asymmetric Effect of P-Glycoprotein on Absorptive and Secretory Transport across Caco-2 Cell Monolayers Pharm. Res. 20:1200-1209.

23. Tran, T. T. , Mittal, A., Gales, T., Maleeff, B., Aldinger, T., Polli, J.W., Ayrton, A., Ellens, H. and Bentz, J. (2004a) An Exact Kinetic Analysis of Passive Transport across a Polarized Confluent MDCK Cell Monolayer Modeled as a Single Barrier. J. Pharm. Sci. 93:2108-2123.

24. Tran, T. T. , Mittal, A., Aldinger, T., Polli, J.W. , Ayrton, A., Ellens, H. and Bentz, J. (2005) The elementary mass action rate constants of P-gp transport for a confluent monolayer of MDCKII-hMDR1 cells. Biophys. J. , 88:715-738.

25. Rautio, J., Humphreys, J. E., Webster, L. O., Balakrishnan, A., Keogh, J. P., Kunta, J. R., Serabjit-Singh, C.J. and Polli, J. W.(2006) In Vitro P-glycoprotein Inhibition Assays for Assessment of Clinical Drug Interaction Potential of New Drug Candidates: A Recommendation for Probe Substrates. In press. Drug Metab Dispos.

26. Gottesman, M. M. and Pastan, I. (1993) Biochemistry of multidrug resistance mediated by the multidrug transporter. Annu. Rev. Biochem. 62:385-427.

27. Lugo, M.R. and Sharom, F.J.(2005a) Interaction of LDS-751 with P-glycoprotein and mapping of the location of the R drug binding site. Biochemistry. 44:643-55.

28. Modok, S., Heyward, C. and Callaghan, R. (2004) P-glycoprotein retains function when reconstituted into a sphingolipid and cholesterol rich environment. J Lipid Res. 45:1910-1918.

29. Troost, J., Lindenmaier, H., Haefeli, W. E. and Weiss, J. (2004) Modulation of Cellular Cholesterol Alters P-Glycoprotein Activity in Multidrug-Resistant Cells. Mol Pharmacol 66:1332-1339.

30. Evers, R., Kool, M., Smith, A. J., van Deemter, L., de Haas, M. and Borst, P.(2000) Inhibitory effect of the reversal agents V-104, GF120918 and Pluronic L61 on MDR1 P-gp-, MRP1- and MRP2-mediated transport. British J. Cancer. 83:366-374.

31. Bentz, J., Tran, T. T., Polli, J. W. , Ayrton, A. and Ellens, H. (2005) The steady-state Michaelis-Menten analysis of P-glycoprotein mediated transport through a confluent cell monolayer cannot predict the correct Michaelis constant K_M. Pharm Res. 22:1667-1677.

32. Butor, C., and Davoust, J.(1992) Apical to basolateral surface area ratio and polarity of MDCK cells grown on different supports. Exp. Cell Res. 203:115-127.

33. Al-Shawi, M. K., Polar, M. K., Omote,H. and Figler, R.A. (2003) Transition state analysis of the coupling of drug transport to ATP hydrolysis by P-glycoprotein. J Biol Chem. 278:52629-52640.

34. Ho, N. F. H., Raub, T. J. ,Burton, P. S., Bausuhn, C. L., Adson, A., Audus, K. L. and Borchardt, R.(2000) Quantitative approaches to delineate passive transport mechanisms in cell culture monolayers. In: Transport Processes in Pharmaceutical Systems. Eds. Amidon, G.L. and Lee, P.I. Dekker, M.New York. pp. 219-316.

35. Shapiro, A. B., and Ling, V. (1998) Transport of LDS-751 from the cytoplasmic leaflet of the plasma membrane by the rhodamine-123-selective site of P-glycoprotein, Eur. J. Biochem. 254:181-188.

36. Hyafil, F., Vergely, C. , Du Vignaud, P.and Grand-Perret, T.(1993) In vitro and *in vivo* reversal of multidrug resistance by GF120918, an acridone carboxamide derivative. Cancer Res. 53:4595-602.

37. Polli, J. W., Wring, S.A., Humphreys, J.E., Huang,L., Morgan, J.B., Webster, L.O. and Serabjit-Singh, C.J. (2001) Rational use of *in vitro* P-glycoprotein assays in drug discovery. J. Pharm. & Exp. Therap. 299:620-628.

38. Shapiro, A. B., Corder, A. B., and Ling, V. (1997) P-glycoprotein mediated Hoechst 33342 transport out of the lipid bilayer, Eur. J. Biochem. 250:115-121.

39. Tang, F., Ouyang, H., Yang, J. Z. and Borchardt, R. T.(2004) Bidirectional transport of rhodamine 123 and Hoechst 33342, fluorescence probes of the binding sites on P-glycoprotein, across MDCK-MDR1 Cell Monolayers. J Pharm Sci. 93:1185-1194.

40. Rosenberg, M. F., Kamis, A. B., Callaghan, R., Higgins, C. F. and Ford, R. C.(2003) Three-dimensional structures of the mammalian multidrug resistance P-glycoprotein demonstrate major conformational changes in the transmembrane domains upon nucleotide binding. J Biol Chem. 278(10):8294-8299.

41. Shitara, Y., Horie, T. and Sugiyama, Y. (2006) Transporters as determinant of drug clearance and tissue distribution. Eur. J. Pharm. Sci., 27:425-446.

42. Shapiro, A. B., Fox, K., Lam, P., and Ling, V. (1999) Stimulation of P-glycoprotein-mediated drug transport by prazosin and progesterone. Evidence for a third drug-binding site, Eur. J. Biochem. 259, 841-850.

43. Loo, T.W., Bartlett, M.C. and Clarke, D.M. (2003b) Substrate-induced conformational changes in the transmembrane segments of human P-glycoprotein. Direct evidence for the substrate-induced fit mechanism for drug binding. J. Biol. Chem. 278:13603-13606.

44. Vandevuer, S., Van Bambeke, F., Tulkens, P. M. and Prvost, M. (2006) Predicting the three-dimensional structure of human P-glycoprotein in absence of ATP by computational techniques embodying crosslinking data: Insight into the mechanism of ligand migration and binding sites. Proteins: Structure, Function, and Bioinformatics. 63:466-478.

45. Omote, H. & Al-Shawi, M. K. (2006) Interaction of transported drugs with the lipid bilayer and P-glycoprotein through a solvent exchange mechanism. Biophys. J. 90: 4046-4059.

46. Loo, T.W., Bartlett, M.C. and Clarke, D.M. (2003a) Drug binding in human P-glycoprotein causes conformational changes in both nucleotide-binding domains. J. Biol. Chem. 278:1575-1578.

47. Ambudkar S.V., C.O. Cardarelli, I. Pashinsky & W.D. Stein. 1997. Relation between the turnover number for vinblastine transport & for vinblastine-stimulated ATP hydrolysis by human P-glycoprotein. J Biol Chem. 272(34):21160-6.

48. Hah, J. S., Ryu, J. W., Lee, W., Kim, B. S., Lachaal, M., Spangler, R. A., and Jung, C. Y. (2002). Transient changes in four GLUT4 compartments in rat adipocytes during the transition, insulin-stimulated to basal: Implications for the GLUT4 trafficking pathway. Biochemistry 41, 14364-14371.

49. Higgins, C.F. and Gottesman, M.M.(1992) Is the multidrug transporter a flippase? Trends. Biochem.Sci. 17:18-21.

50. Borst, P., Zelcerb, N., van de Weteringa, K. and Poolman, B.(2005) On the putative co-transport of drugs by multidrug resistance proteins. FEBS Lett. 580:1085-1093.

51. Hill, T. (1956) An Introduction to Statistical Thermodynamics. Dover. New York, Chapter 20.

Substrate (conc. range)	Inhibitor (conc. range)	IC50	Comments
Amprenavir (50 & 100 uM)	Quinidine (0-20 uM, n=9)	2-5 uM	B>A was inhibited slightly more than A>B
Quinidine (0.1-3 uM, n=4 [a])	Amprenavir (0, 50 & 100 uM)	~100 uM	Only 2 AMP concentrations tested since the solubility limit reached above 100uM
Quinidine (0.1-5 uM, n=5)	Loperamide (0-10 uM, n=8)	5-8 uM	
Quinidine (1-5 uM, n=4)	Hoechst 33342 (0-10 uM, n=5)	2-5 uM	Hoechst 33342 inhibits at the same concentration range as quinidine
Loperamide (1-5 uM, n=4)	Quinidine (0-30 uM, n=10)	B>A: 5 uM A>B: ≥5-20 uM	Fraction inhibition stalled at about 0.5

Figure 9.1: Paper 1: Table 1 - IC50 ranges for P-gp substrates.

Legend for Table 1.

[a] n= number of different concentrations tested from the sequence of 0, 0.1, 0.3 , 1, 2, 3, 5, 10, 20 and 30 μM.

Substrate	"Vmax" $k_2T(0)$ [a] (M/s)	Efflux Active P-gp Density $T(0)$ [b] (uM)	Association to P-gp k_1 [c] ($M^{-1}s^{-1}$)	Efflux to Apical Chamber k_2 [d] (s^{-1})	Dissociation to Apical Membrane k_r [e] (s^{-1})	Partition Coefficient K_{PC} [f]	Binding Constant K_C (M^{-1}) [g] Cytosolic Dissociation Constant "$K_{D,Aq}$" (M)	Steady State Passive Permeability Coefficients [h] (nm/sec)
AMP	$3x10^{-2}$	200	$2x10^{9}$	150	$2x10^{6}$	200	1000 "5 uM"	P_{BA} = 420±50 P_{AB} = 400±50
QND	$1x10^{-3}$	200	$2x10^{9}$	5	$1x10^{5}$	700	15,000 "0.1 uM"	P_{BA} = 500±100 P_{AB} = 500±100
LPM	$4x10^{-4}$	200	$2x10^{9}$	2	$5x10^{5}$	3000	4000 "0.1 uM"	P_{BA} = 350±80 P_{AB} = 400±100

Figure 9.2: Paper 1: Table 2 - Fitted Parameter Values with Single Substrate Experiments.

Legend for Table 2.

[a] The product of k_2T(0) is very rigorously fitted by the first step in the algorithm and the values shown were fixed by at least the first 100 best fits, which all has the same coefficient of variation, CV, i.e. these are robust fits at each concentration. For loperamide, the fits were taken from the higher concentrations only, $\geq 5\mu$M. Lower concentrations did not yield so many stable fits, although the integrated curves using these parameters look reasonable. As mentioned in the Results section, loperamide fits require a basolateral transporter, which is inhibited by GF120918, i.e. the P-gp inhibitor.

[b] The "center of the box" efflux active concentration of P-gp within the inner apical monolayer, as shown in Figure 4 for amprenavir. These units can be converted to a more typical form, assuming a 2nm lipid monolayer thickness for the acyl chain region. T(0) (P-gp/μm^2)=0.8*T(0) (μM, inner apical monolayer)=160 P-gp/μm^2. The ratio of apical membrane to the insert cross section area is irrelevant, since it cancels out in the calculation.

[c] Center of the box estimate for the association rate constant k_1. As shown for amprenavir in Figure 4, the range was $k_1 = (1-10)\text{x}10^9 M^{-1}s^{-1}$. For quinidine and loperamide the range was broader, $k_1 = (0.2-10)\text{x}10^9 M^{-1}s^{-1}$(data not shown; 24).

[d] Center of the box estimate for the efflux rate constant k_2, from P-gp into the apical chamber, given by the ratio of the fitted k_2T(0) for each substrate and the center of the box value of $T(0) = 2\text{x}10^{-4}$ M. See text and footnote (b) above.

[e] Center of the box estimate for the dissociation rate constant k_r, from P-gp back into the

inner apical monolayer.

[f] Equilibrium substrate partition coefficient to 0.1 μm PS/PE/chol (1:1:1) liposomes. This lipid composition is a rough mimic for the inner apical monolayer, as described in (24).

[g] The binding constant to P-gp from the inner apical monolayer, defined by $K_C = k_1/k_r$. Below each binding constant, we show in parentheses the appropriate dissociation constant for each substrate relative to the aqueous cytosol, calculated as $K_{D,Aq}$ =1/(K_C*drug partition coefficient{PS/PE/chol}). These are dissociation constants are more than an order of magnitude smaller than the K_M derived from a steady-state Michaelis-Menten analysis of this data (31).

[h] Steady state passive permeability coefficients measured across the confluent cell monolayer, in the presence of the P-gp inhibitor GF120918, as shown in Figure 3 for quinidine after 1 hour. P_{BA} is shown first and P_{AB} is shown underneath. The values are not always symmetric, since the passive permeability for loperamide is faster in the A>B direction than in the B>A direction before their convergence at steady state. This was also observed in (23).

Figure Legends

Figure 1. Model of a confluent cell monolayer, with the apical membrane on top and the basolateral membrane on the bottom, where it binds to the polycarbonate insert. Passive permeability occurs in both directions. P-gp expressed on the apical membrane transports substrate from the inner apical membrane monolayer into the apical chamber. The concentration of substrate in the apical and basolateral chambers, C_A and C_B, are measured, while the concentration of substrate in the inner plasma membrane, C_{PC}, and the cytosol, C_C, are predicted as part of the data fitting process described in Tran et al. (24).

Figure 2. The total and passive transport of amprenavir into the receiver chamber across the monolayer of confluent MDCK cells is shown with increasing concentrations of the quinidine as the inhibitor. Transport is measured by the nmol of amprenavir transported over time, when the donor side begins with 100 μM amprenavir. The dotted lines show the nmol transported due to passive permeability (+GF120918) A:B>A, that is, to the apical chamber from the basolateral chamber marked with solid squares and B:A>B, that is, to the basolateral chamber from the apical chamber marked by solid triangles. The two curves are nearly indistinguishable, which is expected for symmetric passive transport. Error bars are smaller than the symbols. The total transport, P-gp mediated and passive, A:B>A is shown above the passive permeability lines as a function of the quinidine concentration (μM), which is inhibiting P-gp via its own transport and, thus, reducing the amprenevir transport. The total transport B:A>B is shown below the passive permeability lines as a function of the quinidine concentration (μM). Here the inhibition of P-gp by quinidine increases the transport of amprenavir from the apical chamber. At 10 μM quinidine, the amprenavir transport is nearly the same as pure passive permeability.

Error bars show standard deviation of triplicates. Quinidine at the concentrations shown is preincubated with the cell monolayer for 0.5 hour and then chamber solutions are replaced with 100μM amprenavir in the donor chamber and fresh quinidine solution in both chambers.

Figure 3. The passive permeability coefficient (+GF120918) for quinidine (QND) over 4 hours in the presence of amprenavir or loperamide is shown with their respective standard deviations at each time point for all the grouped data sets. All the quinidine data, B>A and A>B, from 0.1-5μM quinidine, inhibited by either 0-100μM amprenavir (AMP) or 0-10 μM loperamide (LPM) have been included, with a total of 34 data sets. Passive permeability does not depend upon concentrations of substrate or inhibitor. After 2 hrs, there is more variability, due in part to the system approaching steady state where the equation used to calculate the passive permeability coefficient becoming undefined (23). For fitting P-gp mediated transport of quinidine, the time dependent values of the passive permeability coefficient up to 1 hr and then the average steady state value calculated for 1.5 hr and beyond is shown by the arrow at about 500 nm/s. For the other substrates, the crossover time from using the time dependent passive permeability coefficients to using the steady state average values was chosen the same way. Loperamide's passive permeability coefficient in the A>B direction increased to roughly 550 nm/sec at 2 hours and then declined steadily to roughly 400 nm/sec, so all of the time dependent passive permeability coefficients were used.

Figure 4. The distribution of the best fitting pairs of the density of efflux active P-gp, T(0), and the association rate constant, k_1, for amprenavir alone are shown, following the fitting algorithm explained in (24). The amprenavir concentrations are color-coded (black-10μM, red -30μM and blue-100μM). The pairs of {T(0), k_1} randomly distributed

within the box, which looks like a tilted trapezoid shown in blue, give essentially identical best fits to the data for all these substrate concentrations. The arrows point to parameter values at the "center of the box". Table 2 shows these values, i.e. $k_1 = 2\text{x}10^9 M^{-1}s^{-1}$ and T(0)=200μM in the inner apical monolayer, which equals 160 P-gp/μm^2 in the apical membrane, see footnote b of Table 2.

Figure 5. The data and fits for the P-gp mediated transport of quinidine with amprenavir as the inhibitor. All four transport curves are shown here and in the same way in Figures 5-7. For all figures, red denoted concentrations from the apical chamber and blue denotes concentrations from the basolateral chamber. All data symbols are open, since P-gp is active in all cases shown, with squares for B>A data and triangles for A>B data, as used above. Simulations use the parameters given in Table 2, either with the assumption that the substrate and inhibitor are competing for the "single" P-gp binding site (solid line) or the assumption that there is no inhibitor effect (dashed line). Since it is very important to identify which simulation best fits the data, we have made the simulations have thick lines for the B>A direction and thin lines for the A>B direction. From top to bottom the curves are denoted: A:B>A, open red squares (□), for the concentration of substrate in the apical chamber when the basolateral chamber is the donor; B:B>A, open blue squares (□), for the concentration of substrate in the basolateral chamber, blue, when the basolateral chamber is the donor; A:A>B, open red triangles (△), for the concentration of substrate in the apical chamber when the apical chamber is the donor; and B:A>B, open blue triangles (△), for the concentration of substrate in the basolateral chamber when the apical chamber is the donor. Data is shown by the symbols with error bars defined by the standard deviation of triplicate measurements. Fig. 5A shows 0.3μM quinidine transport in the presence of 100μM of amprenavir as the inhibitor. Competitive inhibition fits the data very well, while no-inhibitor effect does not. Fig. 5B shows 0.3μM quinidine

transport in the presence of 50μM of amprenavir as the inhibitor. No inhibitor effect fits the data very well, as if there is no amprenavir in the system, while competitive inhibition does not. There is substantial transport of AMP under these conditions, see Figure 6 below. Fig. 5C shows 3μM quinidine transport in the presence of 50μM of amprenavir as the inhibitor. Competitive inhibition fits the data very well, while no-inhibitor effect does not. As explained in the text, many other cases were tested and the cases shown in the figures were chosen to show the substrate and inhibitor concentrations marking the transition between no-inhibitor effect and competitive inhibition.

Figure 6 shows the data and simulations for the P-gp mediated transport of amprenavir with quinidine as the inhibitor, using the same nomenclature as Figure 5. Fig. 6A shows 50μM amprenavir transport in the presence of 2μM of quinidine as the inhibitor. No inhibitor effect fits the data very well, as if there is no quinidine in the system, while competitive inhibition does not. There is substantial transport of quinidine under these conditions, see Figure 5 above. Fig. 6B shows 50μM amprenavir transport in the presence of 5μM of quinidine as the inhibitor. Competitive inhibition fits the data very well, while no-inhibitor effect does not.

Figure 7 shows the data and simulations for the P-gp mediated transport of quinidine with loperamide as the inhibitor, using the same nomenclature as Figure 5. Fig. 7A shows 1μM quinidine transport in the presence of 2μM of loperamide as the inhibitor. No inhibitor effect fits the data very well. Fig. 7B shows 3μM quinidine transport in the presence of 10μM of loperamide as the inhibitor. Competitive inhibition fits the data very well, while no-inhibitor effect does not.

Figure 8. A representation of microvilli on the apical surface of MDCK II cells with

P-gp expressed on the membrane by arrows. A cartoon path is shown of a random walk of a substrate molecule after being released either by P-gp or by passive permeability at the base of a microvillus. The path will involve many subsequent interactions with the same or a neighboring microvillus. Only substrates released at the tip of the microvilli will have a reasonable chance of diffusing non-stop into the apical chamber and be counted as due to transport mediated by efflux active P-gp or via passive permeability. Any change in microvilli dimension would affect the probability of escape non-stop and, hence, the number of efflux active P-gp and the membrane area for passive permeability.

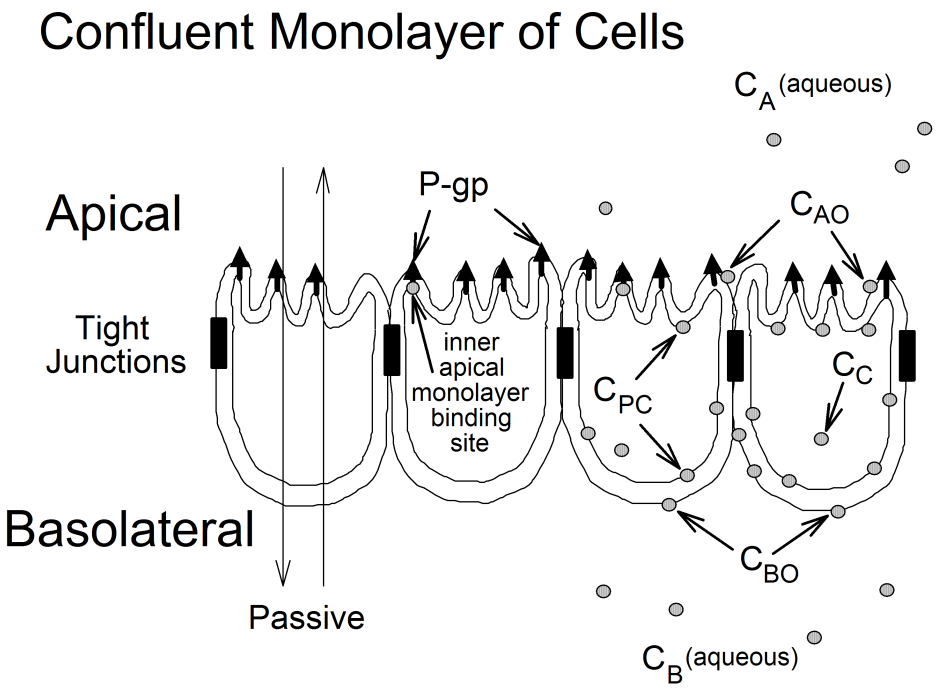

Figure 9.3: Paper 1: Figure 1 - Model of a confluent cell monolayer

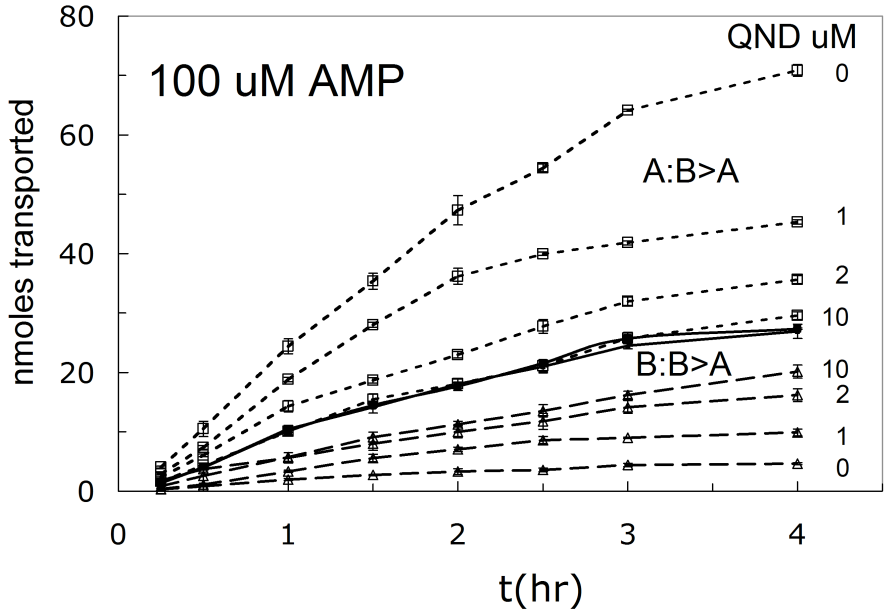

Figure 9.4: Paper 1: Figure 2 - Inhibition of amprenavir transport by quinidine.

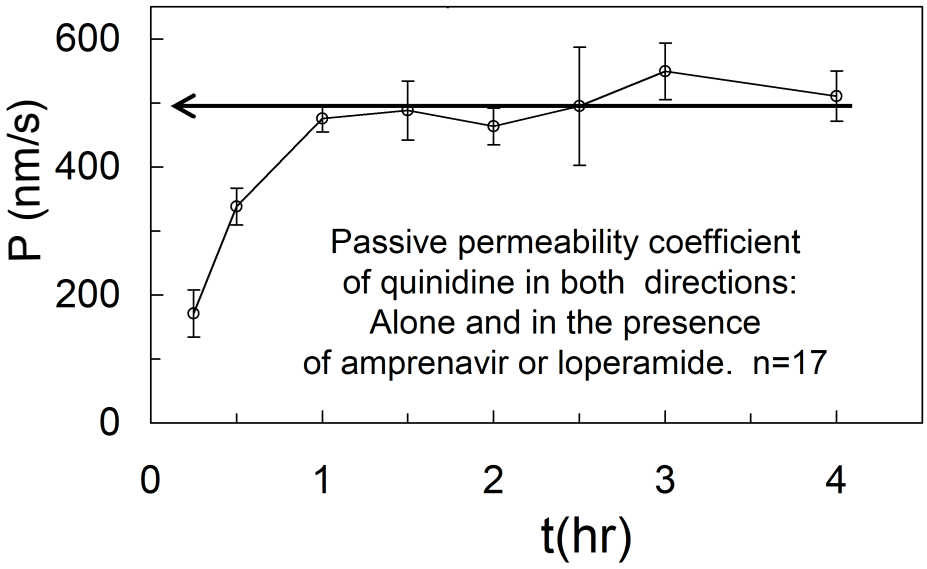

Figure 9.5: Paper 1: Figure 3 - Passive permeability is time-dependent.

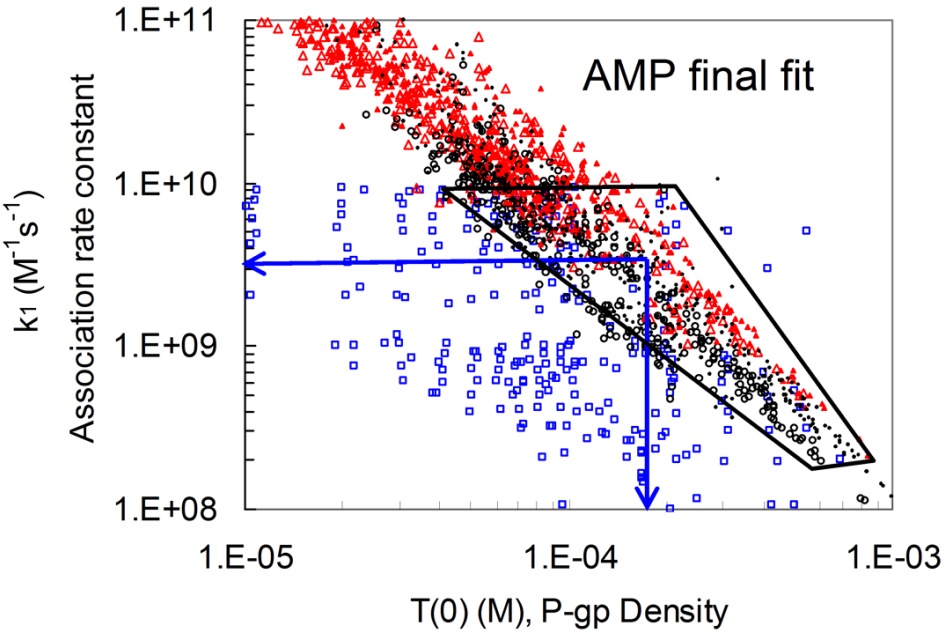

Figure 9.6: Paper 1: Figure 4 - Best fit values for efflux-active P-gp density and the rate of association to it.

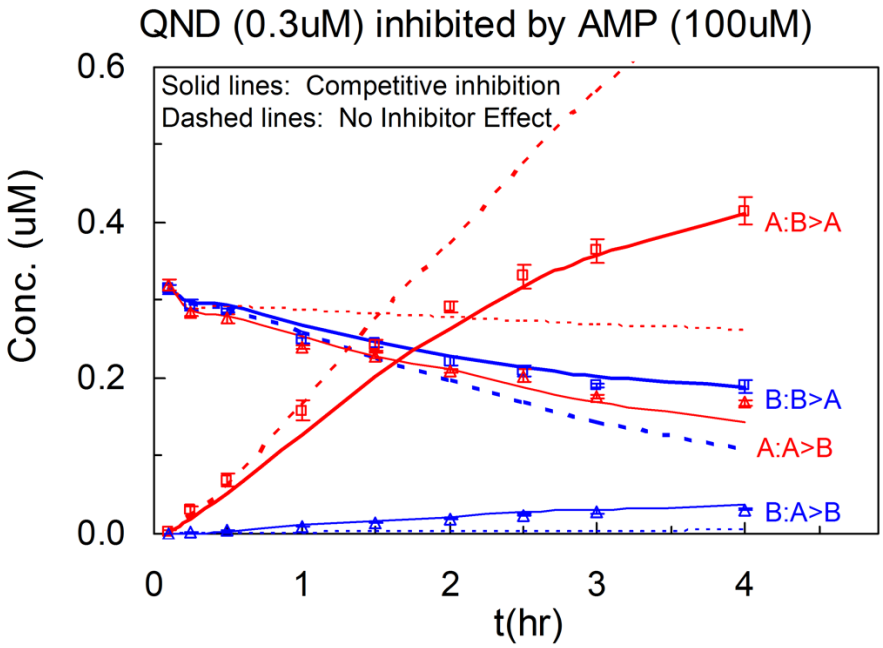

Figure 9.7: Paper 1: Figure 5a - Quinidine transport inhibited by amprenavir : Competitive inhibition at high inhibitor concentrations.

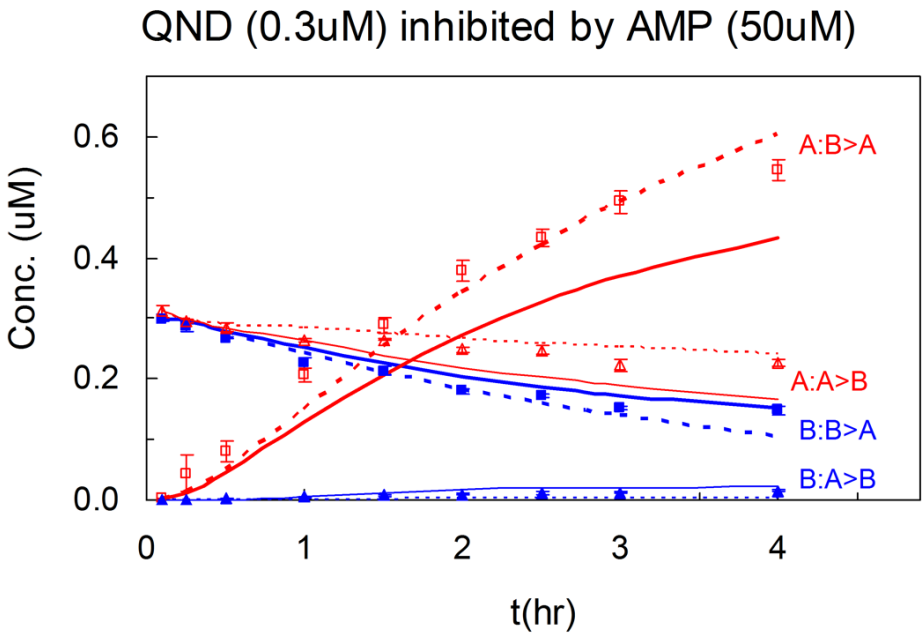

Figure 9.8: Paper 1: Figure 5b - No inhibitor effect provides kinetic evidence for atleast two efflux pathways through P-gp.

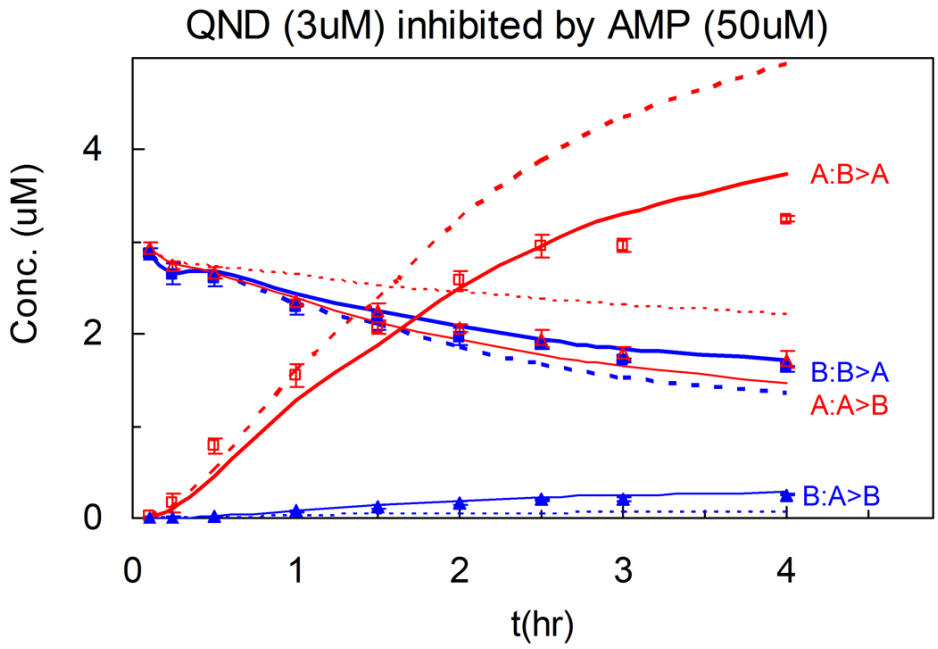

Figure 9.9: Paper 1: Figure 5c - Quinidine transport inhibited by amprenavir : competitive inhibition at high substrate concentrations.

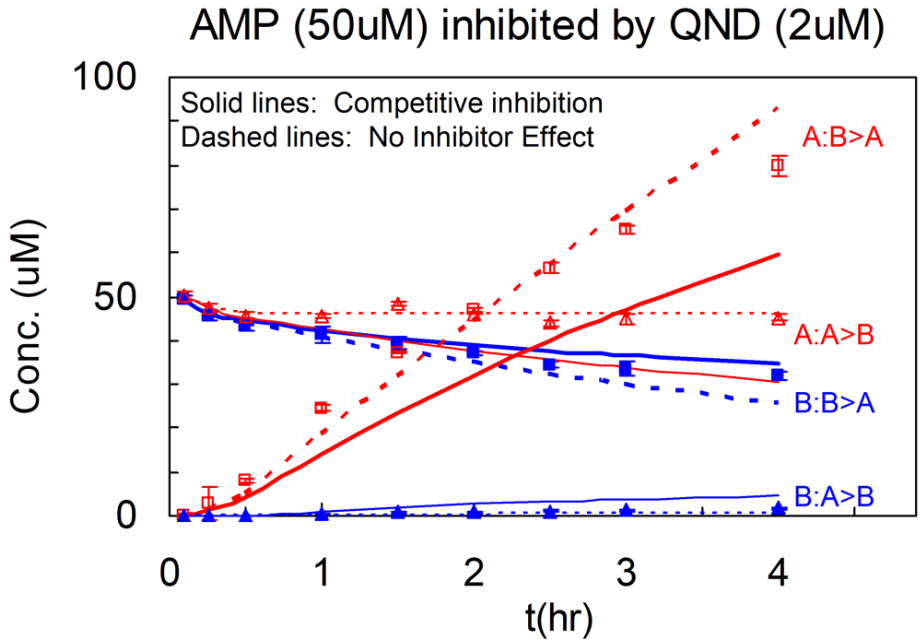

Figure 9.10: Paper 1: Figure 6a - Amprenavir transport inhibited by quinidine : no inhibitor effect.

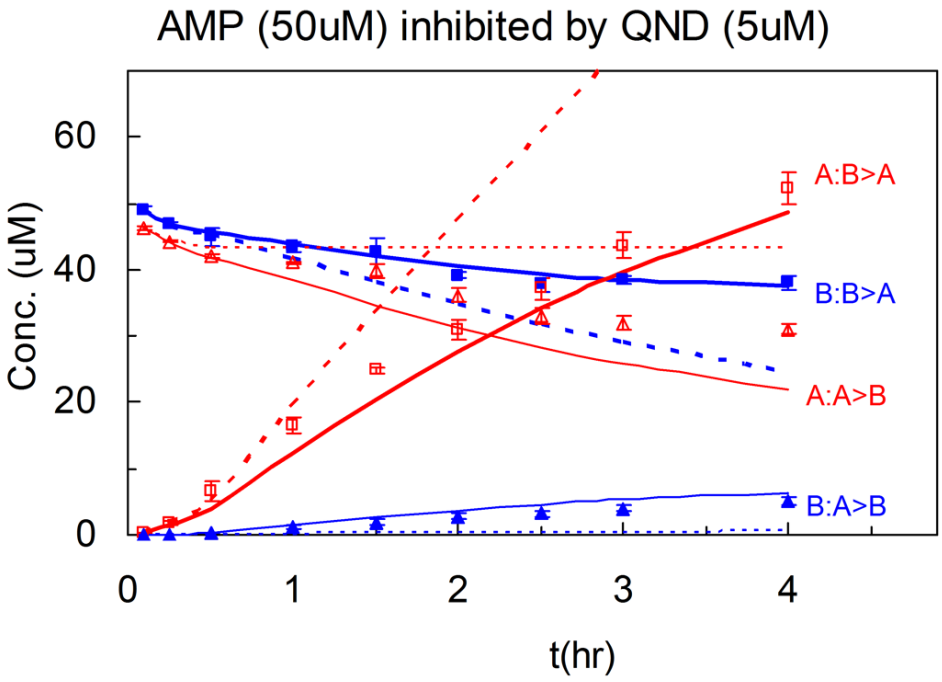

Figure 9.11: Paper 1: Figure 6b - Amprenavir transport inhibited by quinidine : competitive inhibition at high inhibitor concentrations.

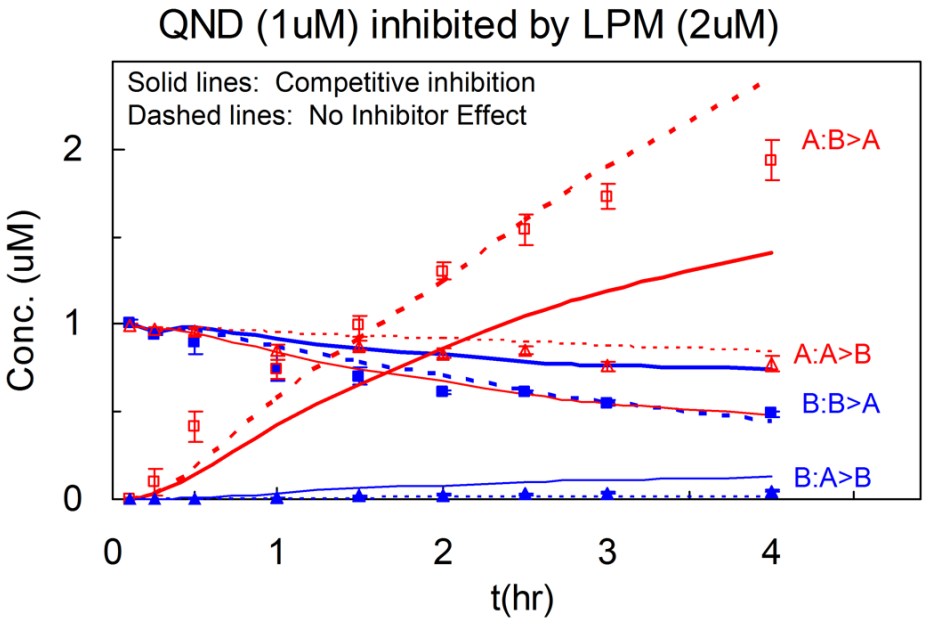

Figure 9.12: Paper 1: Figure 7a - Quinidine transport inhibited by loperamide : no inhibitor effect.

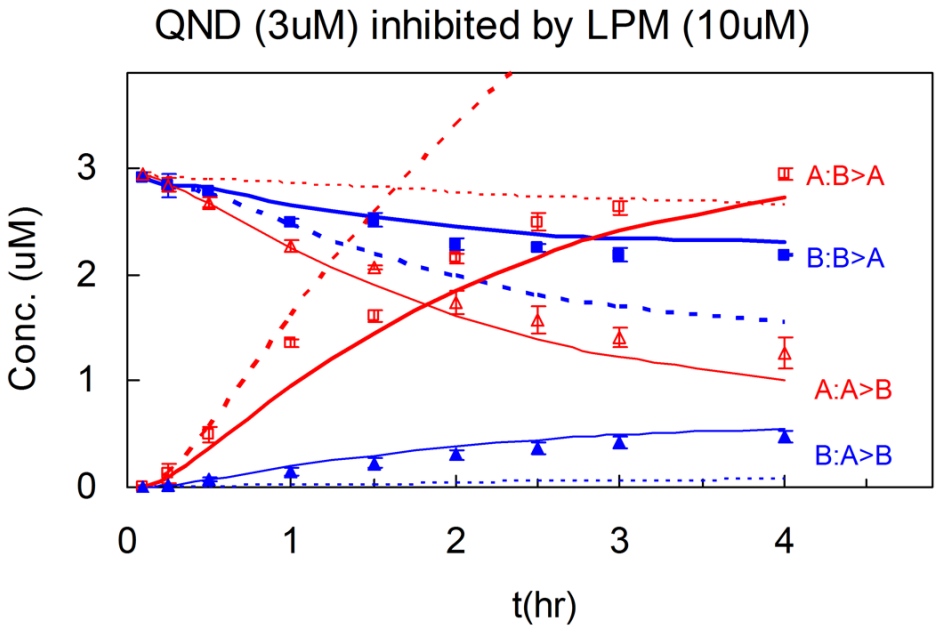

Figure 9.13: Paper 1: Figure 7b - Quinidine transport inhibited by loperamide : competitive inhibition at high inhibitor concentrations.

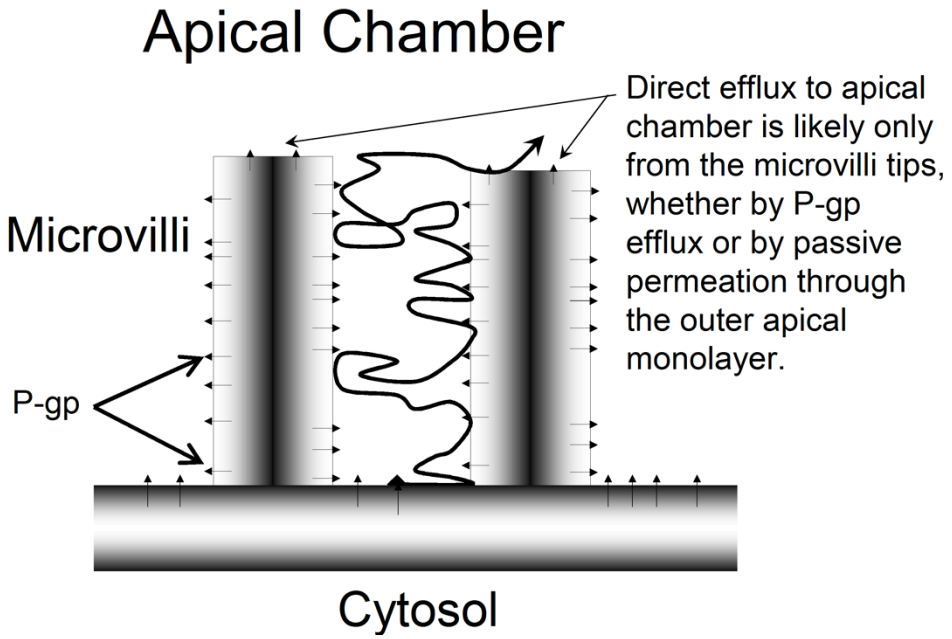

Figure 9.14: Paper 1: Figure 8 - Microvilli morphology plays an important role in the physiological activity of P-gp.

10. Paper 2

Kinetic identification of membrane transporters that assist P-gp mediated transcellular transport of drugs through a confluent monolayer of MDCKII-hMDR1 cells.

Poulomi Acharya[1,2], Joseph W. Polli[3], Andrew Ayrton[4], Harma Ellens[2] & Joe Bentz[1*]

[1] Department of Bioscience & Biotechnology, Drexel University, Philadelphia, PA19104, USA

[2] Preclinical Drug Metabolism and Pharmacokinetics, GlaxoSmithKline, King of Prussia, PA, 19406.

[3] Preclinical Drug Metabolism and Pharmacokinetics, GlaxoSmithKline, Research Triangle Park, NC 27709

[4] Preclinical Drug Metabolism and Pharmacokinetics, GlaxoSmithKline, Welwyn, England

[*] Address correspondence to Dr. Joe Bentz, email: bentzj@drexel.edu, FAX: 215-895-1273.

Running Title: Kinetic identification of apical and basolateral membrane transporters.

Non-standard Abbreviations: Non-standard Abbreviations: P-gp, the P-glycoprotein product of the hMDR1 gene; A>B (or B>A), transport across the confluent cell monolayer when the donor chamber is apical (or basolateral) and the receiver chamber is basolateral (or apical); $K_{D,Aq}$ is the substrate dissociation constant from P-gp relative to the aqueous concentration in the cytosol.

Abstract

Identifying the membrane transporters that move substrates across cells is important for understanding drug absorption / elimination and cell physiology. While the list of membrane transporters involved in intestinal, renal and hepatobiliary transport is extensive, identification of individual transporters responsible for the transport of substrates across the basolateral and apical membranes has been challenging. Using a confluent monolayer of hMDR1-MDCKII cells, the elementary rate constants for the P-gp efflux of digoxin, loperamide, amprenavir and quinidine have been determined. To fit the kinetics of P-gp efflux for digoxin and loperamide, a basolateral transporter has to be introduced into the kinetic model. Our results show that when a compound is tested against digoxin as a probe substrate and shown to inhibit B>A digoxin flux, it could be that the inhibition occurs at the basolateral transporter, rather than at P-gp. Further, digoxin efflux requires an additional apical importer. These putative digoxin and loperamide transporters are completely inhibited by GF120918, a known P-gp and BCRP inhibitor. In contrast to digoxin and loperamide, the P-gp substrates amprenavir and quinidine show no kinetic requirement for these putative transporters. Attempts to identify the additional digoxin and loperamide transporters using specific substrates for a wide range of known kidney epithelial transporters (OCT, OAT, OATP, URAT or MRP) failed to elucidate the identity of these two membrane transporters.

Introduction

The importance of membrane transporters on the metabolism and disposition of drugs is well recognized (Goh et al., 2002; Kim, 2003; Mizuno et al., 2003; Collett et al., 2005; Shitara et al., 2006; Robertson and Rankin, 2006; Sekine et al., 2006). While it is generally believed that membranes transporters mediate the transcellular transport of compounds across the epithelial cells of the colon, kidney and liver, and across the endothelial cells of the blood brain barrier, it has proven very difficult to identify which transporters are involved *in vivo* (Lau et al., 2006). The role of additional non-MDR1 transporters mediating the efflux of digoxin in Caco-2 cells (Lowes et al., 2003) and influx of mitoxantrone (a prototype substrate for ABCG2 or bcrp1) in MDCK II cells (Pan and Elmquist, 2007) have been evidenced. Polarized confluent cell monolayers have be extensively used as a model to study drug transporters (Tang et al., 2002 a,b; Troutman & Thakker, 2003 a,b; Rautio et al., 2006). There has been success in transfecting these model systems with exogenous transporters to study their interactions (Sasaki et al., 2004; Spears et al., 2005). However, the problem is that the interactions are complex and the analysis has been limited to known transporters (Dresser et al., 2001; Shitara et al., 2006).

We have developed a kinetic analysis that can detect the presence of unknown transporters and can assay their inhibition with great sensitivity. Using the polarized MDCKII-hMDR1 confluent cell monolayer, which overexpresses P-gp in the apical plasma membrane, and a detailed mass action kinetic analysis of P-gp efflux, we have been able to answer several fundamental questions about P-gp function (Tran et al., 2005; Bentz et al, 2005; Acharya et al. 2006). The basic experimental design was to measure the total transport (e.g., P-gp and passive permeability) and passive permeability of substrates through the cell monolayer. The difference in these two rates theoretically provides the kinetics of P-gp transport alone.

The objective of this work was to 1) demonstrate the kinetic importance of unknown membrane transporters in the transport of the P-gp substrates loperamide and digoxin across the basolateral and apical membranes of MDCK-hMDR1 monolayers, 2) attempt to identify these unknown transporters using a wide range of transporter substrates and inhibitors.

Materials and Methods

Materials. Amprenavir and GF120918 were from GlaxoSmithKline (USA), loperamide was from Sigma, and quinidine was from Fisher Scientific. ^{3}H-loperamide (10 Ci/mmole) and ^{3}H-amprenavir (21 Ci/mmole) were custom synthesized by Amersham Pharmacia Biotech, England. ^{3}H-quinidine (20 Ci/mmole) was from ICN Biomedical, Inc. USA. Dulbecco's Modified Eagle Medium (DMEM) was from MediaTech, VWR. DMEM with 25 mM HEPES buffer, high glucose (4.5 g/L), L-Glutamine, pyridoxine hydrochloride, w/o sodium pyruvate, and with phenol red was from Gibco. The same medium without phenol red was used for transport experiments, denoted transport media. Transwell 12-well plates with polycarbonate inserts (0.4μm pore size and 12 mm diameter) were obtained from Costar (Acton, MA). All compounds tested in Table 2 were from Sigma (Sigma Chemical Co., St.Louis, MO).

Cell line and culture conditions. The Madin-Darby Canine Kidney II cell line which over-expresses human MDR1 (MDCKII-hMDR1) was purchased from the Netherlands Cancer Institute (Amsterdam, Netherlands) (Evers et al., 2000). MDCK II cells were grown in 175 cm^2 culture flasks using DMEM with 10% fetal bovine serum, 1% L-glutamine and 50 U/mL penicillin, 50 mg/mL streptomycin at 37°C in 5% CO_2 atmosphere. Cells were split twice a week at 70-80% confluency in a ratio of 1:40, after at least 2 washes in PBS and being trypsinized with 0.25% trypsin/EDTA. All transport assays were done with cells from passages 30 to 55. Cells were kept at 37°C in 5% CO_2.

Single substrate efflux assay. Cells were seeded in 12 well Costar-Transwell plates with polycarbonate membrane inserts at a density of 175,000 cells per insert and grown for four days in culture medium. Cells were given fresh media 1 day after seeding. On the day of the experiment, culture media was removed and cells were pre-incubated for 30 minutes with either transport media alone or transport media with 2 μM GF120918, an inhibitor

of P-gp and BCRP. Efflux of a range of substrates across the confluent monolayer of cells was measured in both directions, i.e. apical to basolateral (A>B) and basolateral to apical (B>A) in the presence and absence of GF120918. ^{3}H-amprenavir, ^{3}H-quinidine, or ^{3}H-loperamide (0.5 mCi/mL) was added to each respective substrate concentration to allow quantitation of efflux from donor to receiver chambers. Lucifer yellow (100μM) was added to the donor chamber to monitor integrity of confluent cell monolayer. Samples (25 μL) were taken over a period of 4 or 6 hours, as shown, from both donor and receiver chambers into 96-well Lumaplates, dried overnight and the radioactivity counted by TopCount Model 9912 (Perkin Elmer, USA). The initial concentration measurement was taken at 6 min after the addition of substrate in the first well (Tran et al., 2004, 2005) and subsequent measurements taken at multiple time points up to 6 hours for all experiments (Tran et al., 2005). After taking each aliquot, the Transwell plates were replaced in a shaker at a speed of 30 rpm, at 37°C in 5% CO_2 . Fluorescence of lucifer yellow (Ex max = 438nm, Em max = 530nm) was measured at time zero from aliquots taken directly from the vials and compared to samples aliquoted at the end of the experiment from both the basolateral and apical chambers; the fluorescence was analyzed using a SpectraMax microplate reader. Passive permeability of Lucifer yellow was always <10 nm/s over the experiment.

Inhibition studies. Cells were seeded and fed as described above and on the day of the experiment culture medium was removed by aspiration. The cells were then preincubated with the inhibitor/substrate drug in both chambers for 30 min. During the preincubation, half the wells received inhibitor solution without GF120918 (to study active transport) and the other half received inhibitor solution with GF120918 (to study passive transport). After 30 minutes, the preincubation solutions were removed by aspiration and the labeled substrate was added to the donor chamber, while refilling fresh inhibitor solution in both chambers, again one half without GF120918 and the other half with it.

Digoxin cell concentration exclusion assay. Cells were seeded and fed as described above. On the day of the experiment, culture medium was removed by aspiration. The cells were then pre-incubated for 30 minutes with transport media (TM), TM + quinidine (20μM), TM + GF120918 (2μM), TM + quinidine (20μM) +GF120918 (2μM) in both chambers. All these pre-incubation conditions were in triplicates. Pre-incubation solutions were then removed by aspiration. Donor and receiver solutions contain the radiolabeled substrate digoxin (50μM) in addition to the respective preincubation condition. Basolateral and apical chambers were filled with donor and receiver solutions respectively. Transport from B>A was measured over 4 hours. Since the same concentration of digoxin was used on both sides, a flat curve showing steady state was obtained. At the 4th hour, all solutions were removed. Both chambers were washed 3 times with cold transport media containing 2μM GF120918. The polycarbonate membrane inserts with the cells were carefully cut out and radioactivity associated to the cells on the membrane was counted by liquid scintillation. The same protocol was repeated using 1μM benzbromarone in addition to quinidine.

Cell stability and substrate metabolism. We showed previously that the stability of the cell monolayer and plasma membrane with respect to passive and active transport was not affected by the prolonged exposure times to amprenavir for at least 6 hr (data not shown; Tran et al., 2005). It was also shown that metabolism or decomposition was insignificant for amprenavir, quinidine and loperamide on this time scale using radio-HPLC (data not shown; Tran et al., 2005).

Numerical integrations. We used the stiffest integrator in MATLAB, ode23s, with absolute and relative tolerances set to 10^{-8}. Other MATLAB integrators, while faster, were not accurate enough at the later times of simulations. In data fitting, all concentration curves are simultaneously fitted, so that despite the fact that the A:B>A curve, i.e. substrate concentration in the apical chamber when the basolateral chamber is the donor,

is the most visually striking, all curves contribute to minimizing the difference between data and simulated curves. MATLAB fminsearch minimizes the coefficient of variation between the data and the simulated curves. Further details can be found in Tran et al. (2005) and Bentz et al. (2005).

Mass Action Kinetic Model

Figure 1 is a cartoon of a confluent cell monolayer, featuring the polarized MDCKII-hMDR1 cells, where the basolateral membrane is attached to the polycarbonate filters and P-gp (upward arrows) expressed on the apical surface. The apical and basolateral chambers are kept separate by the tight junctions. Active transport by P-gp occurs vectorially, with substrate binding to a site on P-gp within the apical membrane inner monolayer and with efflux into the apical chamber (Loo and Clarke, 2005; Lugo and Sharom, 2005). For many substrates, including those studied here, passive permeability is a significant fraction of total transport and is quantitatively analyzed separately using the P-gp inhibitor, GF120918 (Tran et al., 2004, 2005; Acharya et al., 2006).

With the confluent cell monolayer system, we measure the concentration of substrate in the apical chamber, denoted C_A, and the basolateral chamber, denoted C_B. However, the concentration of substrate in the cytosol, denoted C_C, and in the inner plasma membrane in contact with the P-gp binding site, denoted C_{PC}, cannot be measured rigorously in real time. These internal concentrations are variables of the mass action model and fitted by elementary rate constants for well-defined kinetic barriers, according to the measured values of C_B and C_A over time (Tran et al., 2005; Acharya et al., 2006).

The simplest Michaelis-Menten mass action reaction to model P-gp is:

$$T_0 + C_{pc} \underset{k_r}{\overset{k_1}{\rightleftarrows}} T_1 \xrightarrow{k_2} T_0 + C_A \tag{10.1}$$

where T_0 is the empty transporter, C_{PC} the substrate in the apical membrane inner monolayer, T_1 is the transporter bound by substrate and C_A the substrate after efflux into the apical chamber. Although P-gp has more than one efflux binding site, when the inhibitor concentrations are near the IC50, P-gp behaves like a simple single competi-

tive site transporter (Acharya et al., 2006). The additional transporters are modeled by Michaelis-Menten steady-state equations

$$\frac{dC}{dt}(Transporter) = \frac{V_{max}[C]}{K_M + [C]} \overset{K_M >> [C_{PC}]}{\longrightarrow} \frac{V_{max}}{K_M}[C] \tag{10.2}$$

This was a compromise between rigor and flexibility, since this model can roughly assess whether there is a kinetically significant binding step with the transporter prior to influx into the cell, without having to fit real binding constants, as done previously for P-gp. For each transporter, both Vmax and K_M are used to fit the data, but we have found, thus far, that only the ratio Vmax/K_M (s^{-1}) was constant. From Eq. (3), this would imply that the K_M of the transporter is much larger than the substrate concentration in the inner apical membrane. For this modeling, we have assumed that the unknown transporters are facilitated transporters, i.e. they support transport in both directions. This was not a strong assumption, since substrate flux was mostly unidirectional during these experiments. Once the transporters are identified, more rigorous modeling can be applied.

The cells do not lose any capacity for drug transport over 6 hour incubations (Tran et al., 2005; Acharya et al., 2006), implying that cellular ATP levels remain adequate for full P-gp function throughout experiment. The passive permeability coefficients used in the mass action model were determined in the presence of 2 μM of the GF120918 (Hyafil et al., 1993; Polli et al., 2001; Tran et al., 2004, 2005).

Results

Loperamide transport requires an additional basolateral transporter. The kinetic parameters for P-gp transport published in Acharya et al. (2006), and shown in part here in Table 1, assumed that P-gp was the sole transporter. This model works very well for amprenavir and quinidine. The transport of loperamide (10μM) in the apical-to-basolateral (A>B) and basolateral-to-apical (B>A) directions across MDCKII-hMDR1 monolayers is shown in Figure 2 and the model, shown by the lines through the data points, fits the experimental data reasonably well.

However, as shown originally in Tran et al. (2005) and confirmed in Acharya et al. (2006), the "P-gp alone" model gave adequate fits for loperamide only with concentrations above 3μM. At lower concentrations, more loperamide transport was observed than could be fitted assuming only passive permeability (i.e. +GF120918) and P-gp mediated transport. The passive permeability coefficients calculated in the presence of GF120918 were too small to account for the measured efflux, even when the P-gp parameters were set to maximal values.

This is shown in Figure 3 by the dotted lines, which substantially underestimate the flux of 1μM loperamide shown by the data points. Addition of a basolateral transporter with $Vmax/K_M = 100s^{-1}$ yields a much better fit to the experimental data (Table 1 and Figures 3, solid lines). Both Vmax and K_M were fitted separately, but only their ratio was constant suggesting that a single transporter is responsible for the increased flux. This kinetic evidence highlights the significant contribution of an uptake basolateral transporter for loperamide at lower concentrations.

After about 4 hours, the fit slightly overestimates the apical concentration. If there were an apical transporter for loperamide, in addition to P-gp, then the final steady state concentration for loperamide in the apical chamber would be smaller. Indeed, a better

fit at 4 hrs can be found with the addition of this second efflux transporter (not shown). However, the deviation is likely experimental error as the parameters in Table 1 support the need for only a basolateral transporter. The effect of a second apical efflux transporter should be more pronounced for even lower loperamide concentrations. As expected the difference between the dotted line and the data points is larger for 0.03μM loperamide (Figure 4). But an additional apical transporter is not required to fit loperamide transport at 0.03 μM (fit not shown).

Digoxin is transported by both a basolateral and an apical transporter. We measured digoxin transport across the MDCKII-MDR1 cell monolayers for 6 hours starting with 1μM digoxin in the basolateral chamber. The flux of digoxin into the apical chamber is linear with time, yielding no "fittable" data, as some degree of saturation is required to derive values for the kinetic parameters. When the cells were incubated for an extended the time (>6 hrs), the transport curves showed a clear toxic effect (data not shown).

This led us to construct a "data stitching" method to measure transport over longer time periods. Once the concentrations of digoxin in the apical and basolateral chambers at the 6^{th} hour are known, the next experiment begins with the initial concentration of digoxin in both chambers matching those at the 6^{th} hour. Using this approach, data is collected for consecutive stretches of 6 hours and stitched together to create a time course curve up to 30 hours (Figure 6). The only artifact in stitching is that the cytosol is initially empty of substrate. However, as the volume of the confluent cell monolayer cytosol is very small, steady state will be reached within the first few minutes of substrate addition (Tran et al., 2004; Acharya et al., 2006).

The kinetic fits for the digoxin concentration time curve are shown in Figure 7. The dotted line shows the fit using just the "P-gp alone" model, which underestimates transport by approximately 50%. The solid line shows the fit using a basolateral transporter

with $Vmax/K_M = 30s^{-1}$ and the parameters given in Table 1. Both Vmax and K_M were fitted separately, but only their ratio was constant, which suggests that only one transporter is responsible. The solid line fits well up to 12 hours. However, beyond 12 hrs, it predicts too much transport. Addition of a second apical transporter with a $Vmax/K_M = 2s^{-1}$ for digoxin, in addition to P-gp and the basolateral transporter, yields a lower final steady state concentration for digoxin in the apical chamber (Figure 7, dashed line). The contribution of the apical transporter is more than experimental error, unlike the case for loperamide (Figure3).

In order to determine the identity of these transporters involved with digoxin transport, inhibition studies were completed with a variety of prototypical substrates or inhibitors for OAT, OCT and MRP transporters (Table 2). The compounds mentioned in Table 2 were selected for inhibition studies because they cover a broad range of possibilities for known transporters on the basolateral and apical membranes of kidney cells. The concentrations of the compounds were chosen based on their K_I or IC50 values reported in the papers cited. To evaluate whether these compounds have any effect on loperamide or digoxin transport, we used concentrations higher than the maximum concentration used for the experiments in the respective papers. This was a reasonable starting point because high concentrations would ensure that any effect on the transport of the probe substrates did not go undetected.

By incubating cells with a high concentration of a substrate or an inhibitor for the basolateral transporter, the transport of digoxin should decrease to the levels predicted by the P-gp efflux alone curves (i.e. a 50% reduction in transport). This makes the kinetic analysis a very sensitive instrument for determining the identity of the basolateral transporter. Except for loperamide, incubations with the prototypical substrates/inhibitors failed to inhibit digoxin transport suggesting these candidate transporters were not the unknown basolateral transporter involved in flux of digoxin across the MDCKII-hMDR1

cell line. The inhibition of digoxin transport by loperamide, and vice versa, certainly involves P-gp, but we further studies are required to determine whether they share a single basolateral transporter, or whether there are two different basolateral transporters.

Out of all the substrates/inhibitors tested, only 100μM and 200μM benzbromarone inhibited 1μM digoxin transport in the B>A direction by 20% and 50% respectively (data not shown), but these concentrations also showed toxic effects on the cells, i.e. the transport curves stopped abruptly after a few hours and the cell monolayer became leaky. These results led us to perform the cell concentration exclusion assay using 1μM benzbromarone with the aim to find out if it actually caused less accumulation of digoxin in the cells.

Cell concentration exclusion assay shows benzbromarone selectively inhibits digoxin accumulation within the cell monolayer. The amount of radioactivity from digoxin associated to the cells was measured in the presence and absence of benzbromarone. Presumably if Benzbromarone inhibits the basolateral and/or apical transporter/s, then less digoxin would be accumulated within the cells. Figure 8 shows cellular digoxin radioactivity by itself, and in the presence of quinidine (a P-gp substrate-inhibitor), GF120918 (inhibits P-gp and the additional basolateral and apical transporters) and benzbromarone. Digoxin, quinidine, benzbromarone and GF120918 are abbreviated as DGX, QND, BZB and 918 respectively. In presence of 20μM quinidine, P-gp is relatively saturated with quinidine (Acharya et al., 2006) and there is more digoxin present within the cells compared to digoxin alone. In presence of 2μM GF120918 , P-gp and the additional transporters are completely inactive and there is even more digoxin present within the cells. In contrast, in presence of 1μM benzbromarone there is significantly less digoxin accumulation, suggesting inhibition of a basolateral and/or apical uptake transporter/s. This led us to investigate the effect of 1μM benzbromarone on digoxin transport (figures 9 and 10) . With 1μM benzbromarone the monolayer was tight up to 4 hours, i.e. the total flux of lucifer yellow remained $<$ 10nm/s. Therefore 1μM benzbromarone

doesn't have toxic effects on cells.

There is no effect of 1μM benzbromarone on the B>A or A>B transport of 1μM digoxin. To investigate if benzbromarone has any effect on digoxin transport due to its possible interaction with the additional basolateral or apical transporter, a bidirectional digoxin transport curve was generated in the presence and absence of benzbromarone. Figure 9A and 9B shows nmoles of digoxin transported B>A and A>B over 6 hours with a starting concentration of 1μM digoxin in the donor side in presence and absence of 1μM benzbromarone. There is no significant effect ($p \gg 0.05$ for both B>A and A>B directions based on linear regression analysis) of 1μM benzbromarone on digoxin transport.

Discussion

The rigorous kinetic analysis of P-gp mediated transport through the confluent MDCKII-hMDR1 cell monolayer has provided a quantitative view of P-gp function through the elementary rate constants (Tran et al., 2005; Acharya et al., 2006). The kinetic modeling work presented here provides evidence for other unknown transporter(s) in the MDCKII cells which facilitate the passage of loperamide and digoxin through the basolateral membrane, so that they can reach P-gp more quickly than by simple passive permeability. In addition, there appears to be an apical transporter that allows digoxin re-entry into the cells after efflux into the apical chamber. Each of these transporters is inhibited by GF120918. These findings have expanded the kinetic modeling from its focus on P-gp mechanism to a tool to elucidate other transporters involved in transcellular transport.

The current fitted parameters for P-gp shown in Table 1. The transcytosis of amprenavir and quinidine across the MDCKII-hMDR1 confluent cell monolayer are quantitatively fitted by P-gp and passive permeability alone. In Tran et al. (2005) and Acharya et al. (2006), it was noted that for loperamide there was another process affecting the B>A transport. By adding a facilitated transporter to the basolateral membrane allows the loperamide data from 12nM to 30μM to be fitted with the parameter values shown in Table 1. At and above 30μM loperamide, P-gp is completely saturated and contributes little to the total transport relative to passive permeability alone. This addition to the kinetic model for loperamide has changed the estimate for loperamide's binding constant from 4,000 M^{-1} (Acharya et al., 2006) to 20,000 M^{-1} (Table 1). The reason for this increase is that the binding constant, K_C, is primarily fitted by the A>B transport (Tran et al., 2005) and the basolateral transporter for loperamide speeds up permeation to the basolateral chamber. Thus, a stronger binding constant to P-gp is required to fit the same A>B flux data.

The flux of loperamide from the basolateral chamber into the cytosol is 60% due to passive permeability (+GF120918) and 40% due to this transporter (-GF120918) (Table 1). This transporter could be active, directed from basolateral to cytosol, but future studies will be required to clarify this point, including finding some compound to inhibit the transporter.

For digoxin, using the stitched data to approximate a 30 hour transport experiment, both a basolateral transporter and an apical transporter are needed to fit the experimental data. The passive flux of digoxin from the basolateral chamber into the cytosol is 30% due to passive permeability (+GF120918) and 70% due to this basolateral transporter. Conversely, from the apical chamber into the cytosol, the flux is 95% due to passive permeability (+GF120918) and 5% due to the apical transporter (-GF120918). In contrast to digoxin and loperamide, neither amprenavir nor quinidine showed any significant improvement in fit with additional transporters aside from P-gp, suggesting that any other transporter has a kinetically insignificant rate.

We have tried to identify these transporters by adding prototypical substrates of known transporters and determining whether the loperamide or digoxin transport curves would drop to the levels predicted by the "P-gp only" curves (Figures 3, 4 and 7). The change in the predicted curves would be very large, making the kinetic modeling an extremely sensitive assay for discovering functional transporters in the confluent cell monolayer. None of the compounds tested in Table 2 affected transport during the first few hours. There were some changes noted after 2-3 hours, but these appeared to be due to toxicity.

A cell concentration exclusion assay was also tried, wherein the concentration of digoxin within the confluent cell monolayer was assayed as a function of benzbromarone concentration, as influx of digoxin into the cytosol is mainly due to transporters. It was anticipated that in the presence of an inhibitor, there should be a large reduction in accumulated digoxin. Addition of benzbromarone resulted in a very significant reduction of digoxin ac-

cumulation within the cell monolayer. However, benzbromarone had no significant effect on digoxin B>A or A>B transport in the same cellular system. Thus, the reduction in cell associated digoxin by benzbromarone is due another mechanism besides the unknown "kinetic" basolateral or apical transporter. The simplest hypothesis is that benzbromarone reduces the cell's cytosolic volume, so less digoxin can accumulate. This would have no predicted change in transport of digoxin, since the kinetic model predicts that most of it diffuses along the inner plasma membrane. Transcellular transport of amphipathic P-gp substrates depends upon plasma membrane area, not on cell volume. This suggests that cell concentration exclusion assays must be carefully controlled when used with amphiphilic compounds effluxed from transporter whose binding sites are within the plasma membrane, like P-gp or the MRPs (Lugo & Sharom, 2005; Borst et al., 2005).

These results lead us conclude that digoxin and loperamide are not good candidates for a probe substrate with the MDCKII-hMDR1 cell line. If a drug inhibits B>A digoxin flux, it could be that the inhibition occurs at the digoxin basolateral transporter, rather than at P-gp. On the other hand, it appears that quinidine or amprenavir are safe probe substrates for this cell line, since their B>A transport could be inhibited only at P-gp.

References

Acharya P, Tran TT, Polli JW, Ayrton A, Ellens H and Bentz J (2006) P-gp expressed in a confluent monolayer of hMDR1-MDCKII cells has more than one efflux pathway with cooperative binding sites. Biochemistry, 45:15505-15519.

Bentz J, Tran TT, Polli JW, Ayrton A and Ellens H (2005) The steady-state Michaelis-Menten analysis of P-glycoprotein mediated transport through a confluent cell monolayer cannot predict the correct Michaelis constant K_M. Pharm Res. 22:1667-1677.

Borst P, Zelcerb N, van de Weteringa K and Poolman, B. 2005. On the putative co-transport of drugs by multidrug resistance proteins. FEBS Lett. 580:1085-1093.

Dresser MJ, Leabman MK and Giacomini KM (2001) Transporters Involved in the Elimination of Drugs in the Kidney: Organic Anion Transporters and Organic Cation Transporters. J. Pharm. Sci. 90(4):397-421.

Dutt A, Heath LA and Nelson J (1994) P-Glycoprotein and Organic Cation Secretion by the Mammalian Kidney. J.Pharm.Exp. Ther. 269(3):1254-60.

Enomoto A and Endou H (2005) Roles of organic anion transporters (OATs) and a urate transporter (URAT1) in the pathophysiology of human disease. Clin. Exp. Nephrol. 9:195-205.

Evers R, Kool M, Smith AJ, van Deemter L, de Haas M and Borst P (2000) Inhibitory effect of the reversal agents V-104, GF120918 and Pluronic L61 on MDR1 P-gp, MRP1- and MRP2-mediated transport. British J. Cancer. 83:366-374.

Goh LB, Spears KJ, Yao D, Ayrton A, Morgan P, Roland WC and Friedberg T (2002) Endogenous drug transporters in *in vitro* and *in vivo* models for the prediction of drug disposition in man. Biochem. Pharmacol. 64:1569-1578.

Harris MJ, Kagawa T, Dawson PA, Arias IM (2004) Taurocholate transport by hepatic and intestinal bile acid transporters is independent of FIC1 overexpression in Madin-Darby canine kidney cells. J Gastroenterol Hepatol. 2004 Jul;19(7):819-25.

Horikawa M, Kato Y, Tyson CA, Sugiyama Y (2002) The potential for an interaction between MRP2 (ABCC2) and various therapeutic agents: probenecid as a candidate inhibitor of the biliary excretion of irinotecan metabolites. Drug Metab. Pharmacokinet. 17, 23-33.

Hyafil F, Vergely C, Du Vignaud P and Grand-Perret T (1993) In vitro and *in vivo* reversal of multidrug resistance by GF120918, an acridonecarboxamide derivative. Cancer Res. 53:4595-602.

Ismair MG, Stanca C, Ha HR, Renner EL, Meier PJ and Kullak-Ublick GA (2003) Interactions of glycyrrhizin with organic anion transporting polypeptides of rat and human liver. Hepatol. Res. 26, 343-347.

Iwanga T, Kobayashi D, Hirayama M, Maeda T and Tamai I (2005) Involvement of Uric Acid transporter in increased renal clearance of the Xanthine Oxidase inhibitor Oxypurinol induced by a uricosuric agent, Benzbromarone. Drug Metab. Disp. 33(12): 1791-95.

Kikuchi R, Kusuhara H, Abe T, Endou H and Sugiyama Y (2004) Involvement of Multiple Transporters in the Efflux of 3-Hydroxy- 3-methylglutaryl-CoA Reductase Inhibitors across the Blood-Brain Barrier. J.Pharm.Exp. Ther. 311(3):1147-53.

Kikuchi A, Nozawa T, Wakasawa T, Maeda T And Tamai I (2006) Transporter-mediated intestinal absorption of Fexofenadine in rats. Drug Metab Dispos. 21,4:308-314.

Lau YY, Okochi H, Huang Y and Benet LZ (2006) Multiple transporters affect the disposition of atorvastatin and its two active hydroxy metabolites: application of *in vitro* and ex situ systems. J. Pharmacol. Exp. Ther. 316, 762-771.

Lee W and Kim R B (2004) Transporters and renal drug elimination. Annu. Rev. Pharmacol. Toxicol. 44:137-66.

Loo TW and Clarke DM (2005) Recent Progress in Understanding the Mechanism of P-Glycoprotein-mediated Drug Efflux. J. Membr. Biol. 206:173-185.

Lowes S, Cavet ME and Simmons NL (2003) Evidence for a non-MDR1 component in digoxin secretion by human intestinal Caco-2 epithelial layers. Eur J Pharmacol. 1;458(1-2):49-56.

Lugo MR and Sharom FJ (2005) Interaction of LDS-751 with P-glycoprotein and mapping of the location of the R drug binding site. Biochemistry 44:643-55.

Mita S, Suzuki H, Akita H, Hayashi H, Onuki R, Hofmann AF and Sugiyama Y (2006) Inhibition of Bile Acid Transport across Na+/Taurocholate Cotransporting Polypeptide (SLC10A1) and Bile Salt Export Pump (ABCB 11)-Coexpressing LLC-PK1 Cells by Cholestasis-Inducing Drugs .Drug Metab Dispos. 34: 1575-1581.

Morita N, Kusuhara H, Sekine T, Endou H and Sugiyama Y (2001) Functional characterization of rat organic anion transporter 2 in LLC-PK1 Cells. J.Pharm.Exp. Ther. 298(3):1179-1184.

Morrow CS, Peklak-Scott C, Bishwokarma B, Kute TE, Smitherman PK, Townsend AJ (2006) Multidrug resistance protein 1 (MRP1, ABCC1) mediates resistance to mitoxantrone via glutathione-dependent drug efflux. Mol. Pharmacol. 69:1499-505.

Noe B, Hagenbuch B, Stieger B and Meier PJ (1997) Isolation of a multispecific organic anion and cardiac glycoside transporter from rat brain. Proc. Natl. Acad. Sci. USA 94:10346-10350.

Pan G and Elmquist WF (2007) Mitoxantrone permeability in MDCKII cells is influenced by active influx transport. Mol. Pharmaceutics Web publication 10.1021/mp060083b S1543-8384(06)00083-9.

Polli JW, Wring SA, Humphreys JE, Huang L, Morgan JB, Webster LO and Serabjit-Singh CS (2001) Rational use of *in vitro* P-glycoprotein assays in drug discovery. J. Pharm. and Exp. Therap. 299:620-628.

Rautio J, Humphreys JE, Webster LO, Balakrishnan A, Keogh JP, Kunta JR, Serabjit-Singh CJ and Polli JW (2006) In Vitro P-glycoprotein Inhibition Assays for Assessment of Clinical Drug Interaction Potential of New Drug Candidates: A Recommendation for Probe Substrates. Drug Metab Dispos. 34:786-792.

Sasaki M, Suzuki H, Aoki J, Ito K, Meier PJ and Sugiyama Y (2004) Prediction of *in vivo* biliary clearance from the *in vitro* transcellular transport of organic anions across a double-transfected Madin-Darby canine kidney II monolayer expressing both rat organic anion transporting polypeptide 4 and multidrug resistance associated protein 2. Mol. Pharmacol. 66, 450-459.

Shitara Y, Horiea T and Sugiyama Y (2006) Transporters as a determinant of drug clearance and tissue distribution. Eur. J. Pharm. Sci. 27:425-446.

Shu Y, Bello CL, Mangravite LM, Feng B and Giacomini KM (2001) Functional characteristics and steroid hormone-mediated regulation of an organic cation transporter in Madin-Darby Canine Kidney cells. J. Pharm. Exp. Ther. 299(1):392-398.

Spears KJ, Ross J, Stenhouse A, Ward CJ, Goh LB, Wolf CR, Morgan P, Ayrton A and Friedberg TH (2005) Directional trans-epithelial transport of organic anions in porcine LLC-PK1 cells that co-express human OATP1B1 (OATP-C) and MRP2. Biochem. Pharmacol. 69: 415-423.

Sugiyama D, Kusuhara H, Shitara Y, Abe T, Meier PJ and Sekine T (2001) Characterization of the efflux transport of 17beta-estradiold-17beta-glucuronide from the brain across the blood- brain barrier. J. Pharmacol. Exp. Ther. 298, 316-322.

Tahara H, Kusuhara H, Maeda K, Koepsell H, Fuse E and Sugiyama Y (2006) Inhibition Of Oat3-mediated renal uptake as a mechanism for drug-drug interaction between fexofenadine and probenecid. Drug Metab Dispos. 34:743-747.

Tang F, Horie K and Borchardt RT (2002a) Are MDCK cells transfected with the human MRP2 gene a good model of the human intestinal mucosa? Pharm Res.;19:765-772.

Tang F, Horie K and Borchardt RT (2002b) Are MDCK cells transfected with the human MDR1 gene a good model of the human intestinal mucosa? Pharm Res. 19: 773-779.

Tran TT , Mittal A, Aldinger T, Polli JW, Ayrton A, Ellens H and Bentz J (2005) The elementary mass action rate constants of P-gp transport for a confluent monolayer of MDCKII-hMDR1 cells. Biophys. J. 88:715-738.

Tran TT, Mittal A, Gales T, Maleeff B, Aldinger T, Polli JW, Ayrton A, Ellens H and Bentz J (2004) An Exact Kinetic Analysis of Passive Transport across a Polarized Confluent MDCK Cell Monolayer Modeled as a Single Barrier. J. Pharm. Sci. 93:2108-2123.

Troutman MD and Thakker DR (2003a) Novel Experimental Parameters to Quantify the Modulation of Absorptive and Secretory Transport of Substrates by P-Glycoprotein in Cell Culture Models of Intestinal Epithelium. Pharm. Res. 220:1210-1224.

Troutman MD and Thakker DR (2003b) Efflux Ratio Cannot Assess P-Glycoprotein-Mediated Attenuation of Absorptive Transport: Asymmetric Effect of P-Glycoprotein on Absorptive and Secretory Transport across Caco-2 Cell Monolayers. Pharm. Res. 20:1200-1209.

Vavricka SR, Montfoort JV, Ha HR, Meier PJ and Fattinger K (2002) Interactions of Rifamycin SV and Rifampicin with organic anion uptake systems of human liver. Hepatology, 36(1):164-172.

Figures

Substrate	P-gp Efflux to Apical Chamber k_2 [a] (s^{-1})	P-gp Dissociation to Apical Membrane k_r [b] (s^{-1})	P-gp Binding Constant K_C (M^{-1}) [c] Cytosolic Dissociation Constant $K_{D,Aq}$ (M)	Partition Coefficient K_{PC} [d]	Steady State Passive Permeability Coefficients [e] (nm/sec)	Basolateral Transporter Vmax/Km (s^{-1}) [f] % Passive Transport into cytosol	Apical Transporter Vmax/Km (s^{-1}) [f] % Passive Transport into cytosol
AMP	150	$2x10^6$	1000 "5 uM"	200	P_{BA}=420±50 P_{AB}=400±50	0 0%	0 0%
QND	5	$1x10^5$	15,000 "0.1 uM"	700	P_{BA}=500±100 P_{AB}=500±100	0 0%	0 0%
LPM	1	$5x10^5$	20,000 "0.1 uM"	3000	P_{BA}=350±80 P_{AB}=400±100	100 40%	0 0%
DGX	10	$4x10^6$	"500"	"100"	P_{BA}=30±8 P_{AB}=25±5	30 70%	2 5%

Figure 10.1: Paper 2: Table 1 - Fitted Parameter Values with Single Substrate Experiments

Legend for Table 1.

[a] Estimate for the efflux rate constant k_2, from P-gp into the apical chamber, given by the ratio of the fitted k_2T(0) for each drug and the center of the box value of $T(0) = 2\text{x}10^{-4}$ M.

[b] Estimate for the dissociation rate constant k_r, from P-gp back into the inner apical monolayer.

[c] The binding constant between P-gp and the inner apical monolayer shown is the average of the best fits (> 160 for each drug concentration). Below each binding constant, we show in parentheses the appropriate dissociation constant for each drug relative to the aqueous phase, calculated as $K_{I,Aq}$ =1/(K_C*drug partition coefficient{PS/PE/chol}), the liposome mimic for the inner apical monolayer. These aqueous dissociation constants are given only to a single significant digit and no error bars were calculated.

[d] Equilibrium drug partition coefficient to 0.1 μm PS/PE/chol (1:1:1) liposomes. This lipid composition is a rough mimic for the inner apical monolayer, as described in Tran et al. (2005).

[e] Steady state passive permeability coefficients measured across the confluent cell monolayer, in the presence of the P-gp inhibitor GF120918. P_{BA} is shown above and P_{AB} is shown beneath. The values are not always symmetric, since the passive permeability for loperamide is faster in the A>B direction than in the B>A direction. This was also observed in Tran et al. (2004).

[f] The fits for the basolateral transporter, where both Vmax and K_M were free, but

only their ratio was constant. Amprenavir and quinidine were completely fitted by P-gp and GF120918 passive permeabilities. This does not mean they cannot use the basolateral transporter, just that little if any of their transport is due to the basolateral transporter. The same is true for the apical transporter, with the addition that loperamide shows no significant transport through it. % GF120918 transport is the fraction of transport into the cytosol, B>C or A>C, due to the transporter, relative to all +GF120918 passive transport.

Compound	Transporter [a]	Drug used		References
		Loperamide	Digoxin	
Benzbromarone	hMRP1,2,3,4,5,6 hURAT1,	Not tested	No effect with 10uM[d]	Enomoto and Endou, 2005; Lee and Kim, 2004; Iwanga et al., 2005.
Digoxin	oatp1a4, 4c1, 1b3, 1b1, roatp2, rOat-K2	moderate inhibition with 10uM DGX	NA	Dresser et al. 2001; Noe et al., 1997.
Fexofenadine	hOAT3,roatp3,	No effect[c] with 300uM	No effect with 300uM	Tahara et al., 2006; Kikuchi et al., 2006.
Glycyrrhizic acid	hOATP1B1,1B3, roatp1a1, 1a4, 1b2	Not tested	No effect with 200uM	Ismair et al., 2003.
Indocyanine Green	rOat2,3, r/hOATP2	Not tested	No effect with 10uM	Morita et al., 2001.
Loperamide		NA [b]	Good Inhibition	
Mitoxantrone	MRP1, BCRP	No effect with 25uM	No effect with 25uM	Pan and Elmquist, 2007; Morrow et al., 2006.
Ouabain	rOatK-2, roatp2, oatp4c1, 1b3	10uM inhibits after 4hrs	10uM shows biphasic transport curve which is reproducible. [c]	Dresser et al., 2001; Noe et al., 1997.
Para-aminohippurate	m/r Oat1, hOAT1, rOat2,3	No effect with 100uM	100uM PAH inhibits after 3hrs	Dresser et al., 2001; Kikuchi et al., 2004.
Probenecid	m/r Oat1,3,4, hOAT1, rOat-K2	No effect with 200uM, Pass perm changes	No effect with 200uM, pass permeability changes	Dresser et al., 2001; Horikawa et al., 2002; Sugiyama et al., 2001.
Rifamycin	rOat2, hOATP-A,C,8,1B1, 1B3	Not tested	No effect with 3uM	Dresser et al., 2001; Vavricka et al., 2002.
Taurocholic acid	Bile acid/salt transporters ASBT,BSEP,NTCP	No effect with 200uM	No effect with 200uM	Mita et al., 2006; Harris et al.,2004.
Tetra-ethyl ammonium	Many OCTs	No effect	Not tested	Dresser et al., 2001; Shu et al., 2001; Dutt et al, 1994.

Figure 10.2: Paper 2: Table 2 - List of compounds tested to identify additional transporters for loperamide and digoxin.

Legend for Table 2.

[a] The compounds used here are substrates and/or inhibitors of known mammalian transporters. Names of all human transporters (OATs, OATPs, MRPs) are in upper case. Transporters in mice or rats are in all lower case (e.g. oatp) or start with an upper case letter followed by the rest in lower case (e.g. Oat).

[b] NA denotes not applicable.

[c] Best inhibition is seen when there is digoxin transport in presence of ouabain without any preincubation. 30mins preincubation with ouabain produces a jump at 4hrs.

[d] 100 and 200μM benzbromarone were tested but these concentrations had toxic effects on cells.

[e] No effect means lack of significant (>10%) inhibition by 2 hrs.

Figure Legends

Figure 1. Cartoon model of a confluent cell monolayer. It shows the apical membrane with microvilli on top and the basolateral membrane on the bottom, where the cells attach to the polycarbonate insert. Passive permeability occurs in both directions. This is measured when P-gp is completely inhibited by GF120918. P-gp expressed on the apical membrane transports substrate from the inner apical monolayer into the apical chamber. The concentration of substrate in the apical and basolateral chambers, C_A and C_B, are measured. The concentration of substrate in the inner plasma membrane, C_{PC}, and the cytosol, C_C, are predicted as part of the data fitting analysis. Transporters other than P-gp are known to operate in the basolateral and apical membrane, that might influence the uptake and efflux rates of P-gp substrates.

Figure 2. 10μM Loperamide transport data can be fitted using just P-gp parameters. This figure shows the concentration of loperamide over time in each chamber starting with 10μM loperamide initially in the donor chamber across the MDCKII-MDR1 cell monolayer. The B:B>A and A:B>A curves denote the concentration of drug in the basolateral and apical chambers when the basolateral chamber was the donor, i.e. transport runs B>A. Similarly, the A:A>B and B:A>B curves denote the concentration of drug in the apical and basolateral chambers when the apical chamber was the donor, i.e. transport runs A>B. B>A data are shown by open squares ($\Box$) when the apical chamber is sampled and by open circles ($\circ$) when the basolateral chamber is sampled. Open triangles ($\triangle$) and diamonds ($\diamond$) represent concentrations measured in the apical and basolateral chambers when transport run from A>B. The fits for the basolateral data are shown by the solid line (–), i.e. both B:B>A and B:A>B. The fits when the apical chamber is sampled are shown by the dotted line (...), i.e. both A:B>A and A:A>B. The same symbols and notations

are used in Figures 3, 4, 5, 6 and 7. All data points represent triplicate measurements at each time point with the corresponding standard deviation. The fits use the parameters published in Acharya et al. (2006) for loperamide, which assumed no other transporters beyond P-gp. There is reasonably good fit to the data as the lines depicting the simulations pass through the data points representing triplicate measurements at each time point.

Figure 3. 1μM loperamide needs a basolateral transporter. This figure shows the concentration of loperamide over time in each chamber starting with 1μM loperamide initially in the basolateral donor chamber. The dotted line shows the fit using the parameters for only P-gp mediated loperamide transport which clearly underestimates amount of transport. The solid line shows the fit using a basolateral transporter with Vmax/K_M=100s^{-1}. Both Vmax and K_M were fitted separately, but only their ratio was constant.

Figure 4. Loperamide only needs a basolateral transporter. This figure shows the concentration of loperamide over time in each chamber starting with 0.3μM loperamide initially in the donor chamber across the MDCKII-MDR1 cell monolayers. The dotted line shows the fit using the loperamide parameters from Acharya et al. (2006), which clearly underestimates transport by about 40% which is much more than was seen in figure 3 for 1μM loperamide. The solid line shows the fit in presence of P-gp and a basolateral transporter with Vmax/K_M=100s^{-1}.

Figure 5. Digoxin transport curve is generated by measuring transport over consecutive stretches of 6 hours. This figure shows the concentration of digoxin over time in each chamber starting with 1μM initially in the basolateral donor chamber across the MDCKII-MDR1 cell monolayers. The increase of digoxin concentration in the apical

chamber is linear, so fitting is not possible. To measure transport for a longer time course, we adopted a "data stitching" method. Once we know the concentrations of digoxin in the apical and basolateral chambers at the 6^{th} hour, we start the next experiment such that the initial concentration of digoxin in both chambers match (as closely as possible) those at the 6^{th} hour.

Figure 6. Digoxin transport curve is generated by stitching transport data upto 30 hours. This figure shows the concentration of digoxin over time in each chamber starting with 1μM initially in the basolateral donor chamber across the MDCKII-MDR1 cell monolayers. The concentration of digoxin in the apical chamber increases over time and finally reaches a steady state.

Figure 7. Digoxin is transported by a basolateral and an apical transporter, in addition to P-gp. This figure shows the concentration of Digoxin over time in each chamber starting with 1μM digoxin initially in the basolateral donor chamber. The dotted line shows the "best" fit using P-gp parameters, basically set to infinite forward values, which clearly underestimates transport by about 50%. The solid line shows the fit using the parameters given in Table 1 of this work, which has a basolateral transporter with Vmax/K_M=30s^{-1} in addition to P-gp. The solid line fits up to 12 hours and beyond that, it predicts more transport than we actually measure. If there were an apical transporter for digoxin, in addition to P-gp, then the final steady state concentration for digoxin in the apical chamber would be smaller. This is shown by the dashed line, with Vmax/K_M=2s^{-1} for the additional apical transporter.

Figure 8. Digoxin cell concentration exclusion by benzbromarone. This figure shows radioactivity in disintegrations per minute from radiolabeled digoxin in MDCKII-

hMDR1 cells by itself (column A) , in presence of quinidine (a P-gp substrate-inhibitor)(column B), GF120918 a potent inhibitor of P-gp and both the additional digoxin transporters (column C) and benzbromarone (substrate for MRP1, MRP2, hURAT1) (column D). In presence of 20μM quinidine (column B), there is more digoxin bound to cells compared to digoxin alone. There is even more digoxin bound when P-gp and the other transporters are completely inhibited by GF120918 (column C). The highlight of this figure is the smallest bar (column D), which shows there is significantly less digoxin bound in presence of benzbromarone, suggesting that it interacts with the basolateral and/or apical transporter for digoxin and blocks digoxin entry into the cells. Digoxin, Quinidine and GF120918 are abbreviated as DGX, QND and 918 to fit them into the figure.

Figure 9. There is no effect of 1μM benzbromarone on the transport of 1μM digoxin. Figure 9A shows nmoles of digoxin transported B>A over 6 hours when the donor starts with 1μM digoxin in the presence and absence of 1μM benzbromarone in both chambers. Circles and triangles represent presence and absence of 1μM benzbromarone during digoxin transport. Same abbreviations are used as in figure 8. Benzbromarone is abbreviated as BZB. The circles and triangles are open ($\circ$, $\triangle$) when there is active transport and closed ($\bullet$,$\blacktriangle$) when there is GF120918 to inhibit both P-gp and the putative transporters.

Similarly, in figure 9B , A>B transport of 1μM digoxin in the presence and absence of 1μM benzbromarone is shown. Open squares ($\square$) represent transport of digoxin alone and open circles ($\circ$) depict digoxin transport in presence of benzbromarone. The corresponding filled symbols represent A>B flux in presence of GF120918. Benzbromarone is not a specific inhibitor for the putative basolateral/apical transporter since it has no effect on digoxin transport.over a period of 6 hours in either direction.

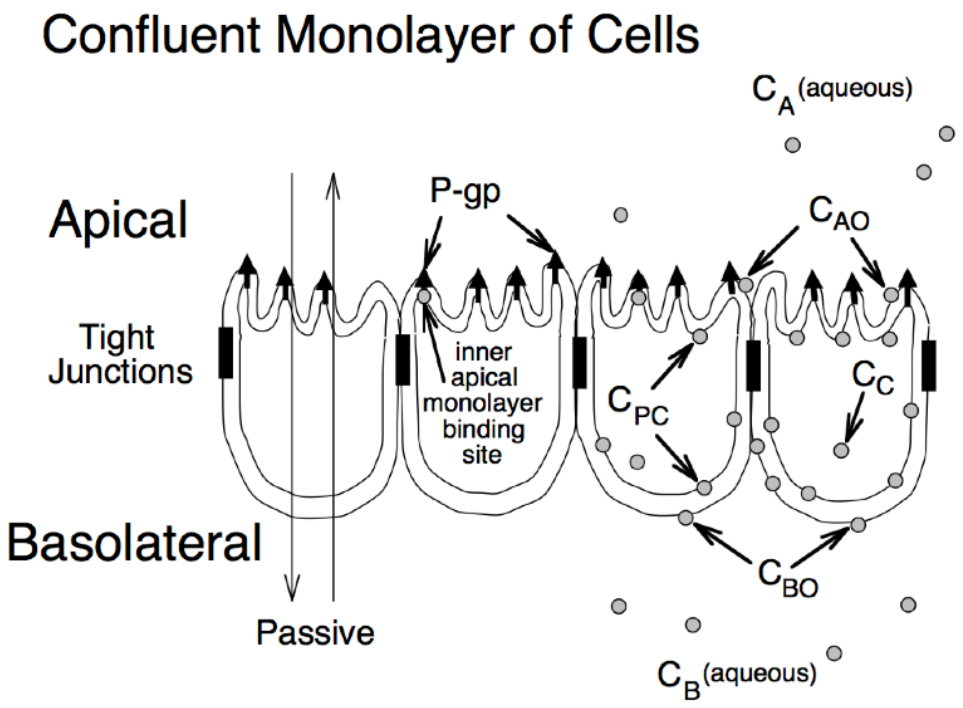

Figure 10.3: Paper 2: Figure 1 - Cartoon model of a confluent cell monolayer.

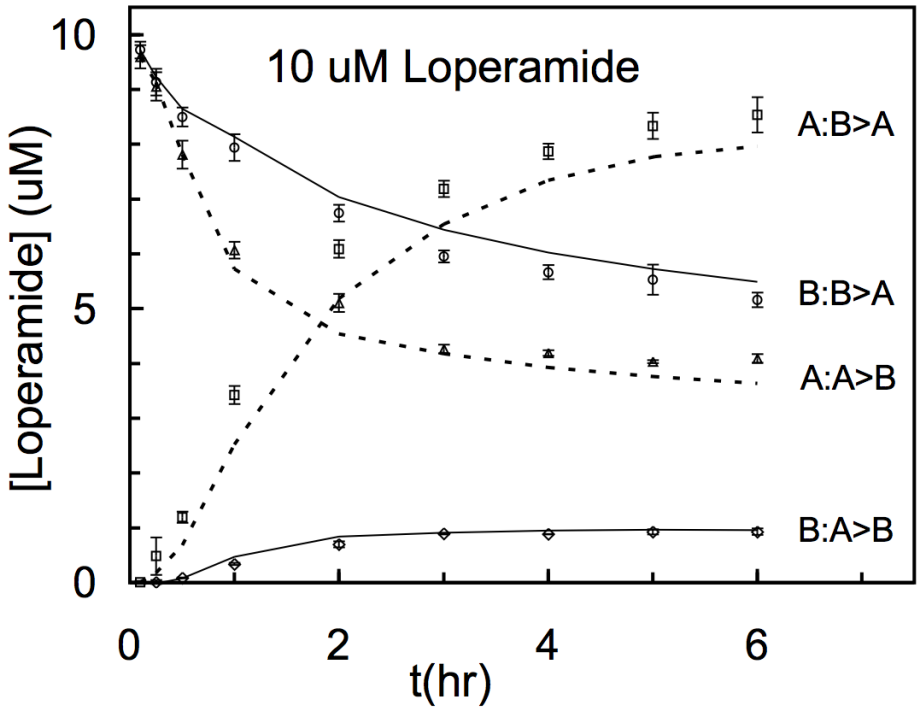

Figure 10.4: Paper 2: Figure 2 - 10μM Loperamide transport data can be fitted using just P-gp parameters.

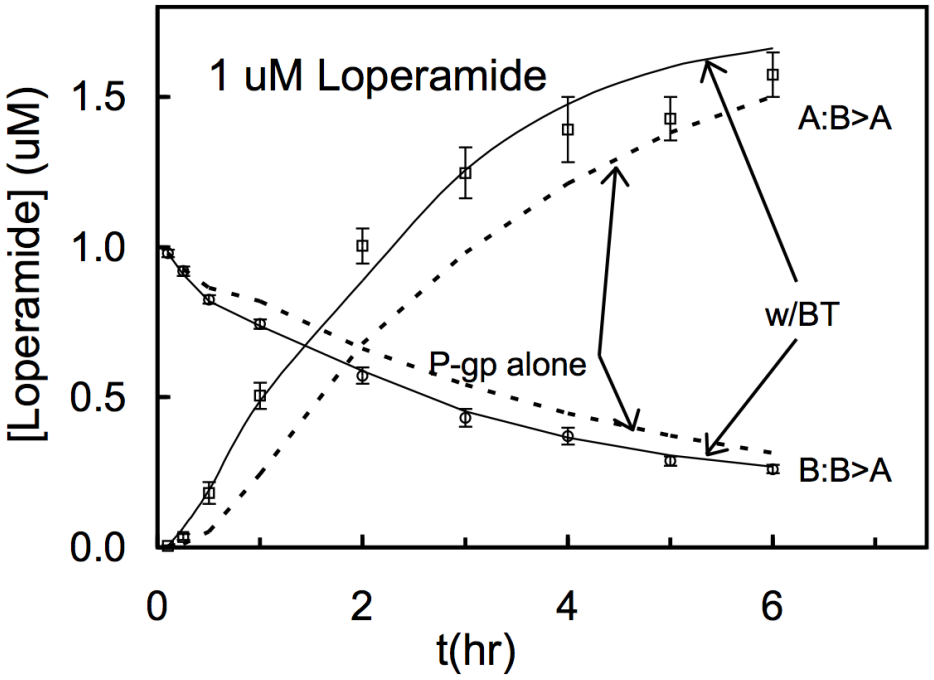

Figure 10.5: Paper 2: Figure 3 - 1μM loperamide needs a basolateral transporter.

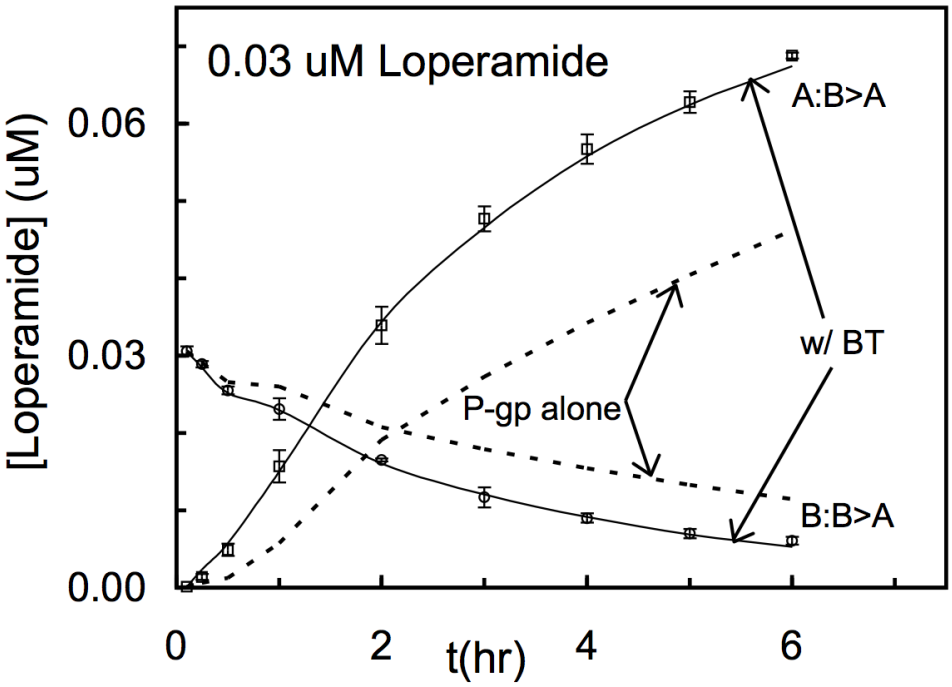

Figure 10.6: Paper 2: Figure 4 - Loperamide only needs a basolateral transporter.

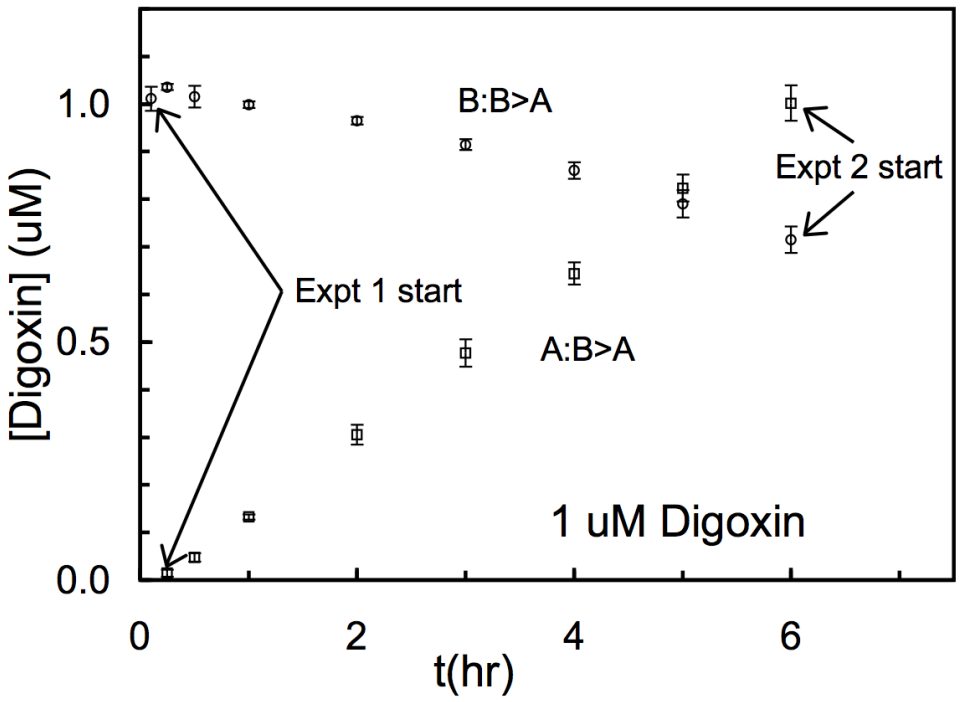

Figure 10.7: Paper 2: Figure 5 - Digoxin transport curve generated by measuring transport over consecutive stretches of 6 hours.

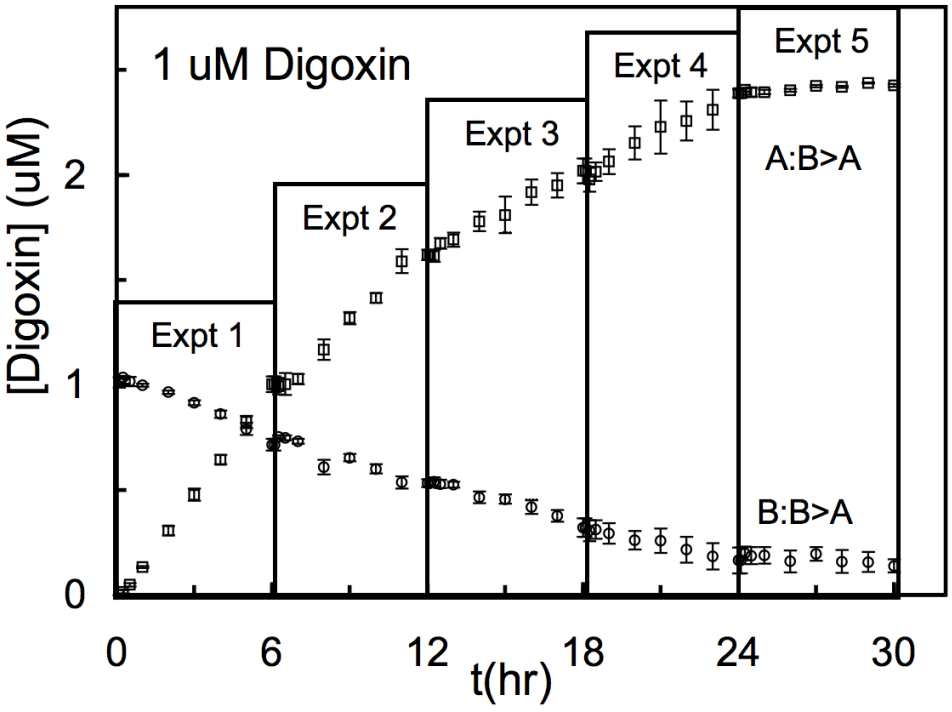

Figure 10.8: Paper 2: Figure 6 - Digoxin transport curve upto 30 hours.

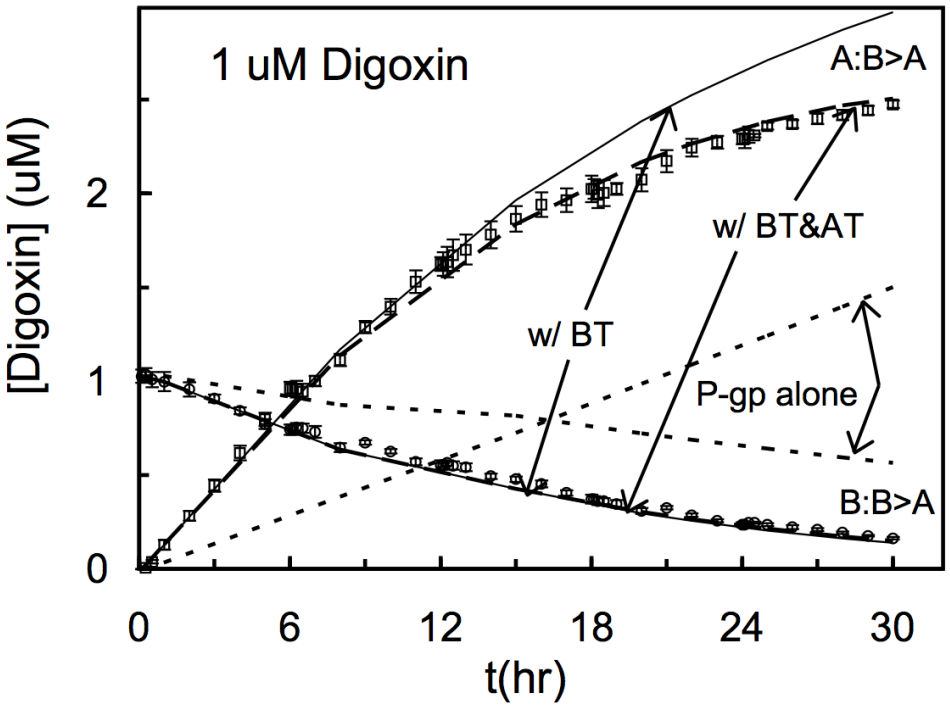

Figure 10.9: Paper 2: Figure 7 - Digoxin is transported by a basolateral and an apical transporter, in addition to P-gp.

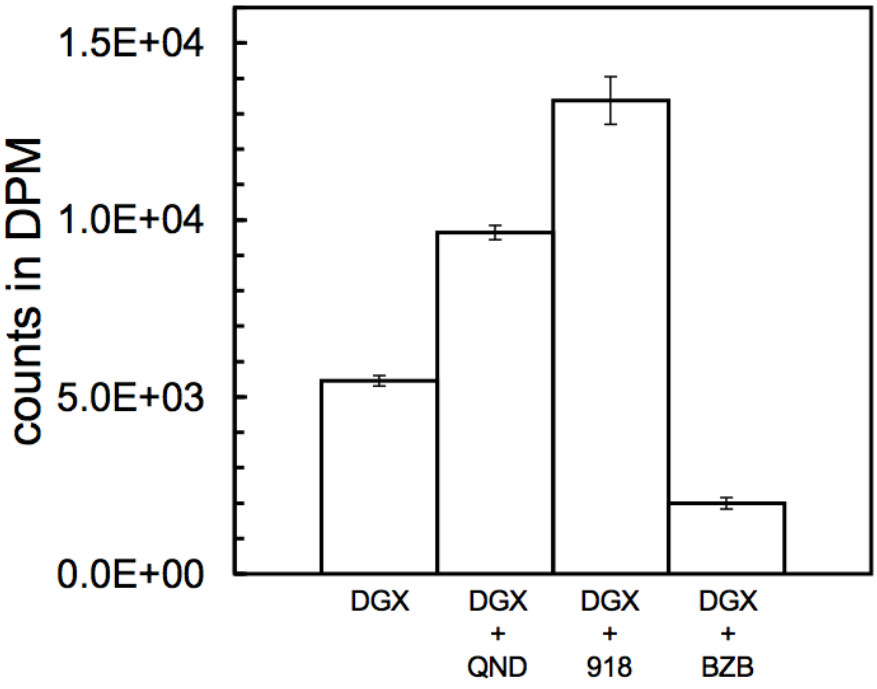

Figure 10.10: Paper 2: Figure 8 - Digoxin cell concentration exclusion by benzbromarone.

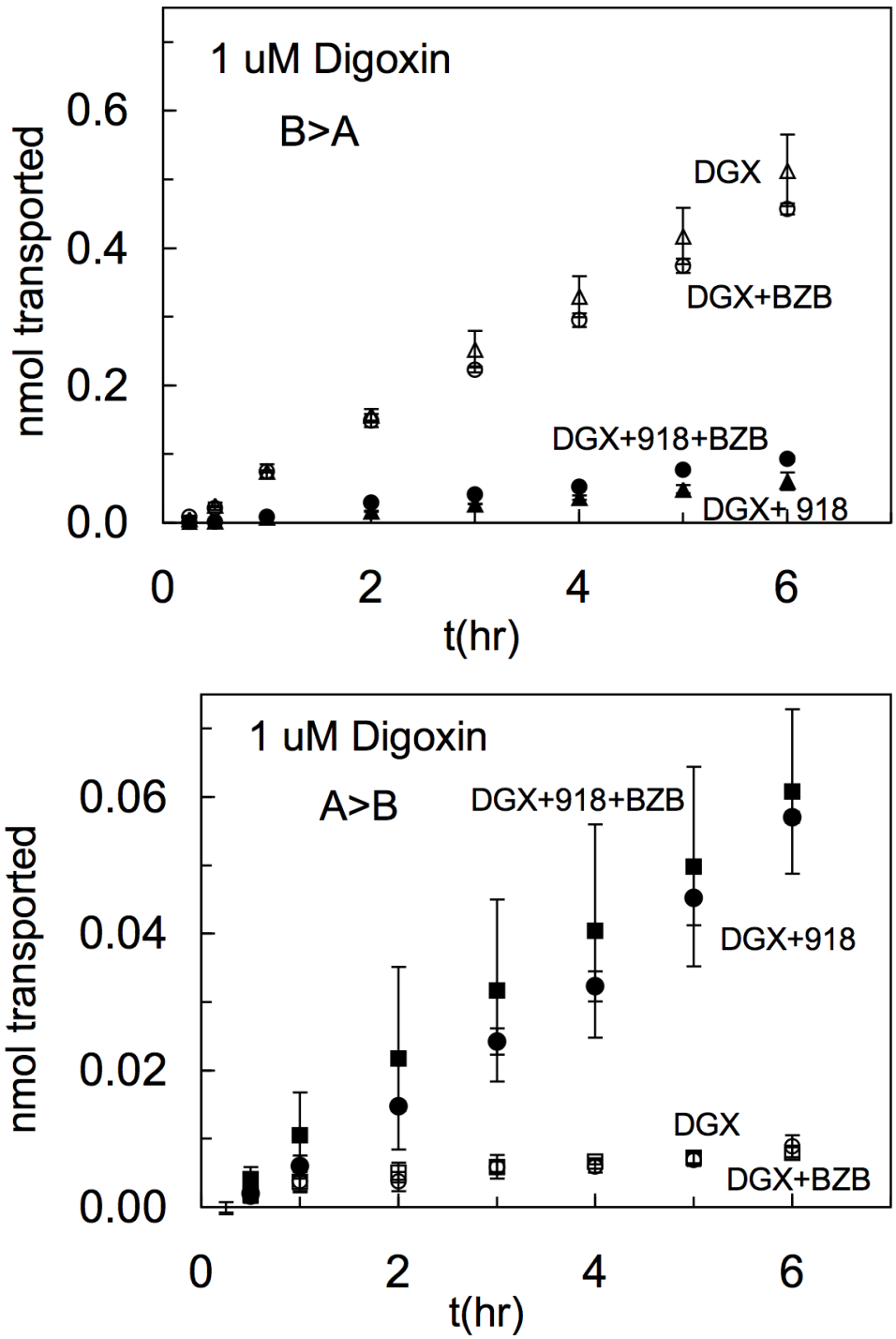

Figure 10.11: Paper 2: Figure 9 - There is no effect of 1μM benzbromarone on the transport of 1μM digoxin.

11. Paper 3

For P-glycoprotein-like mediated transport through a confluent cell monolayer, the IC50 of a P-gp substrate depends upon the probe substrate kinetic parameters.

Joe Bentz[1*], Poulomi Acharya[1,2], Joseph W. Polli[3], Andrew Ayrton[4] & Harma Ellens[2]

[1] Department of Bioscience & Biotechnology, Drexel University, Philadelphia, PA19104, USA

[2] Preclinical Drug Metabolism and Pharmacokinetics, GlaxoSmithKline, King of Prussia, PA, 19406.

[3] Preclinical Drug Metabolism and Pharmacokinetics, GlaxoSmithKline, Research Triangle Park, NC 27709

[4] Preclinical Drug Metabolism and Pharmacokinetics, GlaxoSmithKline, Welwyn, England

[*] Address correspondence to Dr. Joe Bentz, email: bentzj@drexel.edu, FAX: 215-895-1273.

Running Title: Passive permeability and the IC50

Non-standard Abbreviations: P-gp, the P-glycoprotein product of the hMDR1 gene; A>B (or B>A), transport across the confluent cell monolayer when the donor chamber is apical (or basolateral) and the receiver chamber is basolateral (or apical); $K_{D,Aq}$ is the substrate dissociation constant from P-gp relative to the aqueous concentration in the cytosol.

Abstract

Typically, the inhibition of membrane transport is quantified by the IC50, i.e. the concentration of inhibitor required to reduce substrate transport by 50%. This analysis was developed for soluble enzymes and, in the limit of small substrate concentration, the IC50 is equal to the thermodynamic dissociation constant of a competitive inhibitor for the enzyme. For membrane transporters whose binding site resides in the inner monolayer of the plasma membrane, like P-gp and MRP, there is a permeability barrier between the binding site and the extracellular space. For these transporters, there has been no test of the correlation between the IC50 and the dissociation constant of the inhibitor. Previously, we have fitted the mass action elementary kinetic rate constants of P-gp transport of several different drugs through a confluent monolayer of MDCKII-hMDR1 cells. We found that the IC50 values were an order of magnitude or more larger than the dissociation constants derived from the elementary rate constants. Here we use these elementary rate constants to create computer simulations where the transport of probe substrate over time was calculated as a function of inhibitor concentrations, thus yielding IC50 values. These simulations prove that the IC50 value can be orders of magnitude larger than the dissociation constant for the inhibitor. We show that this overestimate is a simple function of cell and substrate parameters, but is independent of inhibitor parameters. We follow A>B transport in detail, where the overestimate is shown to be is due to a rapid steady-state established between the donor chamber and the cytosolic volume, because of the very small cytosolic volume. This shows that extrapolation of an IC50 value from one cell line to another or to *in vivo* will depend upon many factors beyond just the binding constant of the inhibitor to the transporter. All of the conclusions we reach here hold for any small volume system, e.g. suspension or plated cells.

Introduction

The importance of membrane transporters on the metabolism and disposition of drugs is clear (Goh et al., 2002; Mizuno et al., 2003; Chang and Benet, 2005; Collett et al., 2005; Shitara et al., 2005; Robertson and Rankin, 2006; Sekine et al., 2006). One typical experiment in the study of drug-drug interactions is the inhibition of transport of one drug by another, quantified by the concentration of inhibitor required to reduce drug transport by 50%, i.e. the IC50. This analysis was developed for water-soluble enzymes which bind drug, and/or inhibitor, directly from the aqueous phase to which the drug is added initially. So, it is likely to work for membrane transporters that bind their drug directly from the water phase, e.g. glucose permeases (Hah et al., 2002). However, for transporters that bind drug from the inner apical or basolateral monolayer of the cell plasma membrane, e.g. P-gp (Loo and Clarke, 2005; Lugo and Sharom, 2005) and MRP (Borst et al., 2006), the binding site is at least one permeability barrier away from the drug. This suggests, at least, that passive permeability through the plasma membrane may affect the correlation between the inhibitor's dissociation constant and it's IC50.

Using an MDCKII-hMDR1 confluent cell monolayer, we have fitted the elementary rate constants for substrate binding to and efflux from P-gp for amprenavir, quinidine and loperamide (Tran et al., 2005; Acharya et al., 2006). As expected, each of the P-gp substrates inhibited the transport of the other P-gp substrates (Acharya et al., 2006). However, we also found that the IC50's we measured, as well as those in Rautio et al. (2005) for the same substrates/inhibitors, were much larger than the fitted dissociation constants of the inhibitors, even with very low concentrations of substrate. For the confluent cell monolayer, there is a kinetic barrier between the P-gp binding site, within the inner apical membrane, and the extracellular space where the drugs are initially added. This suggested that the substrate parameters describing transport through the intervening

kinetic barrier could be convolved with the IC50, as is the case for the Michaelis constant K_M when the Michaelis-Menten equations are used to analyze P-gp mediated transport through the confluent cell monolayer (Bentz et al., 2005).

This question cannot be answered by experiments alone, since ambiguities can always be ascribed to the use of different cell lines or other effects. A more rigorous analysis of the transport kinetics is required, which starts from the same mass action reactions as used by the standard IC50 and the Michaelis-Menten analyses. This allows computer simulations of substrate transport in the presence of "virtual inhibitors". Following this approach, we have found that the overestimate of the inhibitor's dissociation constant by its IC50 will occur with any cellular system, e.g. confluent cell monolayer, suspension cells or plated cells, wherein the substrate's binding site to the transporter is a permeability barrier away from where the substrate is added. The key component to this overestimate is the small cytosolic volume of the cell systems compared with the extracellular volume, e.g. the Transwell chambers. In this analysis, there are no other transporters in the model, aside from P-gp. If there were additional transporters, which for some substrate/inhibitors there may be, they would become part of the "passive permeability" coefficients.

Materials and Methods

Simulations. For these simulations, we have assumed simple competitive inhibition between the substrate and the inhibitor. Reality is more complex. P-gp has at least 2 efflux pathways which are independent of one another at low concentrations of probe-substrate and inhibitor-substrate like amprenavir and quinidine (Acharya et al., 2006). At high concentrations of either substrate or inhibitor the binding sites of the efflux pathways are competitive and cooperative. When inhibitor concentrations were near their IC50, binding was simply competitive (Acharya et al., 2006).

We also treat the cells as static passive permeability barriers, so that passive permeability coefficients are constant in time. Again, reality is more complex. For all drugs we have tested, there is an initial increase in the passive permeability coefficients and a steady state is achieved eventually (Tran et al., 2005; Acharya et al., 2006). For amprenavir and quinidine, this increase is not due to any "loading" of the cells, as both drugs have essentially perfect mass balance at all times. For our simulations here, these transients will be ignored, since their inclusion would make the analysis more complex without affecting any of our conclusions.

Obviously, we can only measure the overall apical chamber to basolateral chamber, A>B, and overall basolateral chamber to apical chamber, B>A, passive permeability of the drugs to give the measured value for the coefficients P_{BA} and P_{AB}. However, for fitting the mass action kinetics, we need individual membrane passive permeability coefficients P_{AC}, apical chamber to cytosol, and P_{BC}, basolateral chamber to cytosol. Often, $P_{BA} \neq P_{AB}$ until a steady-state occurs, which can be several hours (Tran et al, 2005; Acharya et al., 2006). As explained in Tran et al. (2005), the simplest mix of experiment and theory was to set $P_{AC} = P_{AB}$ and $P_{BC} = P_{BA}$ to account for this asymmetry and to capture the basic elements of the kinetic process.

We used the stiffest integrator in MATLAB, ode23s, with absolute and relative tolerances set up to 10^{-10}. Other MATLAB integrators, while faster, were not accurate enough at the later times of simulations. Further details can be found in Tran et al. (2004, 2005) and Acharya et al. (2006).

P-gp Activity. To fit the [IC50] by P-gp activity, we use the same equation as in Rautio et el. (2006):

$$P-gp\ Activity = \left| \frac{nmol([I], total) - nmol([I]\ or\ [I]=0, GF120918)}{nmol([I]=0, total) - nmol([I]=0, GF120918)} \right| \tag{11.1}$$

where nmol([I],total) is the nmol substrate transported at some time t in the presence of [I]=inhibitor concentration. nmol([I] or [I]=0,GF120918) is the nmol substrate transported at some time t in the presence of the potent P-gp inhibitor GF120918 (Rautio et al., 2006), which is the same whether or not the other inhibitor I is present. We will use the A>B direction to analyze inhibition because it is more sensitive to the binding of substrate to P-gp (Tran et al., 2005), although we have found in this work that analyzing B>A transport gives essentially the same results. Since P-gp reduces total substrate transport in the A>B direction, the equation as stated would give a negative number, so we simply take the absolute value, as shown in the equation.

Thus, in either direction, the fraction of P-gp activity is 1 without inhibitor and decreases as the inhibitor concentration increases. The inhibitor concentration at which the P-gp activity is 0.5 is called the IC50. Without inhibitor, a certain fraction of P-gp will be bound to substrate, depending upon the substrate concentration. At the IC50, half of that fraction of P-gp will be bound by a competitive inhibitor. If the binding is not competitive, different equations must be used.

Kinetic Model of Transport across a Confluent Cell Monolayer

Figure 1 is a cartoon of a confluent cell monolayer, featuring the polarized MDCKII-hMDR1 cells, where the basolateral membrane is attached to the polycarbonate filters and P-gp (upward arrows) expressed on the apical surface. The apical and basolateral chambers are kept separate by the tight junctions. Active transport by P-gp occurs unidirectionally, with substrate binding to a site on P-gp within the apical membrane inner monolayer and with efflux into the apical chamber (Loo and Clarke, 2005; Lugo and Sharom, 2005). For many substrates, including those we use, passive permeability is a significant fraction of total transport and is quantitatively analyzed separately using the P-gp inhibitor, GF120918 (Tran et al., 2004, 2005; Acharya et al., 2006).

With the confluent cell monolayer system, we measure the concentration of substrate in the apical chamber, denoted C_A, and the basolateral chamber, denoted C_B. However, the concentration of substrate in the cytosol, denoted C_C, and in the inner plasma membrane in contact with the P-gp binding site, denoted C_{PC}, cannot (yet) be measured rigorously in real time. These internal concentrations are variables of the mass action model and fitted by elementary rate constants for well-defined kinetic barriers, according to the measured values of C_B and C_A over time (Tran et al., 2005; Acharya et al., 2006). We use the simplest Michaelis-Menten mass action reaction to model P-gp:

$$T_0 + C_{pc} \underset{k_r}{\overset{k_1}{\rightleftarrows}} T_1 \xrightarrow{k_2} T_0 + C_A \tag{11.2}$$

where T_0 is the empty transporter, C_{PC} the substrate in the apical membrane inner monolayer, T_1 is the transporter bound by substrate and C_A the substrate after efflux into the apical chamber. Although we have shown that P-gp has more than one efflux binding site, at inhibitor concentrations near the IC50, P-gp behaved like a simple single compet-

itive site transporter (Acharya et al., 2006). Likewise, while some of these substrates may use other transporters within the MDCKII cell line, that is not part of these simulations, but their effect would only be to change the "values" of passive permeability coefficients.

ATP hydrolysis is not part of this model, since it occurs intracellularly and cannot be measured rigorously over time. However, we found that the cells do not lose any capacity for drug transport over 6 hour incubations (Tran et al., 2005; Acharya et al., 2006), implying that cellular ATP levels remain adequate for full P-gp function throughout the 6 hour long experiment.

Table 1 shows the median consensus values of the elementary parameters used to fit the transport kinetics of amprenavir, quinidine and loperamide (Acharya et al., 2006). Each parameter fitted had a range that gave good fits to all the data for over 6 hours of transport. While the precision of these estimates varies, that precision is not important for this work. We only use these median values for each of the three drugs to create a range the values of the "virtual" substrates and inhibitors which are physiologically and pharmaceutically relevant. If the values of the medians shown in Table 1 were increased or decreased within their standard deviations, there would be no effect upon our conclusions.

We found that all three drugs had essentially the same rate constant for association to P-gp, k_1, and essentially the same estimated surface density for efflux active P-gp, T(0), which was a benchmark for the validity of our mass action model and kinetic analysis (Tran et al., 2005; Acharya et al., 2006). The values in the Table make considerable sense for P-gp function and structure (Tran et al., 2005; Acharya et al., 2006). In our simulations, these two parameters are held fixed at the values shown.

This leaves two other kinetically significant parameters characterizing substrate and inhibitor interactions with the confluent cell monolayer and P-gp, both of which depend upon the substrate:

1. k_2, the efflux rate constant of the substrate and inhibitor from P-gp into the apical

space.

2. k_r, the dissociation rate constant of the substrate and inhibitor from P-gp back into the inner apical membrane. The binding constant of the substrate and inhibitor to P-gp from the inner monolayer of the apical membrane is defined by the ratio of the fitted rate constants, i.e. $K_C = k_1/k_r$.

The partition coefficient of the substrate and inhibitor between the inner monolayer of the apical membrane and the cytosol of the cell is denoted K_{PC}. The product of $K_{PC}K_C$ is the binding constant to P-gp relative to the cytosolic concentration of substrate, so that the dissociation constant of the substrate to P-gp, relative to the cytosol, is $K_{I,Aq} = 1/(K_{PC}K_C)$. This will become quite important below when the question of rank order of inhibitors is addressed.

The two other partition coefficients, K_{BO}, between the basolateral chamber and the outer basolateral membrane monolayer and, K_{AO}, between the apical chamber and the outer apical membrane monolayer, see Fig. (1), have also been estimated independently (Tran et al., 2005). However, while their particular values can shift concentrations slightly, this has no affect on the conclusions we reach.

Results & Discussion

Figure 2 shows the simulation of the nmol transported over time for an "amprenavir-like" probe substrate, starting with 1μM in the apical chamber, in the A>B direction as a function of the concentration of the "quinidine-like" inhibitor, whose concentration [I] in (μM) shown beside each curve. The respective parameters in Table 1 are used. Complete inhibition of P-gp, e.g. by GF120918, is shown by the thick black line, which represents just transcellular and/or paracellular passive permeability since there are no other transporters in this model.

The IC50 in this simulation is clearly in the range of 1-2μM at all times, as indicated by the vertical dotted lines shown at the 2, 4 & 6 hr time points. However, the "quinidine-like" inhibitor has a $K_{I,Aq}$=0.1μM, as can be calculated from Table 1 and shown in Table 2. Thus, the IC50 is 10-20 times larger than the $K_{I,Aq}$ used to calculate these simulations in the first place. The simulations are without error and assume that transport is only by P-gp and passive permeability. Clearly, the overestimate we observe experimentally (Acharya et al., 2006) is due to the elementary rate constants, not experimental ambiguity.

In order to determine which parameters caused the overestimate, we followed the strategy used in Bentz et al. (2005), which was to let the kinetic parameters for both substrate and inhibitor range between and around those values we had fitted for amprenavir, loperamide and quinidine. This creates virtual substrates and inhibitors, with pharmaceutically relevant parameters.

Figure 3 shows the P-gp activity as open squares calculated from Eq.(2), P-gp specific nmol transported, using 2hr data from simulation in Fig. (2), replotted on a log-log plot with 0.1-30μM of inhibitor. This is the same equation used in Rautio et al. (2006). The closed squares show the fraction of P-gp bound by substrate, normalized to the amount bound in the absence of inhibitor. Because we are doing simulations, we "know" this

number, which is the theoretically correct measure of the IC50. While not identical, both measures of relative inhibition are in excellent agreement. The difference is that the nmol transported calculation of P-gp activity ignores backflow of substrate, which slightly underestimates the total amount of substrate actually crossing into the basolateral chamber (Tran et al., 2005). The $K_{I,Aq}$ =0.1μM for the inhibitor is shown by the large X on the x-axis, showing the 14-fold overestimate of $K_{I,Aq}$ by the IC50. We call the ratio of IC50/ $K_{I,Aq}$ the overestimate value, which is what we will explain in this work at the molecular level.

We have found that the inhibitor's parameters do not affect the overestimate value of IC50/ $K_{I,Aq}$ (data not shown). For example, increasing the binding constant of the inhibitor 10-fold did cause the $K_{I,Aq}$ to decrease 10-fold, as expected, but the IC50 also decreased 10-fold. Thus the overestimate was unaffected. Accordingly, decreasing the binding constant of the inhibitor 10-fold caused the commiserate 10-fold increase of $K_{I,Aq}$ and the IC50. None of the inhibitor's kinetic values had a significant effect on the overestimate, at least for the first two hours of transport. Changes in the inhibitor's efflux rate constant, k_2, also did not change the overestimate, basically because the experimental protocol used (Acharya et al., 2006; Rautio et al, 2006) held the inhibitor concentration essentially constant in all compartments.

Thus the value of IC50/$K_{I,Aq}$ is due to only substrate parameters. Starting from the mass action equations (Tran et al., 2005; Acharya et al., 2006), we have found that the ratio of IC50/$K_{I,Aq}$ to be approximated by the equation:

$$\frac{[IC50]}{K_{I,Aq}} \cong \left[\frac{V_{AO}T(0)}{4A}\right]\left[\frac{K_{PC}K_C k_2}{0.5*(P_{BC}+P_{AC})}\right] \tag{11.3}$$

The first bracketed term contains general system parameters: the surface density of P-gp in the apical membrane, i.e. the volume of the apical membrane of the entire con-

fluent cell monolayer (roughly $V_{AO} \approx 0.5$nL, Tran et al., 2005) times the concentration of efflux active P-gp in the apical membrane divided by 4 times the area of the Transwell insert. Thus, the more P-gp there is, the greater the overestimate. The second bracketed term contains the substrate specific kinetic parameters. The overestimate increases with the substrate binding constant to P-gp from the membrane, K_C, the substrate partition coefficient into the cytosolic side of the plasma membrane, K_{PC}, and the efflux rate constant for the substrate, k_2. The fitted values for these parameters are found in Table 1. These terms are responsible for the efflux kinetics. So increased P-gp mediated efflux kinetics decreases the substrate cytosolic concentration and increases the overestimate. On the other hand, increasing the substrate passive permeability coefficients, P_{AC} and P_{BC}, increases the substrate cytosolic concentration and decreases the overestimate. Obviously, if the passive permeability coefficients become large enough, the membranes cease being permeability barriers and the system becomes like an aqueous enzyme.

The deviation of Eq.(3) is straightforward, but quite lengthy and depends upon the simulations for guidance in choosing which terms are significant and which terms are negligible. In lieu of showing the derivation, we will demonstrate its accuracy. When we create a virtual substrate using amprenavir's parameters, from Table 1, except that both P_{AC} and P_{BC} are variable, then Eq.(3) becomes

$$\frac{[IC50]}{K_{I,Aq}} \cong \frac{6,600nm/s}{0.5 * (P_{BC} + P_{AC})} \tag{11.4}$$

To check this approximate equation against exact calculations, we allowed both P_{AC} and P_{BC} to range between 20-2000 nm/s, which more than covers the known range for these parameters, and looked at all possible combinations. Figure 4 shows the of IC50/$K_{I,Aq}$ plotted against these passive permeability on a log-log plot. These values are for the 2hr time point, but any time point from 2-6 hrs gives the same basic result. The

line is Eq. (4), not a least-squares fit, which on a log-log plot has an x-intercept of about 6,600, as predicted. The better fits, shown by O's are for cases where $P_{BC}/P_{AC} < 10$, i.e. where both membranes, apical and basolateral, contribute to the overall passive permeability, which is likely to be the case for biological membranes, in the absence of other transporters. The worse fits, denoted by X's, are for cases where $P_{BC}/P_{AC} \geq 10$, which are cases where only apical membrane determines the transcellular passive permeability, which can also be considered as a mimic for the case where there is a basolateral transporter.

The arrow in Fig(3) points to $0.5 * (P_{AC} + P_{BC}) \sim 6600$ nm/s, which is where the simple approximation of Eq. (5) for IC50/$K_{I,Aq}$ extrapolates to about 1, i.e. where the membrane is as permeable as water. In reality, Eq.(3) would not extrapolate accurately, since it becomes less accurate as the passive permeability increases, which accounts for the greater scatter as $(P_{AC} + P_{BC})$ increases.

To further test the accuracy of Eq.(3), we have made further simulations where the values of k_2, K_C, T(0) or V_{AO} are increased or decreased by 10-fold from the amprenavir values used in Eq.(4). In all cases, the value of IC50/$K_{I,Aq}$ increased or decreased by 10-fold, more or less, showing that Eq.(3) is a reasonable approximation for a broad range of parameters centered around amprenavir and quinidine as probe substrates.

Table 2 shows the IC50 values we extracted from the data in Acharya et al. (2006) for several pairs of P-gp substrates and the fitted values for $K_{I,Aq}$, from the elementary rate constants, calculated from the values shown in Table 1. The experimental ratios of IC50/$K_{I,Aq}$ range from about 20-60. When corrected by Eq. (3), using the parameters in Table 1, the overestimates are reduced to 1.5-4. Thus, the correction by Eq.(3) works well in practice.

What remains is to understand the physical reason for the overestimate, since it suggests a fundamental kinetic property of the confluent monolayer. The simulations show

for A>B transport that the cytosolic concentration of substrate reaches a "quasi"-steady-state within a few minutes, even with substrate passive permeability coefficients as small as 20nm/s, like digoxin (Rautio et al., 2006). This is not the final steady-state achieved eventually, e.g. after several hours, as shown in Fig. 2, when P-gp efflux plus the small amount of B>A passive permeability, is equal to the A>B passive permeability. The initial "quasi"-steady-state in the cytosolic substrate concentration persists as the baso-lateral substrate concentration slowly increases and apical substrate concentration slowly decreases compartment. Eventually, the "quasi"-steady state breaks as the basolateral concentration of substrate approaches that of the cytosolic concentration.

How can this initial "quasi"-steady-state be established in seconds to minutes, when the final steady-state requires hours? The answer lies in the small volume of cytosol compartment of the confluent cell monolayer. In Tran et al. (2004), we showed that the passive permeability between a donor compartment of volume V_D and a receiver compartment of volume V_R, through a single-barrier membrane of area A and a passive permeability coefficient P, gives a receiver side concentration of:

$$C_R(t) = \frac{C_D(0)V_D}{V_D + V_R}\left(1 - exp\left\{-\frac{(V_D + V_R)}{V_D V_R}PAt\right\}\right) \tag{11.5}$$

where $C_D(0)$ is the initial donor side concentration. This equation also assumes that the substrate has no mass balance problems and that there is initially no substrate in the receiver compartment. If this is not the case, then a more complicated equation can be used (Tran et al., 2004), but the same conclusions would be reached. This equation applies only to pure passive permeability, so it eventually reaches true equilibrium.

A convenient measure of the time required to reach a "steady-state" value is the halftime value, where the exponential term=0.5. Then:

$$t_{0.5}(D > R) = \frac{1.44 V_D V_R}{(V_D + V_R) PA} \tag{11.6}$$

For A>B transport, the Transwell system has $V_D = 0.5$mL, $V_R = 1.5$mL and A=1.13 cm^2 (Acharya et al., 2006) When the passive permeability coefficient is P=450 nm/sec, e.g. like amprenavir in Table 1, then $t_{0.5}(A > B) \sim 3$ hours. On the other hand, for the A>C transport to the cytosol, with $V_R = 1\mu$L (Tran et al, 2005), $t_{0.5}(A > C) \sim 20$ sec. Thus, the initial "quasi"-steady-state between the apical chamber and the cytosol can be established within seconds, because the receiver volume is so small.

Now, the simulations show that the greater the efflux rate out of the cytosol relative to the passive permeability into the cytosol, i.e. as the right hand side of Eq. (3) increases, the cytosolic concentration of substrate decreases and the smaller the fraction of P-gp bound by substrate (data not shown). This is the actual mechanism of the overestimate value.

Figure 5 shows the concentration of substrate-bound P-gp as a function of inhibitor concentration. The solid line simulation uses the same parameters as Fig.(2), showing that without inhibitor that about 1μM of P-gp is bound by substrate. To reduce the substrate-bound P-gp by 50% from the inhibitor-free value required IC50=1.2μM inhibitor. The dotted line simulation has the P_{AC} reduced from 400 nm/s to 200nm/s, which reduces the inhibitor-free concentration of substrate-bound P-gp to about 0.5μM. Because a one-site binding curve flattens out as the fraction bound goes to zero, even the Henderson-Hasselbach pH curve, the reduction of substrate-bound P-gp is more shallow per μM inhibitor added than in the first case. More inhibitor is required to reduce the substrate-bound P-gp by 50%, i.e. IC50=2.2μM. In both cases, $K_{I,Aq}$=0.1μM is the same. The overestimate is 12-fold and 22-fold, respectively.

Conclusions

Based upon the fitted elementary kinetic parameters that define the P-gp mediated transport in a confluent monolayer of MDCKII-hMDR1cells (Tran et al., 2005; Acharya et al., 2006), we have investigated the usage of an IC50 experiment to characterize the inhibition of transport and the inhibitor dissociation constant. The simulations show that the IC50 will over-estimate the dissociation constant of the inhibitor to P-gp relative to the cytosol, $K_{I,Aq}$, by a factor which depends upon probe substrate kinetic parameters and cell parameters. This factor is approximated by Eq.(3), whose accuracy is shown in Fig. (4). No part of the derivation for Eq.(3) required that substrate actually pass into the receiver chamber, so that all of the conclusions we reach here hold for any small volume system, e.g. suspension or plated cells.

The basic reason for this overestimate is the small volume of the cytosolic space, as compared with the apical and basolateral chambers, which in the A>B direction causes an initial "quasi"-steady-state in cytosolic concentration to be established in seconds to minutes, even with poorly permeable substrates. This "quasi"-steady-state is established by the balance of P-gp mediated cytosol?apical chamber efflux and the passive permeation apical chamber → cytosol. The steady-state is "quasi" because there is a net donor chamber → receiver chamber flux, which eventually evolves to the final steady-state, where all concentrations are stationary and the cytosolic substrate concentration equals that of the basolateral chamber. In the B>A direction, the derivation of Eq.(3) is more complicated, but the final equation is the same and the calculations give the same answers. Here we have considered only the simpler A>B case.

In the absence of inhibitor, the greater the amplitude of efflux parameters in Eq.(3), the right hand side of the equation, the smaller the cytosolic concentration at this steady-state and, thus, the smaller the concentration of substrate-bound P-gp. Addition of inhibitor

will reduce the concentration of substrate-bound P-gp, but the smaller the "inhibitor-free" substrate-bound P-gp, the larger the amount of inhibitor required to reach the IC50. This is simply the nature of a 1-site binding reaction: more P-gp mediated efflux pushes the system further out onto the tail-end of the binding curve. To use this correction factor to estimate the inhibitor dissociation constant, $K_{I,Aq}$, requires knowing the elementary rate constants of the substrate, as shown in Table 1.

The primary function of IC50 in drug studies is to rank order inhibitors with respect to a particular probe-substrate (Rautio et al., 2006). The rank order of P-gp inhibitors using a single probe substrate with the same *in vitro* cell line would not be affected by the correction factor given by Eq.(3), since it would be the same correction for all IC50 values. Changing the probe-substrate with the same *in vitro* cell line would change the IC50 values, but would not affect the rank order, since the new correction factor would apply to all inhibitor IC50 values.

The stability of the inhibitor rank order in another *in vitro* cell line or *in vivo* is less clear. The correction factor, i.e. the right-hand side of Eq.(3), would not change the rank order. However, in a different cell line or *in vivo*, the relative partition coefficients of the inhibitors to the cytosolic side of the plasma membrane are part of $K_{I,Aq}$. For example, suppose that two drugs had equal binding constants for P-gp from the membrane, then their dissociation constants relative to the cytosol would depend entirely upon the relative partition coefficient to the inner plasma membrane. Whichever drug had the larger partition coefficient would have the smaller IC50. Tran et al. (2005) found quite a lot of sensitivity of partition coefficients between the three drugs we used and the three different lipid compositions, which are crude mimics of biological membranes. In a different cell line or *in vivo*, it is very hard to predict whether the partition coefficients would remain in the same rank order. Independent measurements of the partition coefficients would clarify the extrapolation problem.

Our final point is that equations developed for use with soluble enzymes with soluble drugs cannot be expected to give accurate results for membrane transporters with substrates which must cross a permeability barrier into a much smaller volume to reach the transporter binding site. Our analysis has proven that both the K_M (Bentz et al., 2005) and the IC50 fittings for the confluent cell monolayer do not yield coefficients which mean what they do for soluble enzymes. Only the elementary kinetic parameters derived from the comprehensive mass action kinetic analysis can yield a reliable starting point for extrapolations.

References

Acharya P, Tran TT, Polli JW, Ayrton A, Ellens H and Bentz J (2006) P-gp expressed in a confluent monolayer of hMDR1-MDCKII cells has more than one efflux pathway with cooperative binding sites. Biochemisty, 45:15505-15519.

Bentz J, Tran TT, Polli JW, Ayrton A and Ellens H (2005) The steady-state Michaelis-Menten analysis of P-glycoprotein mediated transport through a confluent cell monolayer cannot predict the correct Michaelis constant K_M. Pharm Res. 22:1667-1677.

Borst P, Zelcer N, van de Wetering K and Poolman B (2006) On the putative co-transport of drugs by multidrug resistance proteins. FEBS Lett. 580:1085-1093.

Chang JH and Benet LZ (2005) Glucuronidation and the transport of the glucuronide metabolites in LLC-PK1 cells. Mol Pharm. 2:428-34.

Collett A, Tanianis-Hughes J, Carlson GL, Harwood MD and Warhurst G (2005) Comparison of P-glycoprotein-mediated drug-digoxin interactions in Caco-2 with human and rodent intestine:Relevance to *in vivo* prediction Eur. J. Pharm. Sci. 26:386-393.

Evers R, Kool M, Smith AJ, van Deemter L, de Haas M and Borst P (2000) Inhibitory effect of the reversal agents V-104, GF120918 and Pluronic L61 on MDR1 P-gp, MRP1- and MRP2-mediated transport. British J. Cancer. 83:366-374.

Goh LB, Spears KJ, Yao D, Ayrton A, Morgan P, Roland WC and Friedberg T (2002) Endogenous drug transporters in *in vitro* and *in vivo* models for the prediction of drug disposition in man. Biochem. Pharmacol. 64:1569-1578.

Hah J S, Ryu JW, Lee W, Kim BS, Lachaal M, Spangler RA and Jung CY (2002). Transient changes in four GLUT4 compartments in rat adipocytes during the transition, insulin-stimulated to basal: Implications for the GLUT4 trafficking pathway. Biochemistry 41:14364-14371.

Hyafil F, Vergely C, Du Vignaud P and Grand-Perret T (1993) In vitro and *in vivo* reversal of multidrug resistance by GF120918, an acridonecarboxamide derivative. Cancer Res. 53:4595-602.

Loo TW and Clarke DM (2005) Recent Progress in Understanding the Mechanism of P-Glycoprotein-mediated Drug Efflux. J. Membr. Biol. 206:173-185.

Lugo MR and Sharom FJ (2005) Interaction of LDS-751 with P-glycoprotein and mapping of the location of the R drug binding site. Biochemistry 44:643-55.

Mizuno N, Niwa T, Yotsumoto Y and Sugiyama Y (2003) Impact of Drug Transporter Studies on Drug Discovery and Development. Pharmacol. Rev. 55:425-461.

Rautio J, Humphreys JE, Webster LO, Balakrishnan A, Keogh JP, Kunta JR, Serabjit-Singh CJ and Polli JW (2006) In Vitro P-glycoprotein Inhibition Assays for Assessment of Clinical Drug Interaction Potential of New Drug Candidates: A Recommendation for Probe Substrates. Drug Metab Dispos. 34:786-792.

Robertson EE and Rankin GO (2006) Human renal organic anion transporters: Characteristics and contributions to drug and drug metabolite excretion Pharmacol. Ther. 109:399-412.

Sekine T, Miyazaki H and Endou H (2006) Molecular physiology of renal organic anion transporters. Am J Physiol Renal Physiol. 290:F251-F261.

Shitara Y, Horiea T and Sugiyama Y (2006) Transporters as a determinant of drug clearance and tissue distribution. Eur. J. Pharm. Sci. 27:425-446.

Tran TT, Mittal A, Gales T, Maleeff B, Aldinger T, Polli JW, Ayrton A, Ellens H and Bentz J (2004) An Exact Kinetic Analysis of Passive Transport across a Polarized Confluent MDCK Cell Monolayer Modeled as a Single Barrier. J. Pharm. Sci. 93:2108-2123.

Tran TT , Mittal A, Aldinger T, Polli JW, Ayrton A, Ellens H and Bentz J (2005) The elementary mass action rate constants of P-gp transport for a confluent monolayer of MDCKII-hMDR1 cells. Biophys. J. 88:715-738.

Figure Legends

Figure 1. Model of a confluent cell monolayer, with the apical membrane on top and the basolateral membrane on the bottom, where it binds to the polycarbonate insert. Passive permeability occurs in both directions. P-gp expressed on the apical membrane transports substrate from the inner apical membrane monolayer into the apical chamber. The concentration of substrate in the apical and basolateral chambers, C_A and C_B, are measured, while the concentration of substrate in the inner plasma membrane, C_{PC}, and the cytosol, C_C, are predicted as part of the mass action modeling and data fitting process described in Tran et al. (2005) and Acharya et al. (2006).

Figure 2. Simulation of nmol transported over time for 0.1μM of an "amprenavir-like" substrate, i.e. using the amprenavir kinetic parameters shown in Table 1, in the presence of increasing concentrations of an inhibitor with the same kinetic parameters as quinidine, which makes $K_{I,Aq}$=0.1μM. Complete inhibition of P-gp by GF120918 is simulated by the thick black line on the top. "Quinidine-like" inhibitor concentrations are shown beside the thin black lines. We use the A>B inhibition because this data is more sensitive to binding to P-gp (Tran et al., 2005), although using B>A simulations give basically the same results. Clearly, the IC50 is in the range of 1-2 μM, i.e. 10-20 times larger than the $K_{I,Aq}$.

Figure 3. The fraction of P-gp mediated transport (open boxes) in the A>B direction substrate at 2 hours from Fig. 2, as a function of inhibitor concentration, on a log plot from 0.1-100μM, with 0.1μM substrate, from Eq.(2). This curve allows us to estimate the IC50 accurately. The closed boxes show the fraction of substrate-bound P-gp, showing that the P-gp activity estimated from nmol transported is quite accurate.

Figure 4. A log-log plot of the calculated values of IC50/ $K_{D,Aq}$ at 2 hours, calculated as shown in Fig. 4 for the amprenavir-like substrate with variable passive permeability coefficients, plotted against the average substrate passive permeability into the cytosol, 0.5*(P_{AC}+P_{BC})(nm/s). The passive permeability coefficients, P_{AC} and P_{BC}, each vary from 20-2000 nm/sec and all combinations are calculated. The linear correlation with Eq.(3) is quite good, with a correlation coefficient of $R^2 = 0.9$ for all the points and $R^2 = 0.98$ for the circles, which are for cases where $P_{BC}/P_{AC} < 10$, i.e. where both membrane contribute to the transcellular passive permeability. The arrow points to 0.5*(P_{AC}+P_{BC})$\sim$ 6600 nm/s, which is where Eq.(4) for IC50/$K_{I,Aq}$ extrapolates to 1 and where the membrane would be as permeable as water.

Figure 5. The concentration of substrate-bound P-gp (fig 5A) or the fraction of P-gp bound by substrate (fig 5B) is shown as a function of inhibitor concentration for A>B transport. The solid line shows the case for the amprenavir-like substrate, with the parameters from Table 1, P_{BC}=500 nm/sec and P_{AC}=400 nm/sec, inhibited by the quinidine-like compound, i.e. the same as in Figs. 2-4. To reduce the inhibitor free value of substrate-bound P-gp from about 1μM to 0.5 μM required 1.2 μM of inhibitor. On the other hand, if the amprenavir-like substrate's P_{AC} is reduced to 200 nm/s, then the inhibitor free value of substrate-bound P-gp is reduced to about 0.5μM, which requires about 2.2 μM of inhibitor to reduce the substrate-bound P-gp concentration by 50%, i.e. nearly twice as much. Given that the "quasi"-steady-state which reduces the cytosolic substrate concentration and, hence, the concentration of substrate-bound P-gp, this is the root cause of the overestimate of the $K_{I,Aq}$ by the IC50.

Figures

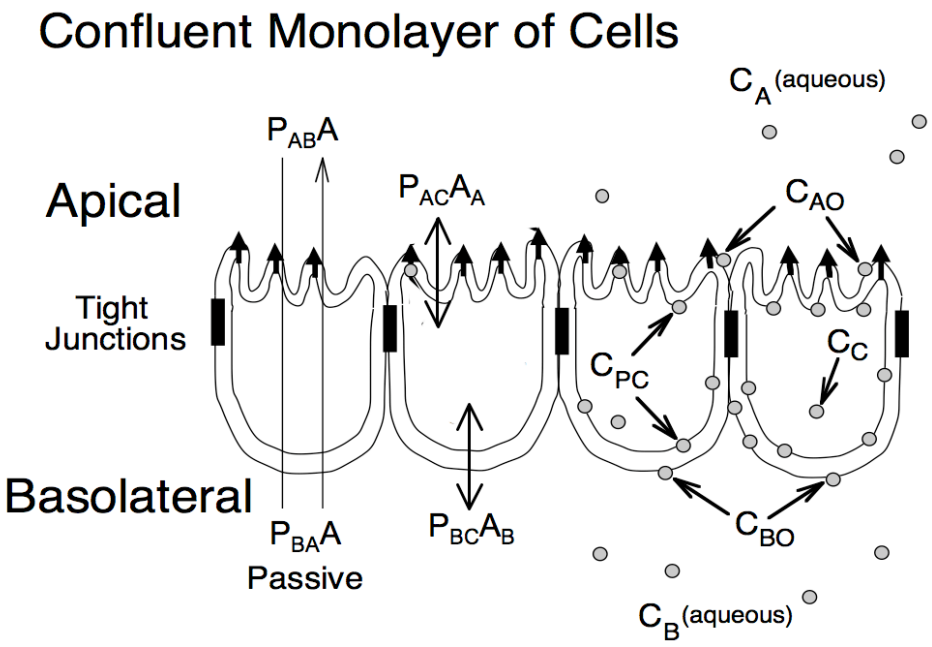

Figure 11.1: Paper 3: Figure 1 - Model of a confluent cell monolayer.

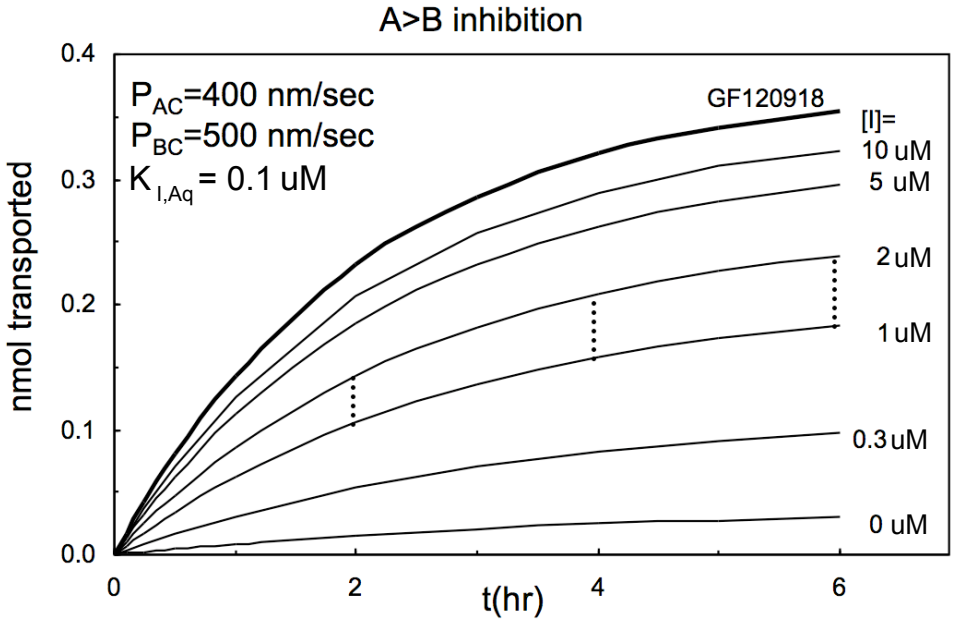

Figure 11.2: Paper 3: Figure 2 - Simulations show IC50 for an amprenavir-like substrate transport inhibited by quinidine-like inhibitor is 1 - 2μM.

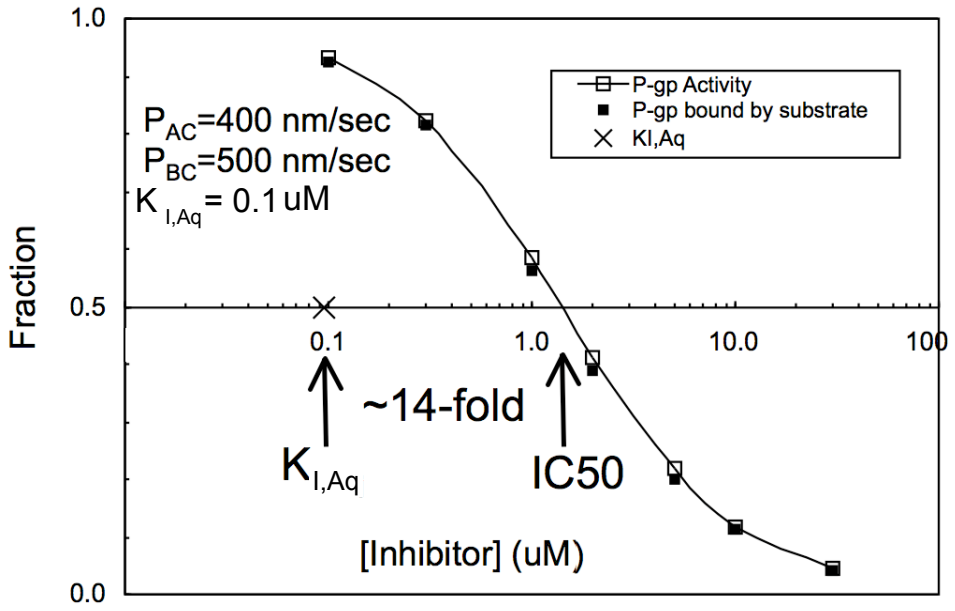

Figure 11.3: Paper 3: Figure 3 - The fraction of substrate bound P-gp as a function of inhibitor concentration.

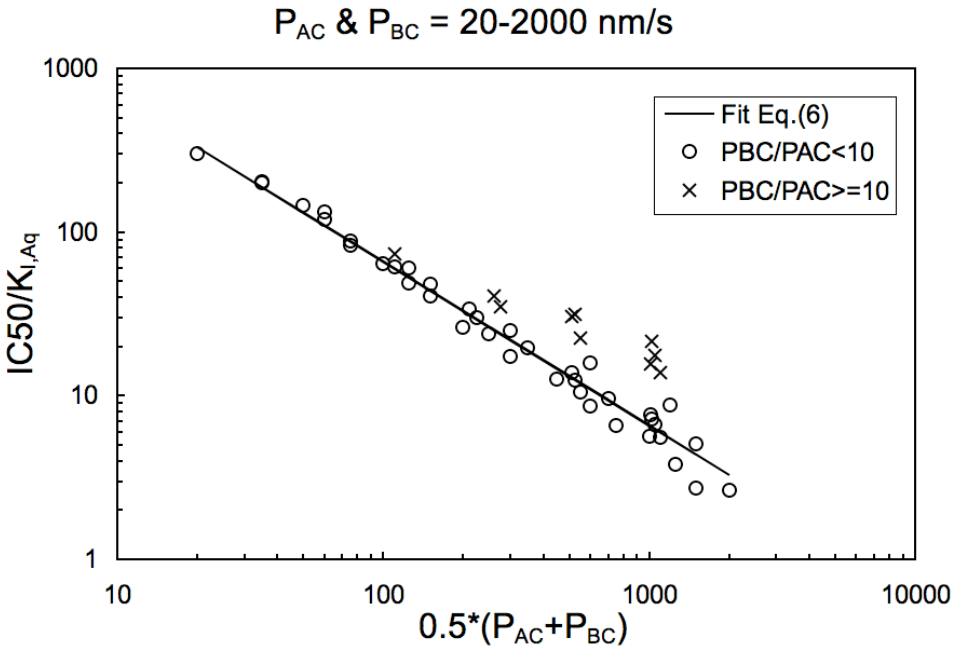

Figure 11.4: Paper 3: Figure 4 - Overestimation of $K_{I,Aq}$ by the IC50 as a function of average passive permeability into the cytosol.

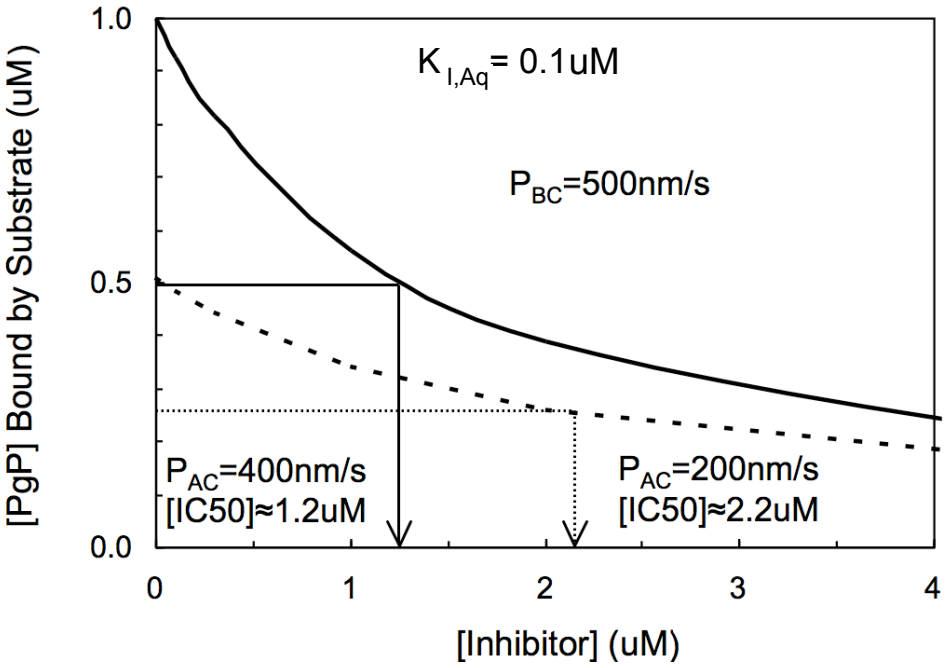

Figure 11.5: Paper 3: Figure 5a - The concentration of substrate-bound P-gp as a function of inhibitor concentration.

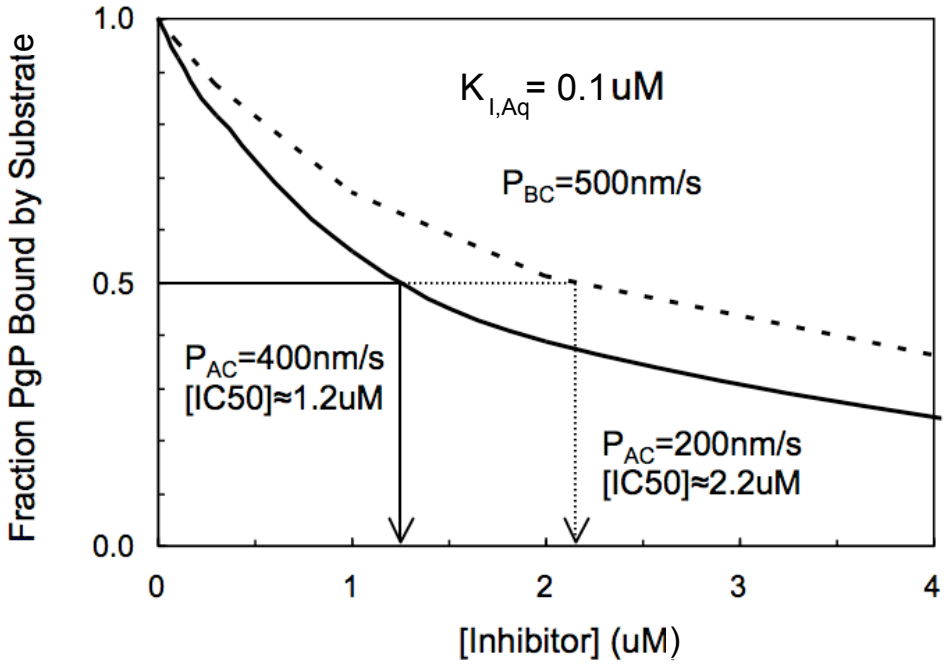

Figure 11.6: Paper 3: Figure 5b - Fraction of substrate-bound P-gp as a function of inhibitor concentration.

Table 1

Substrate	Association to P-gp k_1[a] ($M^{-1}s^{-1}$)	Efflux Active P-gp Density $T(0)$[b] (uM)	"P-gp Vmax" $k_2T(0)$[c] (M/s)	Efflux to Apical Chamber k_2[d] (s^{-1})	Inner Plasma Membrane Partition Coefficient K_{PC}[e]	Binding Constant to P-gp from Inner Plasma Membrane K_C (M^{-1})[f]	Passive Permeability Coefficient at final steady-state (nm/sec) P_{BC}	P_{AC}
AMP	$2x10^{+9}$	200	$3x10^{-2}$	150	200	1,000	500	400
QND	$2x10^{+9}$	200	$1x10^{-3}$	5	700	15,000	500	500
LPM	$2x10^{+9}$	200	$4x10^{-4}$	2	3,000	4,000	350	400

Figure 11.7: Paper 3: Table 1 - Fitted Parameter Values[a]

Legend for Table 1.

[a] These are median values obtained for the association rate constant fitted in Tran et al. (2005) and in Acharya et al. (2006). This is the rate constant from flip-flop across the basolateral membrane to association with the P-gp binding site. The route appears to be lipid lateral diffusion controlled through the inner plasma monolayer.

[b] Median values for the density of efflux active P-gp in the apical membrane inner monolayer for each of the three drugs. As discussed in Tran et al. (2005) and Acharya et al., (2006), this number may be roughly 10 times smaller than the true surface density since only substrate released at the tips of the microvilli are likely to reach the apical chamber, rather than being absorbed back into the microvilli membrane and starting over.

[c] Median values for the product of k_2T(0), or the "Vmax", of P-gp.

[d] Median value for the efflux rate constant k_2.

[e] In reality, three partition coefficients are needed to simulate model data: K_{PC} is between the cytosol and the inner plasma monolayer; K_{BO} is between the basolateral chamber and the outer basolateral monolayer; and K_{AO} is between the apical chamber and the outer apical monolayer. Partition coefficients were estimated using 0.1μm extruded unilamellar liposomes (LUV) whose lipid compositions mimic, in a very crude way, the lipid compositions of the respective membrane monolayers. As explained in Tran et al. (2005), direct measurements using cells would be difficult since the drugs used are so permeable that only overall cell average partition coefficients could be obtained.

[f] Median value for the substrate binding constant from inner apical membrane monolayer to P-gp.

[g] This is the steady-state value for the drug's passive permeability coefficient. In reality, the passive permeability coefficients took from 15 min to 4 hrs to reach steady-state and Pa_{BA} was not the same as Pa_{AB} until their steady-state was reached (Tran et al., 2004, 2005; Acharya et al., 2006). Using these transient conditions would make the calculations and explanations much more complex, without changing any conclusions. We assumed the ideal situation of a static symmetric passive permeability barrier using the values achieved at the final steady-state.

Table 2

Probe Substrate (uM range)	Inhibitor (uM range)	IC50 (A>B)[a] (uM)	$K_{I,Aq}$ Table 1 [b] (uM)	Probe substrate $0.5*(P_{AB}+P_{AB})$ [c] (nm/s)	$K_{I,Aq}$ Eq.(5) [d] (uM)
Amprenavir (50 & 100)	Quinidine (0-20)	5	0.1	450	0.3
Quinidine (0.1-3)	Amprenavir (50&100)	~100	5	500	8
Quinidine (0.1-5)	Loperamide (0-10)	6	0.1	500	0.3
Loperamide (1-5)	Quinidine (0-30)	5	0.1	375	0.4

Figure 11.8: Paper 3: Table 2 - IC50 values and Corrections to estimate $K_{I,Aq}$

Legend for Table 2.

The IC50, passive permeability coefficients Pa_{AB}, and fitted values for the aqueous inhibitor dissociation constant $K_{I,Aq}$ were published in Acharya et al. (2006).

[a] IC50 fitted in Acharya et al. (2006).

[b] The dissociation constant for the substrate relative to the cytosol is $K_{I,Aq} = 1/(K_{PC} * K_C)$, using the parameters in Table 1.

[c]The "average" passive permeability coefficients from the chambers into the cytosol, using the values from Table 1.

[d]The "corrected" $K_{I,Aq}$ using the measured IC50 and Eq.(3).